Titre: Title:	Dynamic Modeling of Tube-Support Interaction in Heat Exchangers
Auteur: Author:	Reza Azizian
Date:	2012
Type:	Mémoire ou thèse / Dissertation or Thesis
Référence: Citation:	Azizian, R. (2012). Dynamic Modeling of Tube-Support Interaction in Heat Exchangers [Ph.D. thesis, École Polytechnique de Montréal]. PolyPublie. https://publications.polymtl.ca/1027/

UNIVERSITÉ DE MONTRÉAL

DYNAMIC MODELING OF TUBE-SUPPORT INTERACTION IN HEAT EXCHANGERS

REZA AZIZIAN

DEPARTEMENT DE GÉNIE MÉCANIQUE

ÉCOLE POLYTECHNIQUE DE MONTRÉAL

THÈSE PRÉSENTÉE EN VUE DE L'OBTENTION

DU DIPLÔME DE PHILOSOPHIAE DOCTOR

(GÉNIE MÉCANIQUE)

DÉCEMBRE 2012

UNIVERSITÉ DE MONTRÉAL

ÉCOLE POLYTECHNIQUE DE MONTRÉAL

Cette thèse intitulée:

DYNAMIC MODELING OF TUBE-SUPPORT INTERACTION IN HEAT EXCHANGERS

présentée par: AZIZIAN Reza

en vue de l'obtention du diplôme de : Philosophiae Doctor

a été dûment acceptée par le jury d'examen constitué de :

M. BALAZINSKI Marek, Ph.D., président

M. MUREITHI Njuki William, Ph.D., membre et directeur de recherche

M. PETTIGREW Michel, post grad.dipl., membre et codirecteur de recherche

Mme ROSS Annie, Ph.D., membre

M. ALIGHANBARI Hekmat, Ph.D., membre

ACKNOWLEDGMENTS

I would like to express my sincere thanks and deep appreciation to my Ph.D supervisor, Professor Njuki Mureithi and co-supervisor, Professor Michel Pettigrew. I am very appreciative of their thoughtful guidance, patience and constant support throughout my doctoral study. They have had a profound impact on the way that I approach scientific problems, find solutions and solve problems. I believe this will be very helpful for my future scientific work and also for real life problems.

I have been privileged to collaborate with members of the chair of fluid-structure interaction during my Ph.D program. I would like to thank Mr. Thierry Lafrance for his technical support and guidance during experimental tests, and for the modifications to the experimental rig, and Mr. Bénedict Besner for his guidance regarding the work with laser displacement devices, force transducers and data accusation system.

I would like to express thanks to Mr. Heung Seok Kang for his help and guidance with damping measurements, Ms. Isabelle Nowlan for sharing her experiences on tube-support experimental tests and finally Mr. Pierre Sawadogo for valuable scientific discussions.

I would like to express my appreciation to Professor Stéphane Étienne for his support and help during writing of this thesis and particularly the translation process of the “Résumé”.

I would like to thank all my colleagues and friends in the department of mechanical engineering at École Polytechnique de Montréal.

Finally, I take this opportunity to convey my profound gratitude to my beloved father, Professor J.Azizian, my mother, Ms. K.Moshiri and my sister, Dr. H.Azizian, for their encouragements and supports throughout the several years of my doctoral work.

RÉSUMÉ

Les forces induites par écoulement dans les échangeurs de chaleur peuvent provoquer des vibrations excessives et des interactions avec les supports. Avec le temps, ces interactions peuvent entraîner de l'usure par frottement et éventuellement mener au bris des tubes. La prédiction précise de l'interaction tube-support est importante pour quantifier l'usure par frottement. Ainsi, l'étude détaillée du frottement et des forces d'impact à l'origine de ces effets est nécessaire à l'établissement d'un modèle d'usure précis. Cette étude porte sur le développement d'un modèle de frottement qui permet de reproduire fidèlement les différents états du phénomène de frottement, incluant les effets d'élasticité, de plasticité et de frottement partiel. Le modèle d'impact tube-support résultant est vérifié numériquement et expérimentalement.

Un modèle de frottement fonction du taux d'amortissement d'un ressort hybride a été développé pour simuler précisément un phénomène de frottement d'une vitesse nulle à une vitesse de glissement importante. Cela a été obtenu en considérant différents phénomènes pendant le phénomène de friction incluant l'effet Stribeck, les forces variables de rupture, l'élasticité des micro-protubérances de paroi ainsi que les comportements de glissement plastique et partiel. Le temps de glissement dans le modèle de friction à limitation de vitesse a été comparé à celui obtenu par le modèle de friction de Lugre. L'incapacité du modèle de frottement à limitation de vitesse à détecter la zone d'adhérence a été expliquée par la dépendance du critère de limitation de la vitesse sur la force variable de rupture et l'effet Stribeck. Ceci a confirmé l'importance d'avoir une limitation de vitesse adaptative pour le modèle de frottement à limitation de vitesse. De plus, la distribution des contraintes à l'intérieur de la zone de contact a été étudiée en détails pour délimiter les différentes régions dans une zone de contact lors du frottement. Cette analyse a permis d'associer une signification physique à chaque composante de ce nouveau modèle de frottement hybride. La capacité du modèle à reproduire précisément le comportement adhérence-glissement a été évaluée à l'aide du modèle de frottement d'Ozaki et Hashigushi ainsi qu'avec les tests expérimentaux de Baumberger et al. Les résultats montrent une meilleure estimation du comportement adhérence-glissement, qualitativement et quantitativement, en utilisant le nouveau modèle hybride. De plus, la capacité du modèle hybride

à reproduire les déplacements qui précèdent le glissement, a été examinée en utilisant le modèle de frottement de Lim et Chen et les diagrammes de phase de stabilité expérimentaux développés par Baumberger et al. Le modèle de frottement hybride reproduit les diagrammes de phase expérimentaux avec un bon accord qualitatif ce qui n'est pas le cas avec le modèle de frottement de Lin et Chen. Toutefois, le niveau de vitesse de stabilité obtenu avec le modèle hybride présente des différences avec les expériences. Cela est principalement attribué à l'importance de la vitesse de Stribeck et aux coefficients d'amortissement dans le modèle de frottement hybride.

Dans la deuxiéme partie de cette recherche, une série de tests expérimentaux d'interactions entre tube et support a été effectuée pour mesurer les forces d'impact et les déplacements à mi-hauteur pour plusieurs amplitudes d'excitations et espacements. Ce programme expérimental a été utilisé comme base de données de référence pour examiner avec attention le modèle d'impact lors de l'interaction tube-support. La théorie des poutres d'Euler-Bernoulli et la technique de superposition modale ont également été utilisées pour les calculs dynamiques d'interaction tube-support. Les mesures d'amortissement structurel varient en fonction du déplacement à mi-hauteur. De plus, les effets d'élasticité et les forces d'impact inélastiques sur la réponse du tube ont été étudiés à l'aide de résultats expérimentaux ainsi que des simulations numériques. Cette étude a apporté d'important éclaircissements sur la relation non-linéaire entre force et déplacement lors de l'interaction tube-support. L'estimation du paramètre optimal *m*, associé à cette relation, a significativement réduit les différences entre les résultats expérimentaux et les simulations numériques. De plus, un programme expérimental prenant en compte le déplacement initial du tube à l'origine des excitations a été entrepris. Cela a permis d'étudier avec attention les déplacements du tube lors de mouvements dissipatifs. Les comparaisons entre les résultats expérimentaux et les simulations numériques indiquent un effet mineur de l'amortissement d'impact sur la réponse du tube en utilisant le modèle de Hunt et Crossley. La différence de déplacement à mi-hauteur a été expliquée comme découlant de la dissipation ajoutée par l'amortissement structurel. Cela a été modélisé par un coefficient qui correspond à l'amortissement structurel lors du contact tube-support. L'estimation de ce coefficient indique que le coefficient augmente lorsque l'espacement entre le tube et le support croit.

ABSTRACT

Flow-induced forces in heat exchangers can cause excessive tube vibration and interaction with their supports. Long term interaction may develop fretting-wear and consequently lead to tube failures. An accurate prediction of the tube-support interaction behavior is important to quantify tube fretting-wear. Therefore, a detailed study of the related friction and impact forces is required for formulating a precise wear model. This study aimed to develop a friction model for accurate representations of various states of the friction process, including elastic, plastic and partial slipping states. In addition, the tube-support impact model is verified both numerically and experimentally.

A hybrid spring-damper rate dependent friction model was developed to precisely simulate the friction process from zero velocity to the gross slip state. This was achieved by considering various physical phenomena during the friction process including the Stribeck effect, varying break-away force, bristle elastic, plastic and partial-slipping behaviors. The slipping time in the velocity-limited friction model was compared to the LuGre friction model. The inability of the velocity limited friction model to detect the sticking region was explained by the dependency of a limiting velocity criterion on the varying break-away force and the Stribeck effect. This confirmed the importance of having an adaptive limiting velocity for the velocity limited friction model. In addition, the stress distribution within the contact region was studied in detail to demarcate different regions within a contact area during the friction process. This analysis attributed a physical meaning to each component of the new hybrid friction model. The ability of the hybrid model to accurately reproduce stick-slip behavior was examined using the Ozaki and Hashiguchi friction model and the Baumberger et al. experimental tests. The result showed better estimation of the stick-slip behavior, both qualitatively and quantitatively, using the new hybrid friction model. In addition, the ability of the hybrid model, to reproduce pre-sliding displacements, was also examined using the Lim and Chen friction model and the experimental stability phase diagram, developed by Baumberger et al. The hybrid friction model reproduced the experimental phase diagram with qualitatively good agreement contrary to the Lim and Chen friction model. However, the magnitude of the stability velocity, in the hybrid model, had some

differences with the experimental result. This is mostly associated with the magnitude of the Stribeck velocity and damping coefficients in the hybrid friction model.

In the second part of the research, a series of tube-support experimental tests was performed to measure the related impact forces and mid-span displacements for various excitation amplitudes and gap sizes. The experimental program results were used as a reference database to carefully examine the impact model during tube-support interaction. The Euler-Bernoulli beam theory and modal superposition technique were also used to perform tube-support interaction dynamics computation. The structural damping measurements showed a varying magnitude depending on tube mid-span displacement. In addition, the effects of elastic and inelastic impact forces on the tube response were studied using the experimental results and numerical simulation comparisons. This study provided important insight into the elastic nonlinear force-displacement relationship during tube-support interaction. The estimation of the optimal parameter *m*, associated with this relationship, significantly reduced the difference between the experimental test results and the numerical simulations. In addition, an experimental program was undertaken considering the tube initial displacement as the origin of the excitation. This enabled a careful study of the tube displacement in a dissipative motion. The experimental tests and numerical simulation comparisons indicated the minor effect of the impact damping on the tube response, using the Hunt and Crossley model. The difference in the mid-span displacements was explained by increased energy dissipation through structural damping. This was modeled using a coefficient which represents a change in the structural damping from the onset of tube-support contact. The estimation of this coefficient indicated an increasing trend of the coefficient with increasing tube-support gap.

TABLE OF CONTENTS

LIST OF TABLES

LIST OF FIGURES

LIST OF SYMBOLS

A	Tube cross-section area[m^2]
a	Contact radius[m]
C	Damping coefficient[Ns/m]
c_p	Plastic damping coefficient[Ns/m]
c_s	Slipping damping coefficient[Ns/m]
c_z	Stribeck damping coefficient[Ns/m]
D_0	Average presliding displacement[m]
D_i	Inner diameter[m]
D_o	Outer diameter[m]
E	Young modulus[Pa]
EI	Bending stiffness[$N.m^2$]
f	Frequency[Hz]
F_d	Impact damping force[N]
F_e	Excitation force[N]
F_{ex}	Excitation force x-direction[N]
F_{ez}	Excitation force z-direction[N]
F_f	Friction force[N]
F_s	Static friction force[N]
F_c	Coulomb friction force[N]

F_n	Normal force[N]
F_t	Tangential force[N]
F_{Ty}	Fretting yield force[N]
G	Shear modulus[Pa]
K	Stiffness coefficient[N/m]
Ku	Internal resistance force[N]
k_e	Tangential elastic stiffness[N/m]
k_{ep}	Tangential elasto-plastic stiffness[N/m]
k_p	Work hardening coefficient[N/m]
k_{ps}	Tangential plastic-slipping stiffness[N/m]
k_s	Support stiffness[N/m]
L	Tube length[m]
L_s	Support length[m]
M	Mass[Kg]
q_{nz},q_{nx}	Modal responses
t	Tube thickness[m], Time[s]
T^*	Amplitude of tangential oscillatory force[N]
v	Poisson ratio
V_0	Limiting velocity[m/s]
V_t	Tangential velocity[m/s]
v_p	Pulling velocity[m/s]

v_s	Stribeck velocity[m/s]
u_0	Zero velocity tangential displacement[m]
u_c	Current velocity tangential displacement[m]
u_z	Normal indentation[m]
w	Contact width[m]
z_e	Elastic displacement[m]
z_p	Plastic displacement[m]
z_s	Partial-slipping displacement[m]

Greek

μ	Friction Coefficient
μ_k	Kinetic friction coefficient
μ_s	Static friction coefficient
ξ	Structural damping ratio
ξ_s	Structural damping ratio during contact
ϕ	State variable[m]
$\varphi_n(x)$	Mode shapes
η	Viscous damping[Ns/m]
σ_0	Friction stiffness coefficient[N/m]
σ_1	Friction presliding damping coefficient[Ns/m]
σ_2	Friction viscous damping coefficient[Ns/m]

Δ_1	Tube-support clearance[m]
ΔE	Friction energy dissipation[N.m]
δ	Total presliding displacement[m]
ρ	Density[kg/m^3]
ω_n	Natural frequency[Hz]

Subscripts

e	Elastic
p	Plastic
ps	Partial-slipping
r	Radial displacement
s	Support
t	Tangential
z	Normal direction
x	Tangential direction

Abbreviation

EPRI	Electric power research institute
FBFM	Force-balanced friction model
VLFM	Velocity-limited friction model
VIBIC	Vibration of beams with intermittent contact (Code)

VITRAN	Vibration transient analysis–nonlinear (Code)
r.m.s	Root mean square
SDFM	Spring-damper friction model

INTRODUCTION

Fretting-wear is a challenging problem which is frequently encountered in different mechanical systems including steam generators. A steam generator is mainly comprised of a tube bundle which transfers heat from the primary loop coolant, within the tubes, to secondary loop water, external to the tubes. The tubes are then subjected to both parallel and cross-flow in different phases, including liquid, gas or two phase. This causes flow-induced forces on the tubes, including fluid elastic and turbulence forces. On the other hand, the concerns associated with thermal expansion, installation and manufacturing may lead to development of a more flexible tube-support structure. Tube-support interaction is therefore unavoidable as a result of flow-induced vibration. The long term interaction may cause tube fretting-wear and subsequently tube rupture. This undesired fretting-wear may affect the safety and performance of a nuclear power station. Data provided by Electric Power Research Institute (EPRI) suggested that, in 1994, 49 percent of all pressurized water reactor steam generators were overhauled as a result of the above mentioned tube-support fretting-wear (Dierecks et al., 1996). The report suggested an average cost of 100-200 million dollars per plant for steam generator tube replacements.

The importance of the tube-support fretting-wear problems has raised a lot of interest among researchers. Many studies have been conducted to investigate and estimate flow-induced forces (Pettigrew et al., 1978; Lever and Weaver, 1982; Pettigrew and Taylor, 1994; Pettigrew et al., 1998; Weaver et al., 2000; Païdoussis et al., 2010). On the other hand, many authors have studied tube-support interaction in terms of impact and friction (Rogers and Pick, 1977; Sauve and Teper, 1987; Fisher, 1989; Chen, 1991; Fisher et al., 1992; Tan and Rogers, 1996; Hassan et al., 2002). The ultimate goal of these studies is to quantify fretting-wear during tube-support interaction. Work-rate is a factor which quantifies wear-rate. This factor is strongly dependent upon sliding distance and normal contact force. It is therefore important to have precise friction and impact models to carefully quantify tube-support fretting-wear.

The velocity-limited friction model (Rogers and Pick, 1977), force-balanced friction model (Karnopp, 1985) and spring-damper friction model (Antunes et al., 1990) are the three main friction models which have been widely used in the tube-support interaction simulation. The main differences between the friction models are the criteria employed to detect the stick-slip

regions and estimation of the sticking friction force. In the friction models above, the criteria to detect the stick-slip regions are not physics based and often lead to errors in the estimation of the sliding distance. Furthermore, in these models, the transition behavior from the stick to slip phases has not been considered. The study of the motion from zero velocity to the gross sliding phase is crucial to obtaining a physics based criterion for detection of the stick-slip regions.

The LuGre Friction model (Canudas de Wit et al., 1995), the Ozaki and Hashiguchi friction model (Ozaki and Hashiguchi, 2010) and the Lim and Chen friction model (Lim and Chen, 1998) are three examples of rate dependent friction models. The friction models consider the transition behavior from the stick to slip phases. Furthermore, the models also take into account the nonlinearity in the vicinity of zero velocity. The precision of the friction models makes them good enough for use in robotic and control systems. However, no attempt has been made to correlate the friction models to the tangential stress distribution.

The study of the tangential stress distribution within the contact region is a crucial step in investigating the bristle behavior during the friction process from the absolute zero velocity to the gross slip state. Cattaneo-Mindlin (Cattaneo, 1938; Mindlin, 1949), Mindlin and Deresiewicz (1953) and Odfalk and Vingsbo (1992) endeavored to correlate the physical phenomena in the friction process to the tangential stress distribution within the contact region. As the result of the studies, the friction process was divided into the three stages of elastic, plastic and partial-slipping regions. From the fretting-wear point of view, the different stages may result in different wear coefficients. Therefore, developing a rate-dependent friction model which can demarcate the different regions of elastic, plastic and partial-slipping is expected to be particularly beneficial.

The estimation of the impact force is a crucial step in the tube-support interaction analysis due to the subsequent effect on the friction force, stick-slip regime and work-rate calculation. Some efforts have been dedicated to modeling the impact force (Axisa et al., 1984; Sauve and Teper, 1987; Yetisir and Fisher 1997). However, the nonlinearity involved in the force-indentation relation has not been studied. Furthermore, the study of the source of energy dissipation during the normal interaction should be a beneficial step. The evaluation of the incorporated impact model in the dynamic modeling of the tube-support interaction, for a real heat exchanger tube, is a challenging step due to the involvement of different factors such as the

fluid-induced forces, multiple supports, support types and friction force. Therefore, for the impact model validation, the replacement of the complicated factors by a simplified laboratory experimental rig may be valuable.

The motivation of the present work may be summarized as follows: fretting wear of nuclear steam-generator tubes remains an important problem in industry both for safety and cost reasons. While significant work has been done too address this problem, and in particular to model tube-support interaction for wear estimation, important questions and challenges remain.

To better estimate the wear work-rate more accurate models for the friction and impact phenomena are needed. In order to develop this next generation of models previously unmodelled details of the tube-support interaction need to be taken into account. This includes consideration of the tangential stress distribution within the contact region as well as correctly modelling the various states or stages of the friction process (including sticking, partial slip and gross slip). In addition the nonlinear impact process needs improved modelling. Finally, the new, inherently more complex models must be verified by incorporation into full multimode tube models. Dynamic analyses then need to be carried out and to the extent possible, comparison with experimental tests done.

CHAPTER 1
LITERATURE REVIEW AND RESEARCH ORGANIZATION

In this section a detailed review of previous work on tube-support interaction is presented. The literature review is followed by a summary of key research questions in Section 1.2. The objectives of the proposed research are presented in detail Section 1.3. The thesis organization is outlined in Section 1.4.

1.1 Review of Previous Studies

This section will review the state of the art on tube-support wear mechanisms, dynamic computation, impact and friction models. In the heat exchanger and steam generator tube bundles, contacts between the tube and support are unavoidable due to the flow-induced vibration. This interaction causes fretting-wear which may consequently lead to tube failure (Fisher et al., 1992; Hassan et al., 2002). Chen (1991) divided the causes of tube failure in heat exchangers into four different phenomena: interaction and wear between the tubes, interaction and wear between the tube and support, joint failure at the tube to tube-sheet interface and tube fatigue. The causes of the excessive vibration and subsequently fretting-wear are flow-induced forces. Flow-induced vibration mechanisms can be classified as fluid-elastic instability, vorticity shedding, turbulence buffeting and acoustic excitation (Pettigrew et al., 1978; Pettigrew et al., 1998). These flow-induced mechanisms can lead to significant tube vibration and interaction with supports. The interaction may then cause tube fretting. The fretting may be classified as fatigue-fretting, fretting-wear and fretting-corrosion (Magaziner et al., 2004). Several authors have studied different aspects of the tube and support dynamics, to come up with better fretting-wear estimation. It is an intricate process to develop a precise contact model due to the difficulties in simulating the fluid forces and unknown contact interface conditions (Popp, 2005). However, several codes have already been developed to simulate the tube-support interaction including VIBIC (Rogers and Pick, 1977), H3DMAP (Sauve and Teper, 1987), GERBOISE (Axisa et al., 1986), INDAP (Hassan, 2000; Hassan et al., 2002; Hassan et al., 2003), VITRAN (Rubiolo, 2006) and FIVDYNA (Toorani et al., 2009).

To have a better estimate of the tube-support interaction behavior during flow-induced vibration, a precise model is needed for each component of the tube-support system including: the fluid excitation forces, tube-support dynamics, tube-support impact, tube-support friction and effects of various system parameters (Chen, 1991).

1.1.1 Tube-support wear mechanisms

An oscillatory relative surface interaction between two objects may result in fretting-wear. Accurate wear-rate estimation is important for the prediction of the life time of the engaged components and their replacement time (Gessesse, 2000). During the interaction, different wear mechanisms may be activated. The type of mechanisms is dependent upon the relative motion of the components, interaction forces magnitude, geometry of the contact, type of materials and operating conditions of the system (Ko, 1986). Due to the flow excitation mechanisms in the steam generator tube bundle, contacts between the tubes and supports occur. These contacts may be categorized as normal, tangential or oblique impacts (Hofmann et al., 1992). The dominant wear mechanism for each type of interaction is different. Therefore, the incident impact angle, which quantifies the type of interaction, plays an important role in the tube-support dynamic computation. The angle may be defined by different system parameters such as: the tube pre-load conditions, flow excitation mechanisms and tube-support interaction forces (Haslinger and Steininger, 1995). To better understand the interaction, it is important to study the interaction forces and subsequently the mechanisms which may be involved in material removal during the wear process.

Different wear processes may be involved during the tube-support interaction such as adhesive, abrasive, delamination, fatigue and corrosion wear (Gessesse, 2000). However, based upon the real working conditions of the heat exchangers, the most dominant wear mechanism in the tube-support interaction may be a combination of the abrasive, delamination and fatigue wear mechanisns (Suh, 1973; Lee et al., 2001; Gessesse and Attia, 2004). Based upon the delamination theory of wear, proposed by Suh (Suh, 1973), the causes of wear are the dislocations at the contact surface, sub-surface crack propagation and void formation (Suh, 1973), (Fleming and Suh, 1977). In an extension of the Suh study (Suh, 1973), different authors have tried to evaluate the wear process both experimentally and theoretically. Argon and Im (1975) proposed a crack propagation criterion to evaluate crack initiation and plastic region formation (Jahanmir and Suh,

1977). The experimental studies conducted by Suh (1973), Gauland and Duquette (1980) and Waterhouse (1981) indicated that cracks may be propagated parallel to the contact surface in the material sub-layer. Furthermore, it was reported that the propagation may take place in an approximate depth of 0.8 to 1.8 times of the micro-contact radius from the contact surface and that due to the numerous cyclic loadings, the crack may grow until reaching the critical length of 1 to 1.4 times of the micro-contact radius. After the crack reaches the critical length, it may progressively change its direction toward the contact interface. The process may consequently form wear debris (Suh, 1973; Fleming and Suh, 1977).

1.1.2 Tube-support interaction

Since the most important causes of tube wear are friction and impact, many authors have tried to model and simulate these phenomena theoretically and experimentally. Different experimental tests have been carried out to establish the relations between the tube-support wear rate and different experimental parameters such as tube-support clearance, support type, friction coefficient and loading conditions.

Axisa et al. (1984) conducted experimental tests to measure the impact force and mid-span displacement during the tube-support interaction for a tube with multiple supports. In the experimental rig, the supports had quatrefoil hole shapes. The tests were conducted for different gap sizes and excitation forces. The results indicated a reasonable trend agreement between the impact forces in the experimental tests and numerical simulations. However, the mid-span displacements indicated significant differences particularly with increasing tube-support gap size.

Haslinger et al. (1990) characterized the squeeze film effect during tube-support interaction. The study investigated the effect of varying gap sizes on the fluid squeeze film phenomenon. The authors also obtained semi-empirical expressions for the effect. Subsequently, Haslinger et al. (1995) conducted experimental tests to estimate the coefficient of friction during tube-support interaction. The results justified the usage of the same friction coefficient for the tube-support oblique impact and gross sliding. Additionally, these results indicated that the friction coefficient is independent of the normal force.

Chen et al. (1985) and Chen (1991) conducted experimental tests to understand the effectiveness of the support. The authors defined two different support modes support active and

support inactive modes. The support active mode may be activated due to relatively small clearance which causes the support to behave effectively. On the other hand, for relative large gaps, the support may not perform effectively which may activate the support inactive mode. The study indicated that during the tube-support interaction, the support mode was usually a combination of the two different modes. Furthermore, the study showed that the tube response may be different depending upon the activation of different modes. The phenomena were then explained based upon changes in the tube-support natural frequency for the different modes. In addition, the Moretti and Lowery (1973) study emphasized the change in the natural frequency depending on the support mode, excitation amplitude and clearance.

Yetisir and Fisher (1997) studied the interaction between fuel channel and fuel elements subjected to a turbulence-induced force caused by an axial flow. For the numerical simulation, the VIBIC code (Rogers and Pick, 1977), based upon the modal superposition method, was used. In the study, different parameters were investigated such as contact stiffness, friction coefficient, damping, support length and gap sizes.

Attia and Magel (1999) carried out experimental tests to investigate the long term fretting-wear behavior in straight and U-bend tubes. The authors tried to study the effect of the tube-support clearance on the wear-rate and subsequently find a relationship between the wear-rate and work-rate. The results indicated that the work-rate decreased with increasing gap-size. However, the trend had a non-monotonic behavior which suggested a self-limiting property for fretting-wear during tube-support interaction.

Lee et al. (2001) conducted experimental tests to evaluate the wear behavior during the tube-support interaction in steam generators. In the experimental tests the tube materials were chosen as Inconel 600MA and 690TT. The support materials were 405 and 409 ferritic stainless steels. The normal load and sliding amplitude were gradually increased and the worn contact interface was carefully observed with the help of a scanning electron microscope. Moreover, the wear coefficient was determined and the effect of the material compositions and surface hardening were investigated. The results indicated that different wear mechanisms may be involved during the tube-support interaction. These mechanisms may strongly depend upon the magnitude of the chromium content which may define the level of the work hardening during the interaction. The morphology investigation of the worn surface indicated that fine wear particles

were formed on the worn surface even after ultrasonic cleaning. The particles were formed due to the high shear plastic deformation on the contact interface and crack propagation in the material sub-layer. These particles became even finer due to the continuous wear process and normal compressive pressure. It was therefore suggested that a wear protective layer may be formed. It is pertinent to note that such a layer behaves differently for Inconel 600MA compared to Inconel 690TT. For Inconel 600MA, the protective layer did not strongly stick to the contact interface. Therefore, it was worn away during the abrasive wear process. In contrast for Inconel 690TT, the protective layer strongly adhered to the worn surface due to the high chromium content. Thus, the wear coefficient may be lower for Inconel 690TT compared to Inconel 600MA.

Attia et al. (2007) elaborated the fretting-wear mechanisms during the tube-support interaction. To achieve this goal, the authors proposed a physical parameter based upon the worn surface morphology and fracture mechanics mechanisms. The new paramater corrolates the energy dissipation to the wear loss by demarcating the different types of the tube orbital motions.

Nowlan et al. (2009) studied the tube-support interaction via a series of sweep test excitations in the direction parallel to a support in contact with a two-span tube. In this study the tube natural frequency was carefully measured. Furthermore, the contact forces were measured for different preload, gap sizes and support orientation. It was concluded that the natural frequency was not changed by the interaction. On the other hand, the stick-slip behavior and normal tube-support interaction transferred energy to the higher tube modes. The results also underlined the sensitivity of the tube response to the tube-support clearance.

Many authors have developed models to simulate the tube response using numerical techniques. Rogers and Pick (1977) used a finite element method to study the tube-support interaction. The study considered the effect of damping, tube stiffness and gap size on the interaction forces. Fisher et al. (1989) validated the work-rate estimation in the VIBIC code against experimental tests. Tan and Rogers (1996) attempted an evaluation of the effect of the force-balanced friction model on the tube-support wear-rate estimation. In the study, the friction model was incorporated into the VIBIC code for different types of supports including circular, semi-circular and scallop-bar types. The work-rates for different gap sizes were also compared against the experimental tests conducted by Yetisir and Fisher (1997).

Hassan et al. (2002) studied the tube-support interaction for a tube subjected to turbulence induced forces. In the study, a nonlinear dynamic analysis based upon a finite element method was used for the simulation. The normal impact model was chosen based upon the Sauve and Teper impact model (Sauve and Teper, 1987). The velocity-limited friction model was incorporated in the numerical simulation and the turbulence excitation modeling based upon the Oengoren and Ziada study (Oengoren and Ziada, 1995) was used. There were also comparisons made between the impact forces among the three different dynamic computation codes including H3DMAP (Sauve and Teper, 1987), INDAP (Hassan, 2000; Hassan et al., 2002; Hassan et al., 2003) and VIBIC (Rogers and Pick, 1977). The results indicated a significant increase in the work-rate estimation due to support offset. The complex behavior of the tube response was investigated by introducing a dimensionless clearance as the ratio of radial clearance to r.m.s support response.

Hassan et al. (2005) simulated the tube-support interaction by considering a new impact model. Due to the difficulties in accurately estimating the contact area and contact pressure distribution, the contact model is commonly simplified to a point contact in which the support is assumed to be a knife edge. However, in Hassan et al.'s study, the real contact region was modeled as a segmental contact. Furthermore, the point and segmental contact stiffness was modeled with a single spring and distributed contact stiffness, respectively. The model indicated that the nature of the tube-support interaction is a combination of the edge and segmental contacts. Furthermore, the study specified a higher possibility of encountering a segmental contact by decreasing the tube-support gap sizes. Different factors such as the support preload, clearance and tube alignment may affect the type of contact during the interaction. For instance when the clearance is small in the presence of a large preload, the interaction may mostly occur in the sliding mode and the appropriate model is the segmental contact. On the contrary, for a large clearance with a small preload, intermittent contacts may mostly occur. In this case the appropriate model is the point contact.

Hassan and Rogers (2005) studied the impact and friction forces during tube-support interaction. In the study, different friction models including the velocity-limited friction model, force-balanced friction model and spring damper friction model were incorporated in the numerical simulations. Furthermore, the work-rate was calculated for the different friction

models and tube-support clearances. The results indicated a good agreement between experimental results and numerical simulations for the large preloads in contrast to the case of small preloads.

1.1.3 Non-linear dynamic computations

Sauvé and Teper (1987) developed an implicit numerical integration scheme for tube-support vibro-impact interaction based upon a finite element method. The program has the flexibility of changing the time-step to minimize errors and obtain the optimum result. Furthermore, the lumped mass approach and Rayleigh proportional model were used to form the mass and damping matrices. The Newmark scheme (Bathe, 1982) was used for integrating the nonlinear equations. As the result, a dynamic computation code, called H3DMAP, was developed to simulate the flow-induced tube-support interaction.

Hassan et al. (2002) developed a computer code called INDAP to simulate the tube-support interaction. The authors used a standard finite element procedure to solve the tube's equation of motion. Using the FEM procedure is extremely costly in terms of time, due to the incipient contact search algorithm. Therefore, the authors adapted a pseudo-force approach developed by Subbaraj and Dokainish (1989). The method simplified the nonlinearity of the system by introducing an external force into the equation of motion.

Another code, developed at AECL, is VIBIC (vibration of beams with intermittent contact) (Fisher et al., 2001). VIBIC is designed for the structural dynamic analysis of tube-support interaction. In the program, the tube dynamic response is determined by the modal superposition technique. Similarly to the Subbaraj and Dokainish (1989) method, the tube-support nonlinearity due to the clearance was modeled by introducing an equivalent external force to the system. The equations of motion are numerically solved using the fourth-order Runge-Kutta algorithm.

VITRAN (vibration transient analysis–nonlinear) (Rubiolo, 2006) is another computer code used to simulate the dynamic response of fuel rods. This nonlinear dynamic analysis code was developed based upon the Euler-Bernoulli beam theory similarly to the study by Antunes et al. (1990). In the governing equations, the rotational inertia and shear deformation are neglected. Further, the unconstrained modal superposition is used to determine the dynamic behavior of the

system. Instead of using the constrained mode shapes the use of the unconstrained mode shapes was explained by the relatively small difference in the results and time consumption cost of using the constrained mode shapes. The numerical analysis by Davies and Rogers (1979) also suggested the admissibility of using unconstrained mode shapes for systems with very low structural damping coefficient.

1.1.4 Impact models

Goyal et al. (1994) divided the impact model into two parts: the first being the detection of the contact between the two bodies and the second the force calculation due to the interaction. An accurate estimation of the normal contact force is an essential part of the interaction modeling due to the subsequent effect on the friction force and stick-slip regime estimation. One of the theories developed to analyze the contact behavior between two bodies is the Hertz's contact theory (Johnson, 1985). In Hertz's theory, the contact region is assumed to be continuous and relatively small compared to the bodies' dimensions (Johnson, 1985). The bodies involved during the interaction are also considered as completely elastic (Johnson, 1985). The contact surfaces are assumed to be frictionless surfaces (Johnson, 1985) and the only force which may be transferred during the interaction is the normal force. Deformation boundary forces are not considered in the model (Johnson, 1985). To take into account the boundary deformation forces, Thornton and Randall (1988) proposed an impact model which considered neighboring deformation based upon a feedback finite element algorithm (Goldsmith, 1960; Johnson, 1985). However, in the case of the tube-support interaction, the thin circular cross-section may affect the contact stiffness by the ovalization phenomenon. Therefore, Morley (1960) studied the ovalization effect for a force couple acting on a thin cylinder. The study assumed that the acting forces are far from the cylinder edges. This enabled the researchers to arrive at an estimate of the stiffness coefficient for the ovalization effect.

During interaction between two bodies, three mechanisms of energy dissipation may be involved including: shear, normal damping and structural damping dissipations. These sources of energy dissipation may be in the form of the elastic waves, viscoelasticity and plastic deformation (Goyal et al., 1994; Stevens and Hrenya, 2005). The coefficient of restitution is the quantity characterizing the energy dissipation during interaction between compact bodies. Different definitions for the coefficient of restitution have been proposed including: the Newtonian

hypothesis based upon the velocity ratio, the Poisson's hypothesis based upon the impulse ratio for the two different impact phases; loading and unloading and the Stronge hypothesis based upon absorbed energy during the interaction (Goyal et al., 1994; Stronge, 2000). There are some difficulties associated with the estimation of the coefficient of restitution. For instance there is no perfect rough surface to prevent sliding and so some of the energy may be dissipated in the form of friction (Goldsmith, 1960). It is also pertinent to point out that due to plastic deformation, torsion and other impact boundary conditions, it is essential to evaluate a precise coefficient of restitution through a semi-empirical formula based upon material properties, impact velocity and impact interface geometry (Goldsmith, 1960).

Hunt and Crossley (1975) developed a model for the normal interaction between two bodies considering energy dissipation. The bodies were assumed to be compact solid bodies and the effect of reflected elastic shock wave was not considered in the model. The three main factors of the model are elastic impact force, coefficient of restitution and impact velocity which may affect the normal damping force estimation.

For a continuous system interaction such as the tube-support system, defining a coefficient of restitution is problematic. The Thomson et al. (1994) study on continuous system interaction indicated that the higher modes are excited. The authors suggested that the measured coefficient of restitution may underestimate the energy dissipation (Wagg and Bishop, 2000). Another study by de Weger et al. (1996) laid emphasis on the higher mode energy transfer (dissipation) during a continuous system interaction. However, the nature of chaotic multi-impact behavior of the tube-support interaction in a short interaction duration introduces uncertainties on the experimental measurements (Werner and Robert, 2008). Different authors have theoretically analyzed the multi-impact behavior and the coefficient of restitution value in continuous systems (Shaw, 1985; Stoianovici and Hurmuzlu, 1996; Bao et al., 2004; Wagg, 2005; Wagg, 2007).

1.1.5 Friction models

Different friction models have been developed for the evaluation of friction induced stick-slip behavior. The incorporated friction model in the tube-support dynamic computation scheme is important particularly due to the nonlinear behavior of the friction force in the vicinity of zero sliding velocity. The main differences among different friction models are their approaches to the detection of the stick-slip regions, estimation of the friction force in the sticking phase and

transition modeling from the sticking to slip phases. In this section, the state of the art in the commonly used friction models in the tube-support interaction modeling is described. In addition the rate-dependent friction models and tangential stress distribution within the contact area are also reviewed.

1.1.5.1 Tube-support friction models

The velocity-limited friction model (VLFM) is one of the friction models which is widely used in tube-support dynamic simulation. In the model, a limiting velocity is defined to demarcate the stick-slip regions. The friction force in the sliding phase is determined similarly to the Coulomb friction model. On the other hand, the friction force in the sticking phase is proportional to the limiting velocity for sticking. The model was described by several authors such as Rogers and Pick (1977) and Tan and Rogers (1996).

Karnopp (1985) proposed a one-dimensional force-balanced friction model (FBFM) by demarcating the slip and sticking regions based upon defining a velocity window. The friction force during the sliding phase in the force-balanced friction model may be defined similarly to the Coulomb friction model. However, the friction force in the sticking region is calculated by balancing the net force to keep the velocity equal to zero in this region.

Antunes et al. (1990) proposed a spring-damper friction model (SDFM). The model was designed to precisely determine the sticking friction force and to take into account the nonlinearity in the vicinity of zero velocity. To achieve these goals, a parallel spring and damper system was implemented to estimate the sticking friction force. In the model, the stick and slip regions may be demarcated by the sign of the dot product of the instantaneous velocity in the current and previous time steps. Furthermore, the spring stiffness and damping coefficient were determined based upon the numerical stability of the model rather than physical quantities.

Tan and Rogers (1996) analyzed a two-dimensional system with two different friction models, including the spring-damper friction model based upon the Antunes et al. (1990) study and the force-balanced friction model based upon the Karnopp (1985) study. The results indicated a weakness of the velocity sign criterion used to detect the stick-slip regions for a two-dimensional dynamic analysis. Comparisons of the models indicated that using the force-

balanced friction model may lead to better numerical stability in the simulation response and more accurate detection of the stick-slip regions.

Tariku and Rogers (2001) improved the force-balanced and spring-damper friction models to have a better estimation of the stick-slip regions. The Karnopp force-balanced friction model (Karnopp, 1985) uses a velocity window to define the sticking region. The boundary condition may result in an error associated with a large time-step since the algorithm may not detect the small velocity window. Therefore, the force-balanced friction model was improved by considering two criteria to precisely detect the sticking regions including, the velocity sign criterion and maximum friction force limitation. The results indicated that the implementation of these criteria rather than using the velocity window may lead to a lower sticking velocity error. For the spring-damper friction model, the authors suggested using three criteria to confirm the occurrence of sticking including, the velocity sign change criterion, net external force limitation and spring-damper force limitation. As a result of the modification, the occurrence of a spike in the beginning of the sticking region was eliminated. The authors also analyzed the effect of different system parameters including the time-step, duration of simulation, initial conditions, spring stiffness and damping coefficient.

1.1.5.2 Rate-dependent friction models

The modeling of the transition from the sticking to slip phases is a challenging problem due to the dependency of the model on elastic, plastic and partial slipping behavior of the bristles within the contact region. Rabinowicz (1951) experimentally studied the transition between the static and dynamic phases. In the study, the transition was explained based upon the breakage of the metallic junctions in the contact interface. Therefore, the transition function may strongly depend upon the relative velocity of the interfaces. Many authors have worked on the development of a mathematical function to precisely reproduce the stick-slip transition (Wojewoda et al., 2008), the Stribeck effect (Stribeck, 1902). The Exponential distribution (Tustin, 1947), Gaussian distribution (Armstrong-Helouvry, 1991) and Laurentzian distribution (Hess and Soom, 1990) have been considered in the modeling.

Dahl (1968) developed a friction model based upon the stress-strain curve of the bonds formed within the contact interface. The author adopted the concept of metallic junctions formation and subsequent yielding and breaking of the junctions in the friction process. In the

model, the bristle deflection was simulated by introducing an internal state variable. The friction force was then proportional to the magnitude of the state variable.

The LuGre friction model, developed by Canudas de Wit et al. (1995), was an upgrade of the Dahl model considering the effect of varying break-away force, pre-sliding displacement, Stribeck effect and friction hysteretic behavior. The model was inspired by the idea of average bristle deflection. Therefore, the friction force in the model was decomposed into three terms depending upon the average bristle deflection, rate of change of the average bristle deflection and the relative velocity of the two interfaces. The Stribeck stick-slip transition function was incorporated in the LuGre model based upon the Gaussian function proposed by Armstrong and Helouvry (1991).

The presliding displacement in the LuGre friction model (Canudas de Wit et al., 1995) was considered to include the plasticity in the whole process of presliding. The assumption may cause an unbounded displacement when a small oscillatory force acts on the system. For this reason, Dupont et al. (2002) tried to eliminate this effect by demarcating the elastic and plastic presliding regions. However, the elastic to plastic demarcation criterion was a challenging step in the model.

Armstrong and Qunyi (2008) studied the presliding behavior in different friction models using internal state-variables. This work indicated that the presliding might be assumed to be elastic or plastic depending on the definition of the state-variable in the friction model. It emphasized the importance of choosing a proper friction model based upon the application and required sensitivity. Astrom and Canudas-de-Wit (2008) studied the LuGre friction stick-slip behavior by considering different system properties such as pre-sliding displacement, invariance and passivity.

Ozaki and Hashiguchi (2010) developed a friction model to study the intermittent stick-slip behavior in an unstable friction-induced phenomenon. In the model, the rate of change in the instantaneous friction coefficient is dependent on the coefficient of friction and plastic sliding velocity. The model also considered the friction coefficient softening effect during the transition from the sticking to slip phases and the hardening effect during the transition from the slip to stick phases.

Baumberger et al. (1994) experimentally studied the motion of a mass-spring system subjected to a driving velocity. The authors investigated the effect of different system parameters including the slider mass, spring stiffness and driving velocity. The study consequently led to the construction of a dynamic phase diagram to demarcate the unstable stick-slip regions from the stable slip regions.

As an extension of the Dieterich (1978) study, Ruina (1983) developed a friction model to represent the unstable stick-slip behavior due to the variation of friction resistance during a movement. The model considered the slip history by introducing a state-variable (Rice and Ruina, 1983). It yielded a critical spring stiffness to demarcate the steady slip from the unstable stick-slip regions. Lim and Chen (1998) developed a simple friction model based upon the conceptual description of the friction process based upon a study by Heslot et al. (1994). The model has a good agreement with the Baumberger et al. experimental phase diagram (Baumberger et al., 1994) demarcating the creep and inertial dominated regions. However, the model cannot properly reproduce the slope of the dynamic phase diagram, particularly in the creep dominated regions.

1.1.5.3 Tangential stress distribution within contact region

Cattaneo (1938) and Mindlin (1949) proposed a tangential stress distribution within the contact region between two elastic bodies subjected to a tangential force. Based upon the proposed distribution, the contact region was demarcated into two sub-regions, the sticking and partial-slipping regions. In the sticking region, the coincident points on the two bodies move together and have the same tangential elastic displacements which may produce the sticking region in the middle of the contact area (Johnson, 1985). In the partial-slipping region, coincident points have a relative tangential displacements which may subsequently develop a peripheral layer of the partial-slipping region in the outer layer of the contact area (Johnson, 1985).

Mindlin and Deresiewicz (1953) investigated the effect of varying the oblique contact force during the interaction between two identical spheres. The study indicated that the force-displacement relation may depend upon the entire history of the loading. Furthermore, the effects of the relative varying normal and tangential forces on the tangential stress distribution were studied. Based upon the history of tangential loading, the energy dissipation associated with the

partial slipping phase was obtained by considering an oscillatory tangential force and using the superposition method.

Johnson (1955) experimentally investigated the Mindlin elastic theory (Mindlin, 1949). In the experimental study, the micro-displacements between a hard steel ball and flat steel support were studied. The steel ball was subjected to a tangential force less than the limiting friction force. To carefully study the micro-slip behavior, the effects of the experimental parameters such as ball diameter, normal load, steady and oscillatory tangential forces were investigated. The results indicated a fairly good agreement between the experimental tests and the Mindlin theory particularly for small tangential forces.

Johnson (1961) conducted experimental tests to study the Mindlin and Deresiewicz (1953) theoretical study. The experimental rig consisted of a steel ball in contact with a flat support subjected to an oscillatory force with different obliquity angles. The experimental observation of the flat bar surface indicated a ring of damaged region on the edge of the circular contact area. The annular region was then extended towards the center of the contact area by increasing the obliquity angle. The measured energy dissipations were consistent with the theoretical analysis of the Mindlin and Deresiewicz (1953) study particularly for small obliquity angles.

Ödfalk and Vingsbo (1992) studied the fretting-wear due to the micro-slip behavior within the contact region. They proposed an elastic-plastic fretting model based upon the Cattaneo-Mindlin theory (Cattaneo, 1938; Mindlin, 1949). The plastic part of the model was developed based on the material properties such as the fretting yield and fretting hardening coefficients. The study indicated that plastic deformation may have a significant effect on the micro-slip behavior and subsequently the amount of the fretting-wear. Vingsbo and Schön (1993) experimentally studied the criteria for incipient gross slip. The study evaluated the fretting scar morphology, displacement amplitude and fretting energy dissipation. Ödfalk and Vingsbo (1990) experimentally studied the fretting wear between spherical bodies. The study indicated that the differences between the pre-sliding displacements based upon the Mindlin and Deresiewicz partial-slipping theory (Mindlin and Deresiewicz, 1953) and measured experimental tests increased with an increase in the forcing frequency. This was explained by the elastic

assumptions in the partial slipping theory whereas the nature of the interaction involves plastic deformation.

1.2 Research Questions

Work rate is a parameter which quantifies fretting-wear during tube-support interaction. This parameter is dependent upon two factors, sliding distance and normal impact force. Many theoretical models, including friction and impact models, have been developed and incorporated in tube-support dynamic computation codes for better work-rate estimation. Yetisir and Fisher (1997) performed a series of work-rate comparisons between experimental measurements and numerical simulations, using the VIBIC code. The results presented up to 50 percent error in the predicted work-rate comparisons. Hassan and Rogers (2005) also simulated the Yetisir and Fisher experimental measurements, using the INDAP code. These authors adopted different friction models, including the VLFM, FBFM and SDFM, in the simulations. The results indicated a significant difference of 50 percent, for 0 mm gap size, similarly to the VIBIC code simulation. However, the difference was reduced, adopting a larger tube-support preload. These work-rate differences, reported by different researchers, underline on a need for more precise study of friction and impact models.

The velocity-limited (Rogers and Pick, 1977), force-balanced (Karnopp, 1985) and spring-damper friction models (Antunes et al., 1990) are the friction models which are commonly used for tube-support interaction modeling. Their simplicity is the key advantage of using these friction models. However, there are some weaknesses associated with them. The presliding displacement, varying break-away force and Stribeck effects are not considered, in the above mentioned friction models. On the other hand, these effects may influence a criterion to detect stick-slip regions. An accurate estimation of this criterion plays an important role to estimate sliding distance, particularly in a system with an intermittent stick-slip behavior. To define a physics based criterion to detect stick-slip region, the study of friction process from zero velocity to the gross-slip state is important.

Hofmann et al. (1992) categorized the types of tube-support interaction into tangential sliding, oblique impacting and perpendicular impacting. The study suggested different wear

coefficients as resulting from different type of interaction. The differences in wear coefficients may be partially explained as a result of different types of displacements during the friction process, including elastic, plastic and partial slipping displacements. Some friction models, including the LuGre (Canudas de Wit et al., 1995) and Lim and Chen friction models (Lim and Chen, 1998) were developed to model pre-sliding displacement, using internal state variables. However, there are some difficulties to attribute their parameters to physical meaning.

This study aims to carefully study tangential stress distribution within a contact area and develop a new hybrid elasto-plastic friction model to precisely consider different stages of friction process, including elastic, plastic, partial slipping and gross-slip regions.

Normal impact force plays an important role in friction force calculation and work-rate estimation. Having a precise friction model may not be beneficial without considering an accurate normal impact model. Fisher et al. (1989) made normal impact force comparisons for tube-support interaction between experimental measurements and numerical simulations, using the VIBIC code. The predicted normal impact force significantly overestimated the experimental measurements by about a factor of 2. This difference is directly associated with the normal impact model incorporated in the numerical code. The normal impact model in most of tube-support interaction dynamics computation codes, including VIBIC, H3DMAP, INDAP and VITRAN, simply consists of a parallel spring and damper. The spring stiffness is calculated, using the Morley technique (Morley, 1960), and the damping coefficient is determined, using the Hunt and Crossley model (Hunt and Crossley, 1975). It is important to investigate this impact model in greater detail to identify the source of the above mentioned differences. Therefore, this research aims to perform tube-support experimental tests, with various combinations of gap sizes and excitation forces. This will make it possible to accurately measure parameters which represent the dynamics of interaction, including normal impact force and tube mid-span displacement. In addition, this investigation includes the study of the nonlinear force-displacement relationship and mechanisms of energy dissipation, to improve tube-support impact model.

1.3 Objectives

The general goal of the proposed thesis research is to precisely study the factors that play major roles in the tube-support fretting-wear estimation. The study focuses on the friction and impact models which may affect the stick-slip regime and normal interaction forces. For the friction model, the need for a physics based model which represents the real bristle behavior during the friction process has been clearly inferred from the state of the art review. This requires a comprehensive study of the stress distribution within the contact region. The ultimate goal of developing the friction model is to demarcate the elastic, plastic and partial slipping displacement during the friction process. For tube-support interaction, having a precise friction model may not be beneficial without developing an accurate impact model. Therefore, a comprehensive experimental study is needed to study the nonlinearity in the force-displacement relation during the tube-support interaction. A study of the source of energy dissipation during the normal impact may additionally be valuable.

The detailed objectives of this study are the following:

1. Design and development a hybrid spring-damper rate dependent friction model based upon the elastic, plastic and partial-slipping phenomena which may occur during a friction process from the absolute zero velocity to the gross slip state. Furthermore, validating the friction model against an experimental instability phase diagram.
2. Detailed study the effect of the varying break-away force and Stribeck effect on the stick-slip regime.
3. Performance of a series of experimental tests to measure the tube-support normal impact force and mid-span displacement for different gap sizes and excitation forces as a reference for the impact model validation.
4. Development of a numerical code based upon the Euler-Bernoulli beam theory to simulate the tube-support dynamics. The code will incorporate the friction and impact models.

5. Study of the nonlinear relation between the elastic impact force and normal displacement by validation of the code against the experimental tests and estimation of the empirical parameters associated with the nonlinearity.
6. Conduct experimental tests to study the source of energy dissipation during the tube-support interaction particularly the effect of the Hunt and Crossley model and nonlinearity in the structural damping.

1.4 Thesis Organization

This thesis is divided into four chapters. The first chapter presents the purpose and inspiration behind the study, a full state of the art review of previous studies and the thesis objectives. The state of the art review includes works on tube-support wear mechanisms, nonlinear dynamic computation, friction and impact models. The second and third chapters are in the form of papers and are constructed to include an abstract, introduction, methodology, results and a conclusion. In the second chapter, the details of the development of a hybrid spring-damper friction model are presented. The third chapter provides details of the experimental tests for the impact model evaluation. The normal elastic and inelastic impact models are also discussed. Finally, the discussion and conclusions are addressed in the fourth chapter including a review of objectives, further discussion, contributions and recommendations for future work.

CHAPTER 2
NUMERICAL ANALYSIS OF FRETTING-WEAR WITH A HYBRID ELASTO-PLASTIC FRICTION MODEL

This chapter is presented in the form of a paper submitted to *Journal of Pressure Vessel Technology* on 28 May 2012. Authors: Reza Azizian and Njuki Mureithi.

ABSTRACT

Fretting wear is a common problem in different industries especially when it comes to interactions between metallic components. Flow induced excitation forces in heat exchangers for instance cause tube-support interactions. The long-term interaction is an important phenomenon which may cause fretting-wear of the tubes. Experimental tests of the interaction show the occurrence of stick-slip intermittent behaviour in the tube response. To precisely simulate the intermittent stick-slip behaviour, it is crucial to refine the conceptual model of the coefficient of friction for the entire motion form absolute zero velocity to gross slip phase. The incorporated friction model plays an important role in the determination of the level of fretting-wear in the system. The friction model should satisfy two important criteria: the first important aspect is the strategy of the friction model to detect the cessation of sticking, the beginning of partial slipping and the establishment of the sliding region. The second important aspect is defining a friction coefficient function for the entire system response to precisely represent the transient stick-slip regions. In the present work, the velocity limited friction model was compared with the LuGre model which is a rate dependent friction model. The effect of varying the break-away force and Stribeck effect on the stick-slip region were also investigated. Furthermore, the criteria to demarcate the stick-slip region in the LuGre model are discussed and a different method to incorporate the Stribeck effect and presliding damping in the Dahl friction model is proposed. Using the tangential stress distribution in the contact area, a new hybrid spring-damper friction model is developed. The model is able to estimate the elastic, plastic and partial slipping distances during relative motion. The ability of the model to reproduce experimental tests is investigated in the present work.

2.1 Introduction

During interaction between metallic components, friction and wear play important roles. These phenomena cause material to be removed at the points of the interaction which may lead to the component failure. Different wear processes may be involved during the interaction such as abrasion, delamination, fatigue, corrosion and fretting wear (Ko, 1986; Gessesse, 2000). Tube-support interaction in heat exchanger tube bundles may cause the same problem. Different experimental tests have been carried out to determine the exact mechanism of the wear process and material removal (Suh, 1973; Gauland and Duquette, 1980). The results indicate that cracks propagate in the sub-layer parallel to the contact surface and gradually turn toward the contact surface due to the stress concentration (Suh, 1973; Fouvry et al., 1997). The process may cause wear debris which explains the main mechanism of material removal during the wear process (Suh, 1973; Fleming and Suh, 1977).

In heat exchangers, the fretting-wear process is associated with the long term tube-support interaction (Pettigrew and Taylor, 2003b). In numerical simulations of the phenomenon the type of incorporated friction model plays an important role. Nonlinearities of the friction models in the vicinity of zero velocity pose serious difficulties when developing and incorporating these models in numerical simulations. Experimental studies of tube-support interaction show significant chattering between the stick-slip regions (Haslinger and Steininger, 1995; Pettigrew and Taylor, 2003b). For the tube-support interaction simulation, especially in the presence of wear, it is vital to incorporate a proper friction model. The friction model should have certain capabilities to precisely reproduce the interaction behaviour. During the interaction, three phases of relative motion may be considered: sticking, partial-slip and gross-slip. It is important for the friction model to be able to demarcate the boundaries between the different phases of the relative motion and to quantify the magnitude of the relative motion in each phase. Switching between different phases of the relative motion has been observed in different experimental tests (Rabinowicz, 1951; Baumberger et al., 1994; Heslot et al., 1994). In the mathematical models, different functions have been incorporated to reproduce the intermittent stick-slip behavior especially in the vicinity of zero velocity where there is nonlinear transient behavior from the stick to slip phases (Baumberger et al., 1994; Canudas de Wit et al., 1995; Lim and Chen, 1998; Ozaki and Hashiguchi, 2010).

For numerical simulation of the tube-support interaction, different numerical codes have been developed to reproduce the interaction behavior. Examples, include VIBIC (Rogers and Pick, 1977), H3DMAP (Sauve and Teper, 1987) and FIVDYNA (Toorani et al., 2009). As noted above, a proper friction model is vital to determine the amount of wear in the simulations. The Velocity Limited Friction Model (VLFM), Force-Balanced Friction Model (FBFM) and Spring-Damper Friction Model (SDFM) are the three major friction models which have been commonly used in the simulations.

In the present work, the advantages and weaknesses of the velocity-limited friction model compare to a rate dependent friction model were investigated for a simple mass-spring system. The process of transition from absolute zero velocity to entirely gross slipping was conceptually refined by considering the tangential stress distribution within the contact region. The results indicate the three main regions of elastic, yielding (plastic) and partial slipping before incipient gross-slip. Each region of the motion is represented by a theoretical model. The elastic displacement is represented by the Cattaneo-Mindlin theory (Cattaneo, 1938; Mindlin, 1949). The plastic displacement and yielding are characterized with the Odfalk and Vingsbo method (Ödfalk and Vingsbo, 1992). The partial-slipping displacement is associated with a damping coefficient inspired by the Mindlin and Deresiewicz method (Mindlin and Deresiewicz, 1953). Moreover, the Stribeck effect is modeled with a transient function based on the LuGre model (Canudas de Wit et al., 1995).

Finally, to consider the different effects, a hybrid elasto-plastic spring damper friction model is designed. A simple mass-spring system is then chosen according to experimental tests by Baumberger et al. (1994) to test the new friction model.

2.2 Friction Models

The main purpose of developing different friction models is to have capabilities to reproduce the exact behaviour of the relative motion before the cession of sticking. Moreover, due to nonlinear friction behaviour in the vicinity of zero velocity, it is important for the friction model to have a realistic transient behaviour for this period in contrast with the simple Coulomb friction model.

The Coulomb friction model is the fundamental basis of all friction models. The model gives the friction force in the gross slip state. The model, however, cannot predict incipient gross slip or estimate the friction force in the sticking region. All the different types of friction models use the Coulomb friction model to determine the friction forces during sliding. However, different methods are used for demarcating between the stick-slip regions. The latter play an important role in our research since more slipping regions may increase the work-rate and consequently increase the estimated fretting during the tube-support interaction. Different friction models have been developed to evaluate the stick-slip regions and estimate the sticking friction forces as follows (Hassan and Rogers, 2005):

2.2.1 Velocity-limited friction model (VLFM) (Tan and Rogers, 1996)

In the velocity-limited friction model, the friction force during gross-slip phase may be determined based on Equation (2-1) similarly to the Coulomb friction model. Moreover, a limiting velocity, V_0, is defined to demarcate stick-slip regions. The friction force, F_f, is given by,

$$\left|F_f\right| = \mu F_n \qquad if \quad \left|V_t\right| > V_0 \quad , \tag{2-1}$$

$$\left|F_f\right| = \frac{\left|V_t\right|}{V_0}\mu F_n \qquad if \quad \left|V_t\right| \le V_0 \ , \tag{2-2}$$

where V_0 , μ and F_n are the limiting velocity, friction coefficient and normal contact force, respectively. The choice of the limiting velocity is crucial in the VLFM to demarcate the stick-slip regions. The magnitude of the limiting velocity was quantified as a ratio of the average sliding velocity. The ratio was reported in the literature in the range of 0.001-0.1 depending on the condition of the interaction (Tariku and Rogers, 2001).

2.2.2 Force balanced friction model (FBFM) (Karnopp, 1985)

In the force-balanced friction model, the friction force during slipping is determined similarly to the Coulomb's friction model but the sticking friction force is determined as follows (Hassan and Rogers, 2005):

$$F_f = Ku - F_e \ , \tag{2-3}$$

where Ku and F_e are system internal resistance and applied external force, respectively. To have a sticking phase in the FBFM, similarly to the VLFM, a limiting velocity is defined. However, the friction force in the range of the limiting velocity must be less than the break-away force to maintain the sticking phase.

2.2.3 Spring damper friction model (SDFM) (Hassan and Rogers, 2005)

In the spring-damper friction model, the friction force during sticking is composed of two terms: damping force and spring force terms. The model is formulated as,

$$F_f = \mu F_n \qquad \text{sliding}, \tag{2-4}$$

$$F_f = K_a(u_c - u_0) + C_a V_t \qquad \text{sticking}, \tag{2-5}$$

where the parameters u_c and u_0 are, respectively, the current and the zero velocity tangential displacement. K_a and C_a are the stiffness and damping coefficients. The coefficients were determined based on numerical consistency and stability rather than physical coherency (Antunes et al., 1990).

2.3 Rate Dependent Friction Models

A more precise friction model should be able to reproduce the process from an absolute zero velocity to the condition of incipient gross slip. The contact interaction process contains the different regimes of elastic, plastic and partial slipping before the complete cession of sticking (Johnson et al., 1971; Johnson, 1985; Ödfalk and Vingsbo, 1992). Much effort has been dedicated to precisely simulate the different parts of the process especially the creep dominated regime. Three rate dependent friction models are discussed below.

2.3.1 Ozaki and Hashiguchi friction model (Ozaki and Hashiguchi, 2010)

Ozaki and Hashiguchi (2010) developed a rate-dependent friction model based on a conceptual definition of a friction coefficient for the entire motion. The model has the following mathematical form:

$$\dot{\mu} = -k\left(\frac{\mu}{\mu_k} - 1\right)v_p + \xi\left(1 - \frac{\mu}{\mu_s}\right), \tag{2-6}$$

where k and ξ are the rate of decrease and recovery of the friction coefficient, respectively. The coefficients are material constants and the typical values which were used in the Ozaki and Hashiguchi (2010) simulation are 10mm^{-1} and 0.01s^{-1} for k and ξ, respectively. The quantities v_p, μ_s, μ_k are the plastic sliding velocity, static coefficient of friction and kinetic coefficient of friction, respectively.

In the model, the instantaneous friction coefficient depends not only on the plastic velocity, static and dynamic friction coefficients but also on the coefficient friction's rate of change. The model can simulate plastic-sliding and the Stribeck effect during motion. Creep deformation which plays an important role in estimating the pre-sliding displacement was also included in the model. However, experimental comparisons indicated the inabilities of the model to quantitatively reproduce the experimental test.

2.3.2 Lim and Chen friction model (Lim and Chen, 1998)

As an extension of the Rice and Ruina (1983) friction model, Lim and Chen (1998) developed a model considering a conceptual choice of the friction coefficient, μ, by taking into account the velocity weakening and creep before the cession of sticking as follows:

$$\mu(\phi,\dot{x}) = A\,\mathrm{sgn}(\dot{x})\sinh^{-1}\left\{\frac{1}{2}\exp\left[\frac{\bar{\mu}}{A}\right]\right\} + \eta\dot{x}, \tag{2-7}$$

where,

$$\bar{\mu} = a_v + b_v \ln\frac{\phi V_0}{D_0} + A\ln\frac{\phi|\dot{x}|}{D_0}, \tag{2-8}$$

and

$$\dot{\phi}(t) = 1 - \frac{|\dot{x}|\phi}{D_0}. \tag{2-9}$$

ϕ is a state variable which describes the slipping history. D_0 is an empirical parameter associated with an average pre-sliding displacement. The quantity a_v and b_v are experimental parameters which were chosen equal to 0.369 and 0.014, respectively. The model was characterized to simulate and demarcate the creep and inertia dominated slipping regions.

2.3.3 LuGre friction model (Astrom and Canudas de Wit, 2008)

The LuGre friction model is an elastic rate-dependent friction model. The model is competitive due to incorporating different friction features such as varying break-away force, friction hysteretic behavior and presliding displacement (Canudas de Wit et al., 1995). The different effects make the LuGre model capable of precisely estimating the frictional system response especially when it comes to measure the exact stick-slip regions during frictional contact. In the model, the friction force is expressed mathematically as follows:

$$F_f = \sigma_0 z + \sigma_1 \frac{dz}{dt} + \sigma_2 \dot{x} \,, \tag{2-10}$$

where,

$$\frac{dz}{dt} = \dot{x} - \sigma_0 \frac{|\dot{x}|}{g(\dot{x})} z \tag{2-11}$$

and

$$g(\dot{x}) = F_c + (F_s - F_c)\exp(-(\dot{x}/v_s)), \tag{2-12}$$

The parameters σ_0, σ_1 and σ_2 are the stiffness, presliding damping and viscous damping coefficient, respectively. F_s , F_c and v_s are the static friction force, Coulomb friction force and Stribeck velocity, respectively. The friction force as formulated in equation (10) is composed of three terms. The first term is the force associated with the elastic bristle deflection, z. The second term considers the effect of the rate of the average bristle deflection, $\frac{dz}{dt}$, which is determined by equation (2-11). The third term is the viscous friction force. Moreover, in the LuGre model the Stribeck effect is considered based on the Armstrong-Helouvry (1991) Gaussian distribution. The Stribeck effect as formulated in equation (2-12) is incorporated in equation (2-11) which formulates the rate of average bristle deflection. Typical values of the LuGre friction model parameters which were determined based on the Armstrong experimental test (Armstrong, 1990) are (Canudas de Wit et al., 1995),

Table 2.1 The LuGre model parameters (Canudas de Wit et al., 1995)

σ_0 (N/m)	σ_1 (Ns/m)	σ_2 (Ns/m)	F_s (N)	F_c (N)	v_s (m/s)
10^5	$10^{2.5}$	0.4	1.5	1	0.001

In the LuGre model, the Stribeck effect is considered by introducing an exponential function as shown in equation (2-12). The Stribeck velocity, v_s, determines the rate of change from the sticking phase to the gross slipping phase.

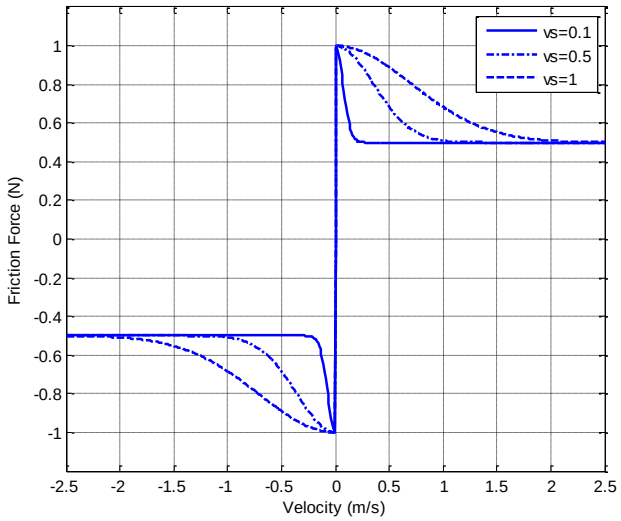

Figure 2-1 The Stribeck velocity effect on switching from stick state to slip states.

Figure 2-1 shows the transient function modeling the switching between the sticking state and slip state in the LuGre model. The effect of varying the Stribeck velocity, v_s, is also shown. The Stribeck velocity is the parameter which defines how fast switching takes place in the friction model. For the Stribeck velocity, magnitudes smaller than 0.001(m/s) are reported in the literature (Rabinowicz, 1951; Armstrong, 1990; Armstrong and Canudas, 1994; Canudas de Wit et al., 1995).

2.4 Comparison of the LuGre and VLFM Models

In this section, the velocity limited friction model is compared with a rate dependent friction model. The purpose of the comparison is to clarify the weaknesses and advantages of the

models to precisely simulate the stick-slip regions. To make a comparison between the VLFM and LuGre models, the mass-spring system in Figure 2-2 was chosen. The system allows us to precisely study the effect of the friction model parameters on the predicted friction force and slick-slip regions. In this study, different types of pulling velocities are chosen to examine friction model behavior under various conditions. The first applied excitation consisted of a constant pulling velocity, v_p, applied to the spring free end. The constant excitation velocity in the presence of the spring may excite the mass with a periodic excitation. At the same time, due to the motion in one direction, the expected differences between the mass displacements in the two friction models may accumulate during the process and can thus be clearly observed.

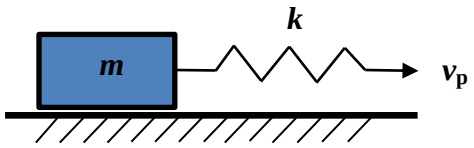

Figure 2-2 Mass-spring system.

For the mass-spring system the equation of the motion is,

$$m\ddot{x} + kx = kv_p t - F_f . \tag{2-13}$$

In Equation (2-13), the mass, m, and stiffness, k, are chosen respectively equal to 1 kg and 20 N/m. v_p and F_f are the pulling velocity and friction force, respectively. In Figure 2-3, the friction force histories obtained using the velocity-limited friction model and LuGre model are shown. For the pulling velocities of 0.1, 0.2 and 0.3 m/s, the break-away forces of 1.39, 1.34 and 1.26 N were, respectively, obtained for the LuGre model.

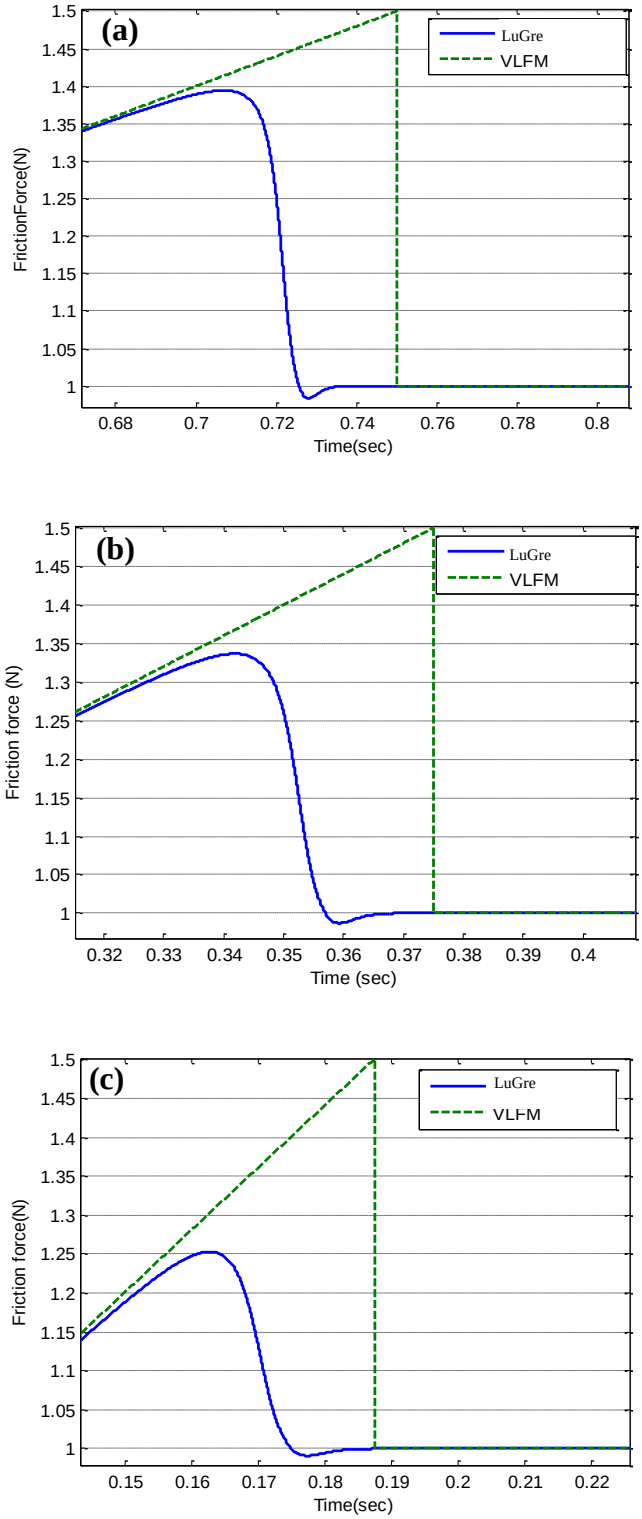

Figure 2-3 Break-away forces comparison for the Velocity Limited Friction Model and the LuGre model with different pulling velocity (a) vp = 0.1 (m/s), (b) vp = 0.2(m/s), (c) vp = 0.4 (m/s).

The results show that the break-away force in the LuGre model decreases with increasing excitation force in contrast with the velocity-limited friction model which gives a constant break-away force of 1.5 N. The LuGre break-away friction behavior is consistent with the Johannes et al. (1973) and Rabinowicz (1951) experimental tests which demonstrate the dependency of the magnitude of the break-away force on the rate of increase of the friction force during the transient stick-slip state (Wojewoda et al., 2008). The LuGre and VLFM comparison shows not only the importance of the varying break-away force but also the change in the stick-slip regions due to the differences. In other words, the LuGre model switches to the gross-slip regime sooner than the velocity-limited friction model due to the varying break-away force in the study.

The differences between the percent duration of slip for different simulation times for both models are presented in Figure 2-4. The results show an increase in the slipping time percentage with increase in simulation time for both models which eventually attains a steady state after passing a certain time. The results indicate approximately a 4% difference in the slipping duration between the LuGre and VLFM models.

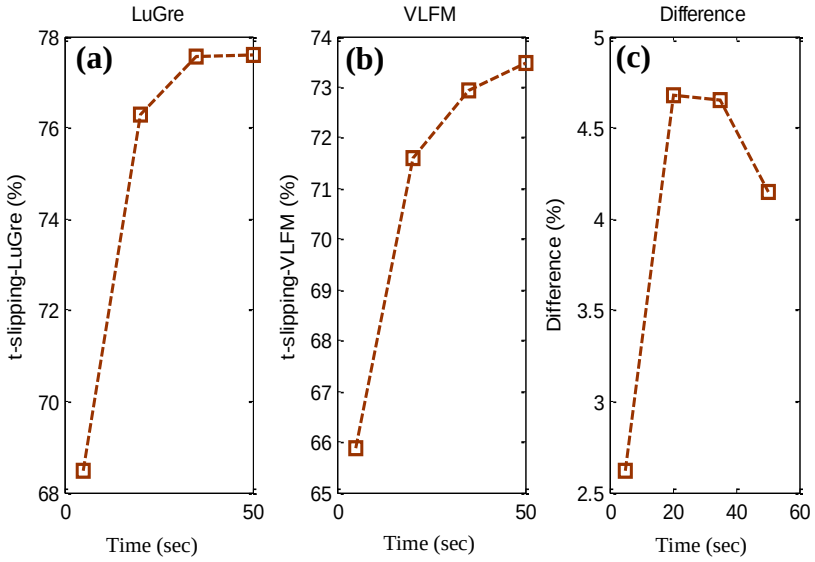

Figure 2-4 Slipping time for the LuGre Model and Velocity-Limited Friction model (a) The LuGre slipping time (b) The VLFM slipping time (c) Difference between the LuGre and VLFM.

To more carefully investigate the ability of the friction models to capture the stick-slip regions, the chirp excitation function was chosen. The chirp is a cosine function with a linearly

increasing instantaneous frequency with time. As shown in Figure 2-5, four different chirp excitation functions are applied to the pulling velocity. The chirp functions with 0.2 m/s amplitude have target frequencies increasing from 5 Hz to 30 Hz for cases 1 to 4, respectively, in a 10 second simulation duration. The results indicate a decrease in the slipping time for the LuGre model in contrast with the VLFM. The constant velocity limited magnitude may restrict the VLFM from capturing the entire sticking region. The inability of the VLFM to detect the sticking region may be explained based on the essence of having an adaptive velocity limited magnitude for the VLFM.

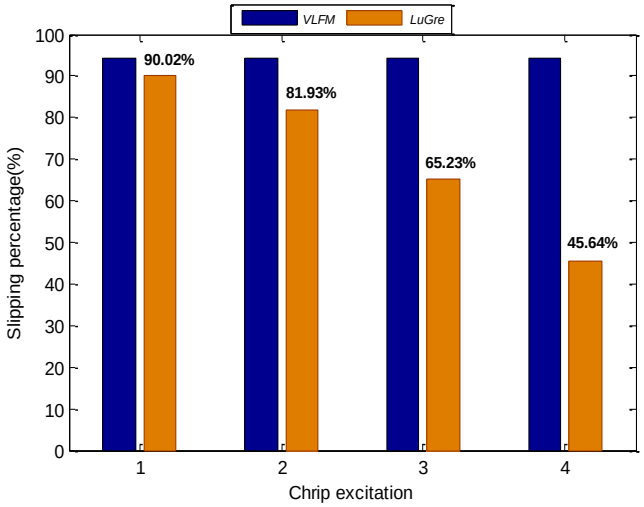

Figure 2-5 Slipping time comparison the VLFM and LuGre (1) chirp [1,5] (2) chirp [1,10] (3) chirp [1,20] (4) chirp [1,30].

The slipping time durations for the LuGre and the VLFM models shows that it is vital to choose a proper criterion to demarcate the stick-slip regions. In the LuGre model, the rate of average bristle deflection is chosen as the criterion for detection of incipient gross-slip displacement. From the mathematical formulation of the LuGre model, the parameter, *dz/dt*, needs to be chosen small enough to capture all sticking regions. In Figure 2-6, the effect of decreasing the rate of the average bristle deflection is investigated. Decreasing the parameter from 1e-9 m/s to 1e-12 m/s shows only a slight difference in the slipping time until the critical point of 1e-12 m/s. The results indicate that by choosing an average bristle deflection smaller than 1e-11 m/s, the LuGre model assumes a big portion of the movement to fall in the sticking region. Therefore, a steep decrease from 62.37% to 3% of the slipping time is observed. The

change is due to the sensitivity of the model to choice of the time step. However, the choice of *dz/dt* equal to 1e-10 m/s is in a reasonable range for the time-step equal to 1e-6s.

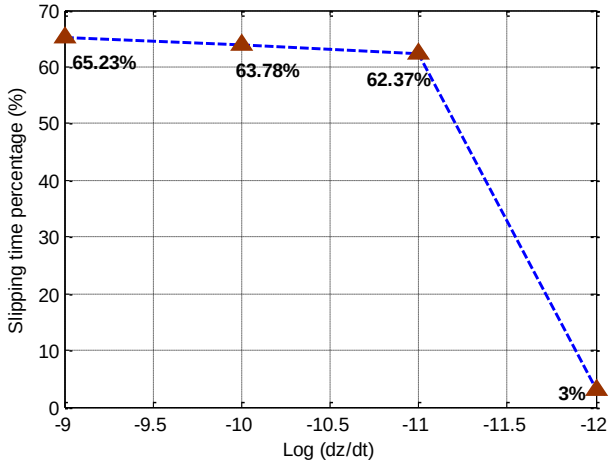

Figure 2-6 Slipping time percentage versus logarithmic average bristle deflection.

2.5 Equivalent Spring-Damper Friction Model

Some advantages of the rate-dependent friction model compared to the VLFM were discussed in the previous section. However, to use the LuGre model, it is important to understand the relation between the empirical parameters and the mathematical formulation. The LuGre model is a friction model which was developed based on the Dahl friction model (Dahl, 1968) by considering the hysteretic behavior and presliding displacement (Armstrong, 1990; Canudas de Wit et al., 1995). To achieve these goals, the Dahl friction model (Dahl, 1968) was upgraded to the LuGre model by incorporating the Stribeck function (Armstrong-Helouvry, 1991) ,Equation (2-12), into Equation (2-11). Moreover, two additional damping terms were introduced (Equation (2-10)) which represent the damping associated with the rate of the average bristle deflection and viscous damping. However, the approach to correlate the empirical parameters to the mathematical formulation may not represent the physical response of the system. Therefore, in this section the LuGre model is reorganized in the form of an equivalent physical nonlinear spring-damper model with the same constant parameters.

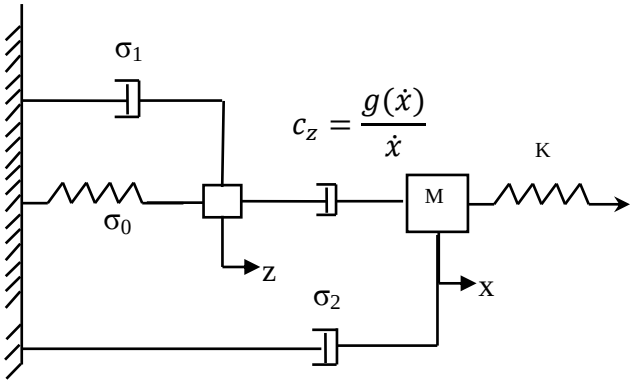

Figure 2-7 Spring-damper model equivalent to the Lugre Model.

As shown in Figure 2-7, it is proposed to represent the Stribeck function and damping terms in the LuGre model by a physical hybrid spring-damper model. The spring with the constant σ_0 and dampers with the constant σ_1 and σ_2 are configured in parallel to reproduce Equation (2-10). Moreover, the Stribeck effect in Equation (2-12) is transformed to an equivalent Stribeck damping, C_z. The damping element is configured in series with the rest of the system to be able to shift the system from the sticking state to the slip state depending on the velocity of the mass. As shown in Figure 2-8, the simulation results show 5-9% difference for the slipping time between the LuGre model and the physical equivalent spring-damper friction model. The advantage of the latter model is that it gives an intuitive physical meaning to the mathematical functions in the LuGre model.

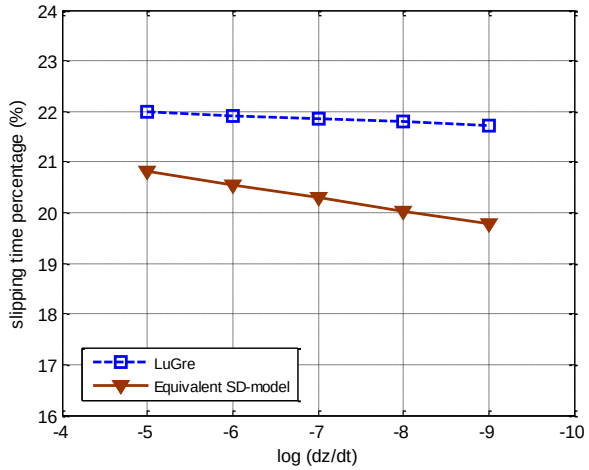

Figure 2-8 Slipping time comparison between the LuGre and Revised SDFM for different logarithmic rate of average bristle deflection.

2.6 Stress Distribution within the Contact Area

The equivalent spring damper friction model which was proposed in previous section contains physical parameters. The role of the parameters is to articulate the exact behaviour in the different phases of the motion from absolute zero velocity to the gross-slip phase. To upgrade the equivalent spring-damper friction model with a more physical model capable of demarcating different regions in the contact area, it is necessary to consider the tangential stress distribution in the interface between two objects. For contact between spherical objects, Cattaeno (1938) and Mindlin (1949) developed a mathematical formula to describe the tangential stress distribution within the contact area as follows:

$$q(r)=\begin{cases}\mu p_0\left\{\left(1-\dfrac{r^2}{a^2}\right)^{1/2}-\left(1-\dfrac{r^2}{c^2}\right)^{1/2}\right\} & 0\le r<c\\ \mu p_0\left(1-\dfrac{r^2}{a^2}\right)^{1/2} & c\le r\le a\end{cases}, \tag{2-14}$$

where μ is the coefficient of friction, P_0 the normal stress and a the contact radius.

Based on equation (2-14), the contact area is divided into two regions: a sticking region with elastic displacement and a partial slip region. Figure 2-9 shows the differences in the stress distribution in the two regions which are demarcated by the parameter ‘c’

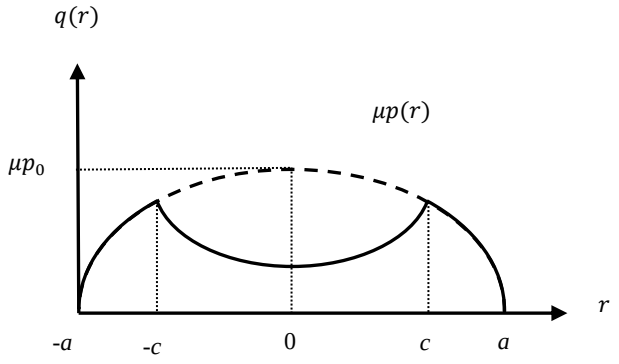

Figure 2-9 Cattaneo-Mindlin tangential stress distribution (Johnson, 1955).

In the region $0 \leq | r | \leq c$, the coincident contact points on the interface move together which represents the sticking region as shown in Figure 2-10 by the point 'A' (Mindlin, 1949; Johnson, 1985). However, for the region $c \leq | r | \leq a$, the contact points on the two bodies have a relative tangential movement which represents the slipping region as shown in Figure 2-10 by the points 'B' and 'C' (Mindlin, 1949; Johnson, 1985).

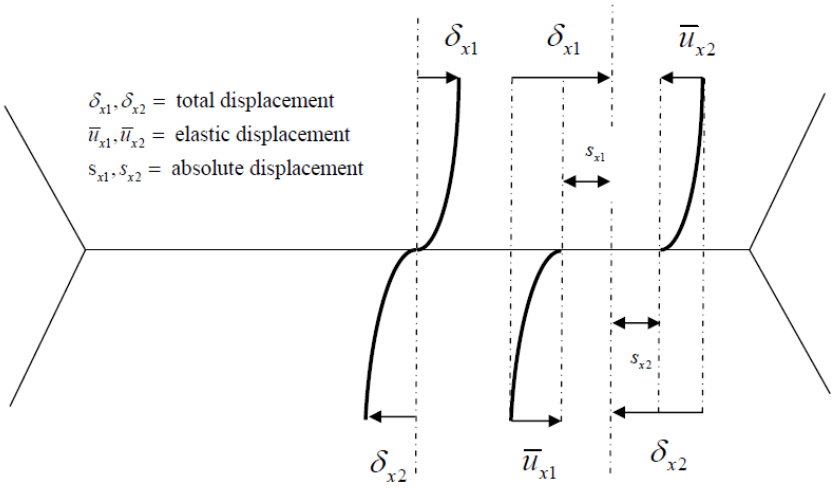

Figure 2-10 Stick and slip point in contact region (Johnson, 1985).

Consequently, the relative tangential displacement in the contact region is determined as follows (Johnson, 1985):

$$\delta_x = \frac{3(2-\nu)\mu F_N}{8Ga}\left\{1-(1-\frac{F_T}{\mu F_N})^{2/3}\right\}, \tag{2-15}$$

where F_N is the normal contact force, ν the Poisson's ratio μ the coefficient of friction and G the shear modulus.

In later development of the Cattaneo-Mindlin theory (Cattaneo, 1938; Mindlin, 1949), Mindlin and Deresiewicz (1953) studied the effect of varying tangential force on the stress distribution within the contact area. Consequently, the study determined the energy dissipation per cycle during the oscillatory tangential displacement as in equation (2-16) by integrating the force-displacement history for a cycle.

$$\Delta E = \frac{9(2-\nu)\mu^2 F_N^2}{10Ga}\left\{1-\left(1-\frac{T^*}{\mu F_N}\right)^{5/3}-\frac{5T^*}{6\mu F_N}\left[1+\left(1-\frac{T^*}{\mu F_N}\right)^{2/3}\right]\right\}, \tag{2-16}$$

where T^* is the amplitude of the tangential oscillatory force and a the contact radius.

In other work, Ödfalk and Vingsbo (1990) measured the presliding displacement, δ, dependence on the excitation frequency. The results indicated underestimation of presliding displacement by the Cattaneo-Mindlin elastic theory. To correct for this, Ödfalk and Vingsbo (1992) developed a plastic model to consider yielding in the contact region based upon equations (2-17)-(2-20).

$$\delta_p = \beta\left[\gamma\frac{(F_T-\alpha F_{Ty})}{k_p}-\alpha\frac{(T^*-F_{Ty})}{2k_p}\right] \tag{2-17}$$

where F_T, k_p, F_{Ty} are the tangential force, work hardening coefficient and fretting yield point, respectively. δ_p is the presliding displacement associated to yielding. In equation (2-17), the three constant parameters α, β and γ may be determined as follows (Ödfalk and Vingsbo, 1992):

$$\alpha = \begin{cases} 1 & \frac{d\delta}{dt} > 0 \\ -1 & \frac{d\delta}{dt} < 0 \end{cases} \tag{2-18}$$

$$\beta = \begin{cases} 1 & T > F_{Ty} \\ 0 & T <= F_{Ty} \end{cases} \tag{2-19}$$

$$\gamma = \begin{cases} 1 & |F_T| > F_{Ty} \text{ and } \frac{dF_T}{dt}F_T > 0 \\ 0 & \text{else} \end{cases} \tag{2-20}$$

where δ is the total presliding displacement.

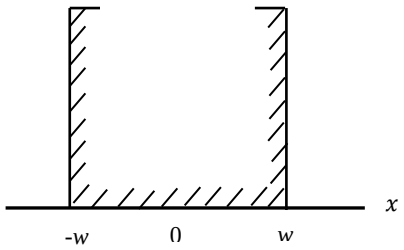

Figure 2-11 Two flat surfaces in contact.

Using the Cattaneo-Mindlin theory for flat surfaces without losing its cogency needs to be explained and justified. As shown in Figure 2-11, considering two flat surfaces in contact, with the condition of neither gross-slip nor partial-slip, the system is similar to a flat punch with the same displacement in the loading direction all over the contact region. The tangential stress distribution is (Johnson, 1985),

$$Q(x) = \frac{Q_x}{\pi (w^2 - x^2)^{1/2}} \ , \tag{2-21}$$

where x is the position of the coincident points within the contact width and w is the contact width. As shown in Figure 2-12, the tangential stress increases to infinity on the border line $|x|=w$ which brings into question the condition of no-slip. In other words, the coefficient of friction needs to be infinite to sustain the condition of no-slip on the border of the contact area. This leads us to infer the presence of the partial-slipping region for two-flat surfaces similarly to the circular contact case (Johnson, 1985).

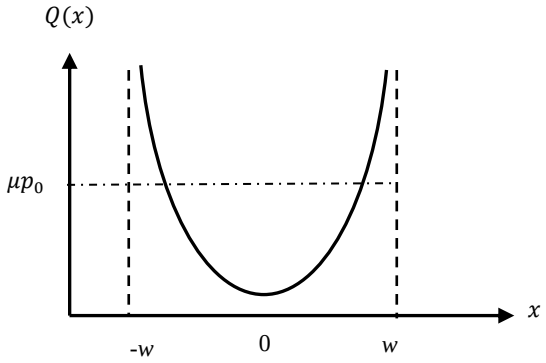

Figure 2-12 Tangential stress distribution for a flat punch (Johnson, 1985).

Ödfalk and Vingsbo (1990) have attempted to justify the use of the Cattaneo-Mindlin theory for flat surfaces in contact by considering the micro structure of the bristles in the contact interface. Since the Cattaneo-Mindlin theory is valid for a circular contact, certain assumptions needed to be considered to be able to use the theory for flat surfaces including (Ödfalk and Vingsbo, 1990): (1) two smooth flat surfaces in contact with each other and one of them includes certain waviness, (2) the surfaces are in contact at least in three contact points, (3) considering a spherical shape for the contact tip between flat surfaces. Based upon these assumptions, conceptual incorporation of the Cattaneo-Mindlin theory in a friction model for flat surfaces is admissible. The experimental test conducted by Ödfalk and Vingsbo (1990) confirmed that the presliding displacement is proportional to the *2/3* power of the normal force which supports the validity of the Cattaneo-Mindlin theory for flat surfaces.

2.7 New Hybrid Spring-Damper Friction Model

In the preceding sections, different weaknesses and advantages of the LuGre model were investigated. In the development of the new model, two important aspects of the friction model are considered. The first aspect is the criterion to demarcate the stick-slip regions. The second aspect is incorporation of different friction phenomena such as the Stribeck effect and presliding displacement based on a physical hybrid spring-damper model. The issues are vital due to the sensitivity of fretting-wear to slipping distance. For the LuGre model, the demarcating parameter was chosen as the rate of the average bristle deflection. However, as shown in Figure 2-6, the slipping time may depend on the magnitude of the limiting parameter. Researchers have investigated the micro-behaviour in the contact area during the stick-slip states. As mentioned earlier, Cattaneo-Mindlin developed a model for the tangential stress distribution in the contact area. The model suggests two regions within the contact area. A sticking region in the center of the contact area and a partial slipping region in the peripheral region outside of the contact area which progressively develops towards the contact center with increase in the friction force (Johnson, 1985). Johnson (1961) experimentally proved the theory. The Cattaneo-Mindlin theory was further developed to consider the effect of plastic deformation and yielding in the border between the sticking and slip regions (Ödfalk and Vingsbo, 1992). Based upon the stress distribution in the contact region, different phases of displacement may be identified in the

contact area (Johnson, 1985; Ödfalk and Vingsbo, 1992). The three main regions of elastic displacement, plastic displacement and slipping are shown in Figure 2-13. In addition, to have a precise friction model, two transient regions of elastic-to-plastic and plastic-to-slipping transition are considered.

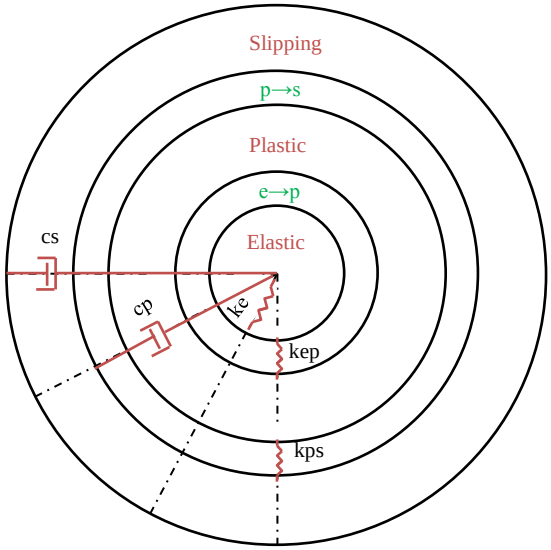

Figure 2-13 Displacement field in the contact area and hybrid spring-damper model.

2.7.1 Model formulation

A hybrid spring-damper friction model is formulated based upon consideration of the different regions in the contact area. From Figure 2-13, the friction force and relative displacement are given by:

$$F_f = k_e z_e + c_p \dot{z}_p + c_s \dot{z}_s \ , \tag{2-22}$$

$$z = z_e + z_p + z_s \ , \tag{2-23}$$

where z_e , z_p and z_s are the elastic, plastic and partial slipping displacements, respectively. k_e , c_s , c_p are the stiffness, plastic-damping and slip-damping coefficients, respectively.

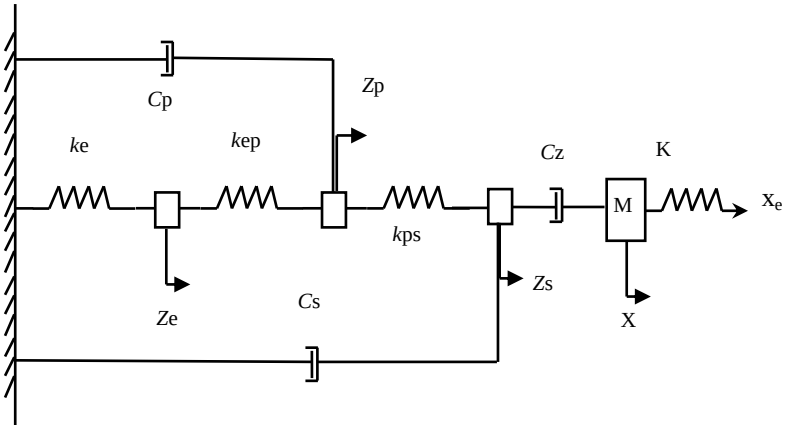

Figure 2-14 New hybrid spring-damper friction model.

The proposed hybrid friction model is shown schematically in Figure 2-14. The model considers four important effects: The first effect considered is the average elastic bristle displacement inspired by the Cattaneo-Mindlin theory based on equation (2-15) by introducing the parameter k_e. The second effect considered is the plastic displacement inspired by the Odfalk-Vignsbo method (Ödfalk and Vingsbo, 1992) based on integrating the force-displacement relation (equation (2-17)) and introducing the parameters c_p and k_{ep} for the resulting equivalent damping and stiffness, respectively. The third effect considered is the partial-slipping displacement inspired by the Mindlin-deresiewicz method (Mindlin and Deresiewicz, 1953) based on equation (2-16) by introducing the parameters c_s and k_{ps}. Finally, the Stribeck phenomenon is introduced based on the LuGre model (Astrom and Canudas de Wit, 2008) according to equation (2-12). The Friction model can be expressed in the form of equations (2-24)-(2-26) which include the four different effects as follows:

$$\underset{\textit{bristle elastic}}{k_e z_e} + \underbrace{k_{ep}(z_e - z_p)}_{\textit{transient } e\to p} = 0, \tag{2-24}$$

$$\underbrace{k_{ep}(z_p - z_e)}_{\textit{transient p}\to e} + \underbrace{k_{ps}(z_p - z_s)}_{\textit{transient p}\to s} + \underset{\textit{plastic dissipation}}{c_p \dot{z}_p} = 0, \tag{2-25}$$

$$\underbrace{k_{ps}(z_p - z_s)}_{\textit{transient s}\to p} + \underbrace{c_z(\dot{z}_s - \dot{x})}_{\substack{\textit{transient} \\ \textit{partial-slip}\to\textit{slip}}} + \underset{\substack{\textit{slipping} \\ \textit{dissipation}}}{c_s \dot{z}_s} = 0, \tag{2-26}$$

where c_z in equation (2-26) is the Stribeck damping which is given by:

$$c_z = \frac{g(\dot{x})}{\dot{x}}, \tag{2-27}$$

where $g(\dot{x})$ may be determined based on equation (2-12). Considering these effects, the pre-sliding displacement may be more accurately modeled. The new model consists of two damping coefficients for the plastic and partial slipping. Moreover, three stiffness coefficients for the elastic, elasto-plastic and elasto-slipping displacements are incorporated in the model.

2.7.2 Verification of model capabilities

One of the important properties of the new hybrid friction model is the capability to explicitly determine the elastic displacement (z_e), plastic displacement (z_p) and partial slipping displacement (z_s). To demonstrate this, the system of Figure 2-14 is excited below the break-away force with the following excitation function:

$$x_e = 0.1\cos(10t) + 0.1. \tag{2-28}$$

To show a comparison between the hybrid spring-damper friction model and the LuGre model, the system parameters for the hybrid model are defined equal to the equivalent parameters for the LuGre model as shown in Table 2.1 based on the following:

$$c_s = c_p = \sigma_1/2 \ , \tag{2-29}$$

$$k_e = k_{ep} = k_{ps} = 3\sigma_0 \ , \tag{2-30}$$

Using a precise physics based relation between the damping and stiffness coefficient strongly depends on the contact condition and the object material properties. Therefore, the relations (2-29) and (2-30) are assumed in order to demonstrate the capability of the model to demarcate different regions of elastic, plastic and partial slipping regions.

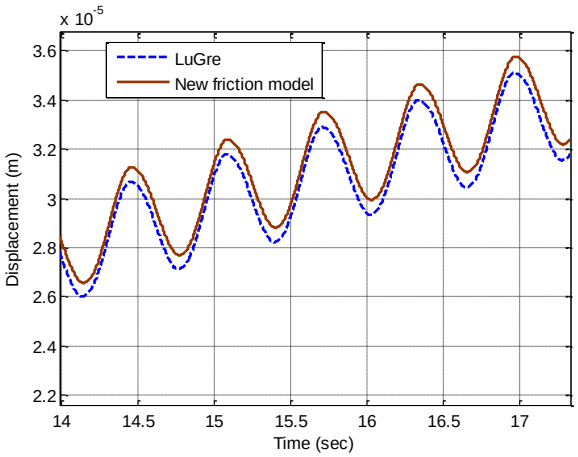

Figure 2-15 Displacement comparison between the LuGre and the new friction models using Equation (2-28) as the excitation.

In Figure 2-15, the displacements of the mass-spring system obtained using the LuGre and the new friction model are presented. Both models behave similarly with slight differences in the displacements. However, as shown in Figure 2-16 the new friction model has the capability to demarcate elastic, plastic and partial slipping displacements during the motion.

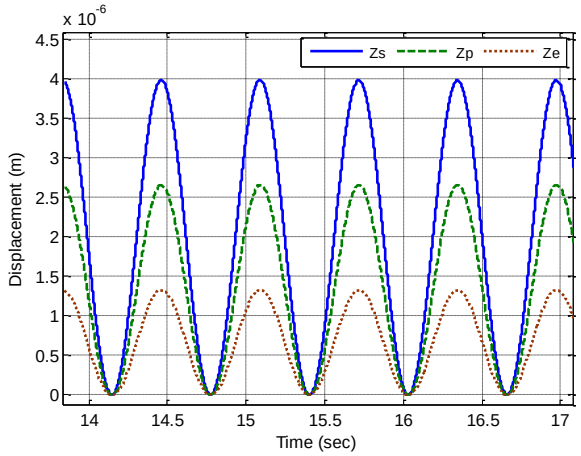

Figure 2-16 Elastic, plastic, partial slipping displacement.

In the numerical simulation of the stick-slip motions, it is important to precisely estimate the pre-sliding displacement. The LuGre model is an elastic model with the weakness of inability to demarcate between the elastic, plastic and partial slipping regions within the presliding displacement. As shown in Figure 2-16, the new hybrid model overcomes this difficulty. Furthermore, the demarcating capability makes the new hybrid friction model more flexible in terms of reproducing the pre-sliding displacement. To examine the flexibility, another

comparison between the LuGre model and the new friction model is made by implementing the following excitation displacement:

$$x_e = \left\{0.05 + e^{-0.05t}\right\} \cos 2t. \tag{2-31}$$

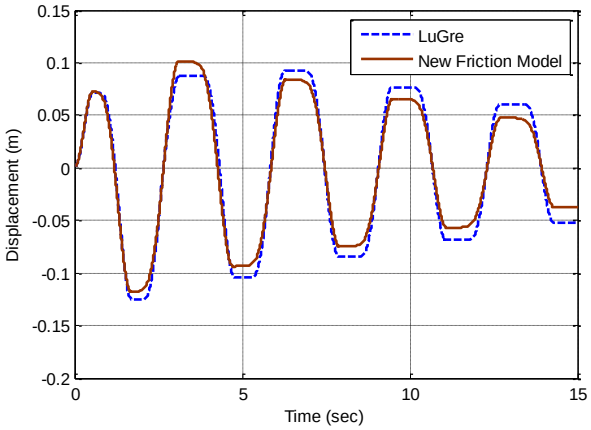

Figure 2-17 Displacement comparison the LuGre and new friction models.

The displacements of the mass-spring system are compared in Figure 2-17 for the two friction models. The results indicate the same general motion of the two models with a difference in the pre-sliding displacement.

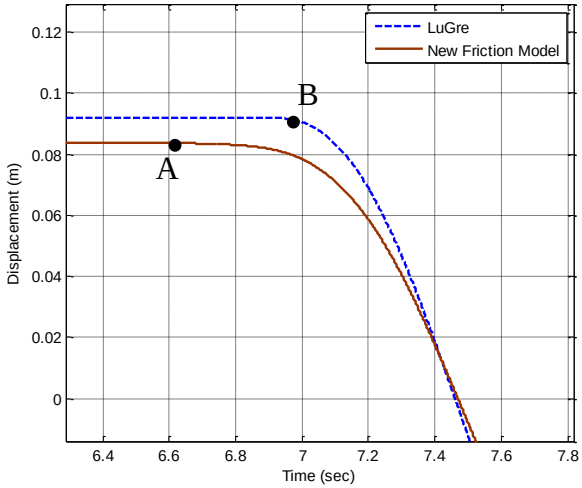

Figure 2-18 Presliding displacement in the LuGre model and new hybrid friction model.

In Figure 2-18, the presliding displacement in the LuGre model and new hybrid friction model are presented in greater detail. The points ‘A’ and ‘B’ represent the beginning of the

presliding displacement in the new hybrid friction model and LuGre model, respectively. The results emphasize the flexibility of the new hybrid friction model to reproduce a bigger presliding displacement while maintaining the general trend of the motion.This suggests a more flexible friction model able to reproduce the experimental measurements. In contrast with the LuGre model, the new friction model is an elasto-plastic model. The elasto-plasticity property enables the new friction model to not only reproduce a more precise presliding displacement by including elastic and plastic deformations but also to reproduce the nonlinear behaviour in the vicinity of zero velocity by demarcating different regions as shown in Figure 2-16.

2.8 Model Verification

The accuracy of the friction model is important especially when it is used in a practical application such as the tube-support interaction and its fretting-wear evaluation. The presliding displacement and its effect on the fretting-wear estimation make the friction model even more crucial in representing the true physics of the phenomena. To achieve a precise friction model, identification of the model parameters is important. This leads us to consider a semi-empirical approach.

To compare the new friction model against experimental test, it is crucial to come up with a correct set of model parameters. Defining a set of physics based parameters for the friction model is challenging due to the dependency of these parameters on the contact geometry, material and contact conditions. Therefore, for model verification, an inverse numerical method is adopted. The verification is conducted in two stages. The first stage is to train the model against one set of experimental test data and optimize the model capability to reproduce the experimental results. The second stage is using the first stage parameters to reproduce experimental test results for different test conditions.

The hybrid friction model is evaluated by comparing it with the experimental test results by Baumberger et al. (1994). The latter was the only fully documented test program the authors could find in the open literature. As shown in Figure 2-1, the experimental rig consists of a mass attached to a spring subjected to a constant pulling velocity, V_p. The set-up makes it possible to produce periodic stick-slip motion due to the spring force and friction resistance to the motion.

Table 2.2 shows parameters for the mass-spring system. In the numerical simulation, the parameters were chosen to be consistent with the experimental test for the model verification.

Table 2.2 Mass-spring model parameters.

M (kg)	K (Nm^{-1})	Vp (μms^{-1})
0.8	58000	1

To estimate the parameters, the nonlinear least-squares method was used. Four parameters k_e , F_s , F_c ,v_s affect the general stick-slip behavior. On the other hand, four other parameters k_{ep} , k_{ps} , c_s , c_p mostly affect the presliding distance.

The optimization was conducted in two steps. The first step involved defining the general motion behavior by optimizing the first set of parameters. In this step the objective function is the quadratic difference between the displacement time-history in the experiment and numerical simulation for the entire stick-slip motion. In Table 2.3, the first set of the optimized parameters is presented.

Table 2.3 New friction model parameters.

$k_e\,(N/m)$	$F_s\,(N)$	$F_c\,(N)$	$v_s\,(m/s)$
5.2e+7	1.07	0.707	1e- 6

The second optimization step contains the estimation of the second set of parameters which is more sensitive in terms of defining the presliding displacement. In this step the objective function is the quadratic difference for the time-history of the presliding displacement. In Table 2.4, the second set of the optimized parameters is presented.

Table 2.4 New friction model parameters.

$k_{ep}\,(N/m)$	$k_{ps}\,(N/m)$	$c_s\,(N.s/m)$	$c_p\,(N.s/m)$
1.9e+7	8.5e+7	2.3e+3	6.3e+2

The first-step of the optimization is more costly since the objective function is highly sensitive to these parameters. On the other hand, the second step of the optimization captured the

presliding displacement which required a more refined time step to more accurately run the simulation and capture the entire process. The time step is chosen equal to 1e-6 sec.

Figure 2-19 shows a comparison of the Baumberger et al. experimental test data (Baumberger et al., 1994) with the new hybrid friction model as well as the Ozaki and Hashiguchi model (Equation (6)) (Ozaki and Hashiguchi, 2010). Clearly, the new friction model can reproduce the same number of sticking regions as reported in the experiment contrary to the Ozaki and Hashiguchi (Ozaki and Hashiguchi, 2010) model which detects only five out of eight sticking phases. Furthermore, the duration of the sticking region in the new friction model shows reasonable agreement with the experimental test.

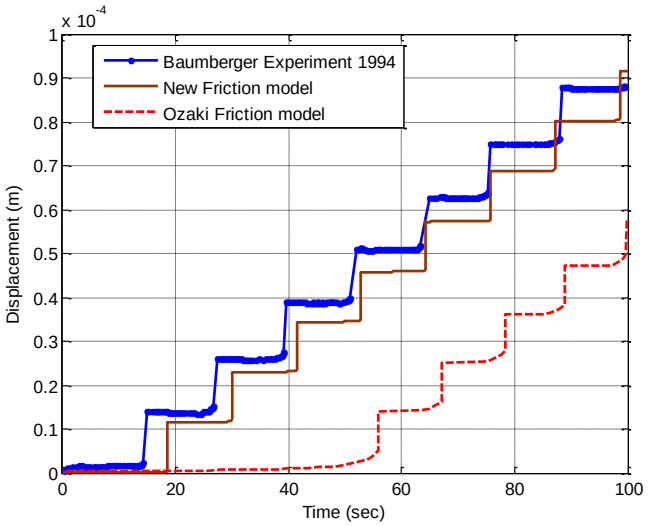

Figure 2-19 New hybrid friction model, Ozaki and Hashiguchi friction model (Ozaki and Hashiguchi, 2010) and Baumberger et al. experiment (Baumberger et al., 1994) comparisons.

After identifying the system parameters with the optimization method, the friction model is evaluated with different inputs for the spring stiffness and pulling velocity. The K-V stability diagram based upon Baumberger et al. experimental test data (Baumberger et al., 1994) is used to compare the stability velocities. The velocity may be determined for each spring stiffness coefficient by subjecting the mass-spring model to a linearly increasing velocity. For low velocity the motion begins with the stick-slip behavior until it reaches the stability velocity which transfers the motion to a more stable mode of gross-slip.

As shown in Figure 2-20, the stability velocities, for different spring stiffness coefficients, are compared between the hybrid spring damper and Lim-Chen friction model (Lim and Chen, 1998). For each set of data, transient stick-slip behavior may occur below the curve whereas more stable motion occurs for velocities above the curve.

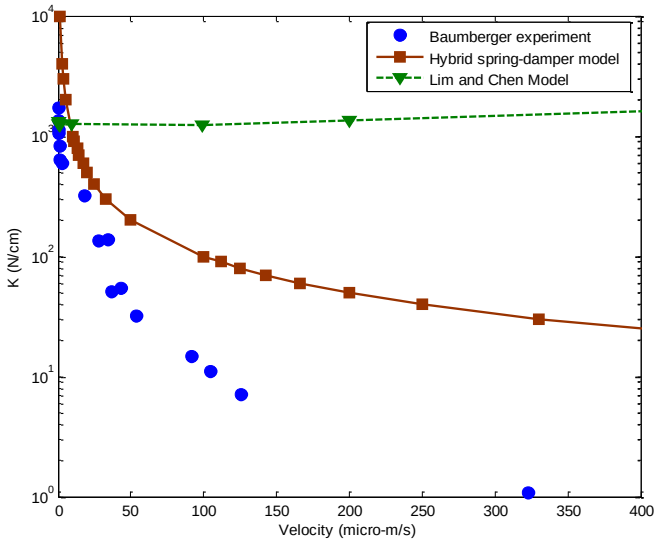

Figure 2-20 K-V dynamic phase diagram for the stick-slip stability for the Baumberger et al. experimental tests (Baumberger et al., 1994) , Lim and Chen model (Lim and Chen, 1998) and Hybrid spring-damper model.

As reported by Lim and Chen (1998), their friction model has a good agreement with the theoretical friction model developed by Rice and Ruina (1983). However, the models have the limitation that they cannot correctly reproduce the slope of the dynamic stability diagram. As shown in Figure 2-20, the Lim and Chen model produced approximately a constant line for the stability curve with highly sensitive stability velocity to the stiffness in contrast to the experimental results. The new hybrid spring damper friction model with the optimized parameters may be able to reproduce the experimental result with a qualitatively good agreement. Quantitatively, the dynamic stability diagram is divided into three regions based on the agreement between the experimental test and hybrid friction model. The first region of the stability velocity of $0 \leq v_c \leq 10$ (μms^{-1}) shows differences in instability velocity between the model and experimental test. The differences may be explained based upon the nature of the creep dominated region which may need a higher Stribeck velocity as the motion changes slowly

from the static to the dynamic regime. However, the trends of the experimental test and numerical simulation are in good agreement showing v_c tends to zero for high spring stiffness. The second region of $10 \leq v_c \leq 50$ (μms^{-1}) has a fairly good agreement with the experimental test. Furthermore, in the third stability region of $50 \leq v_c \leq 350$ (μms^{-1}) the numerical simulation is able to reproduce the general experimental trends. However, the simulations overestimate the stability velocity. This is likely due to overestimation of the damping coefficients in the friction model.

2.9 Conclusions

In this study, commonly used friction models for tube-support interaction simulation were discussed. The weaknesses and advantages of the models are compared with a rate dependent friction model. For comparison a simple mass-spring system was used. The Stribeck effect and effect of changing the break-away force on the stick-slip regions were investigated. To have better comparison between the models, different excitation forces were applied to the mass-spring system and the capabilities of the models to capture all the sticking regions were examined.

Two features of the LuGre model were investigated. The first is the criterion for demarcating the stick-slip regions and the second the incorporation of the Stribeck effect and presliding damping in the Dahl friction model (Dahl, 1968). A modified and extended LuGre model based on an equivalent spring-damper was then proposed. The slipping time comparison was made for the two models which indicated 5-9% difference.

To have a precise estimation of the slipping distance, it is important for the friction model to be able to detect different regions during the motion especially before incipient gross slip. To achieve this, a new hybrid spring-damper friction model was conceptually designed incorporating different phenomena which have a role in establishing the stick-slip regions. Simulation results confirm the capability of the new friction model to accurately demarcate the different regions of elastic, plastic and partial-slipping within the presliding displacement. Moreover, the hybrid spring-damper friction model was compared to experimental tests and shown to correctly predict not only the number of the stick-slip events but also the correct duration of the sticking phase. The model is therefore a significant improvement over the Ozaki and Hashiguchi model. Other comparisons were made against a series of experimental tests

conducted by Baumberger et al. The numerical simulation results indicated a qualitatively good agreement with the measured stability velocity. However, differences in the stability velocity magnitude were reported. The differences were attributed, in part, to underestimation of the Stribeck velocity and overestimation of the damping coefficients in the hybrid friction model parameters.

2.10 References

Antunes, J., Axisa, F., Beaufils, B. and Guilbaud, D. (1990). Coulomb friction modelling in numerical simulations of vibration and wear work rate of multispan tube bundles. Journal of Fluids and Structures 4(3): 287-304.

Armstrong-Helouvry, B. (1991). Control of machines with friction. Boston, Kluwer.

Armstrong, B. (1990). Control of machines with non-linear, low-velocity friction: A dimensional analysis. Experimental Robotics I. Heidelberg, Springer 139**:** 180-195.

Armstrong, D. and Canudas, C. (1994). A survey of models, analysis tools and compensation methods for the control of machines with friction. Automatica 30(7): 1083-1138.

Astrom, K. J. and Canudas de Wit, C. (2008). Revisiting the LuGre friction model. Control Systems, IEEE 28(6): 101-114.

Baumberger, T., Heslot, F. and Perrin, B. (1994). Crossover from creep to inertial motion in friction dynamics. Nature 367(6463): 544-546.

Canudas de Wit, C., Olsson, H., Astrom, K. J. and Lischinsky, P. (1995a). A new model for control of systems with friction. IEEE Transactions on Automatic Control 40(3): 419-425.

Canudas de Wit, C., Olsson, H., Astrom, K. J. and Lischinsky, P. (1995b). A new model for control of systems with friction. IEEE Transactions on Automatic Control 40(3): 419-425.

Cattaneo, C. (1938). Sul contato di due corpo elastici. Accademia dei Lincei, Rendiconti, 27: pp342-348, 434-436, and 474-478.

Dahl, P. R. (1968). A solid friction model, Technical report, Space and Missile Systems Organization Air Force Systems Command.

Fleming, J. R. and Suh, N. P. (1977). Mechanics of crack propagation in delamination wear. Wear 44: 39-56.

Fouvry, S., Kapsa, P., Zahouani, H. and Vincent, L. (1997). Wear analysis in fretting of hard coatings through a dissipated energy concept. Wear 203-204: 393-403.

Gauland, D. J. and Duquette, D. J. (1980). Cyclic wear behavior (Fretting) of a tempered martensite steel. Metallurgical Transactions 11(9): 1581-1588.

Gessesse, Y. B. (2000). On the fretting wear of nuclear power plant heat exchanger tubes using a fracture mechanics approach: Theory and verification. Ph.D, Concordia University

Haslinger, K. H. and Steininger, D. A. (1995). Experimental characterization of sliding and impact friction coefficients between steam generator tubes and avb supports. Journal of Sound and Vibration 181(5): 851-871.

Hassan, M. A. and Rogers, R. J. (2005). Friction modelling of preloaded tube contact dynamics. Nuclear Engineering and Design 235(22): 2349-2357.

Heslot, F., Baumberger, T., Perrin, B., Caroli, B. and Caroli, C. (1994). Creep, stick-slip, and dry-friction dynamics: Experiments and a heuristic model. Physical Review E 49(6): 4973.

Johannes, V. I., Green, M. A. and Brockley, C. A. (1973). The role of the rate of application of the tangential force in determining the static friction coefficient. Wear 24(3): 381-385.

Johnson, K. L. (1955). Surface Interaction between Elastically Loaded Bodies under Tangential Forces. Proceedings of the Royal Society of London. Series A. Mathematical and Physical Sciences 230(1183): 531-548.

Johnson, K. L. (1961). Energy Dissipation at Spherical Surfaces in Contact Transmitting Oscillating Forces. Journal of Mechanical Engineering Science 3 (4): 362-368

Johnson, K. L. (1985). Contact Mechanics. Cambridge, Cambridge University Press.

Johnson, K. L., Kendall, K. and Roberts, A. D. (1971). Surface energy and the contact of elastic Solids. Proceedings of the Royal Society of London, Mathematical and Physical Sciences 324(1558): 301-313.

Karnopp, D. (1985). Computer Simulation of Stick-Slip Friction in Mechanical Dynamic Systems. Journal of Dynamic Systems, Measurement, and Control 107(1): 100-103.

Ko, P. L. (1986). Metallic wear-a review, with special references to vibration-induced wear in power plant components. Proceedings ASME Pressure Vessels and Piping Conference. Chicago, Illinois. 20**:** 66-78.

Lim, Y. F. and Chen, K. (1998). Dynamics of dry friction: A numerical investigation. Physical Review E 58(5): 5637–5642.

Mindlin, R. D. (1949). Compliance of elastic bodies in contact. ASME Journal of Applied Mechanics 16(3): 259-268.

Mindlin, R. D. and Deresiewicz, H. (1953). Elastic Spheres in Contact under Varying Oblique Forces. ASME Journal of applied mechanics 20: 327-344.

Ödfalk, M. and Vingsbo, O. (1990). Influence of normal force and frequency in fretting. Tribology Transactions 33(4): 604-610.

Ödfalk, M. and Vingsbo, O. (1992). An elastic-plastic model for fretting contact. Wear 157(2): 435-444.

Ozaki, S. and Hashiguchi, K. (2010). Numerical analysis of stick-slip instability by a rate-dependent elastoplastic formulation for friction. Tribology International 43(11): 2120-2133.

Pettigrew, M. J. and Taylor, C. E. (2003). Vibration analysis of shell-and-tube heat exchangers: an overview--Part 2: vibration response, fretting-wear, guidelines. Journal of Fluids and Structures 18(5): 485-500.

Rabinowicz, E. (1951). The nature of the static and kinetic coefficients of friction. Journal of Applied Physics 22(11): 1373-1379.

Rice, J. R. and Ruina, A. L. (1983). Stability of steady frictional slipping. Journal of applied mechanics 50(2): 343-349.

Rogers, R. J. and Pick, R. J. (1977). Factors associated with support plate forces due to heat-exchanger tube vibratory contact. Nuclear Engineering and Design 44(2): 247-253.

Sauve, R. G. and Teper, W. W. (1987). Impact simulation of process equipment tubes and support plates: a numerical algorithm. ASME Journal of Pressure Vessel Technology 109(1): 70-79.

Suh, N. P. (1973). The delamination theory of wear. Wear 25(1): 111–124.

Tan, X. and Rogers, R. (1996). Dynamic friction modelling in heat exchanger tube simulations. Flow-Induced Vibrations. Montreal, ASME. 328**:** 347–358.

Tariku, F. A. and Rogers, R. J. (2001). Improved Dynamic Friction Models for Simulation of One-Dimensional and Two-Dimensional Stick-Slip Motion. Journal of Tribology 123(4): 661-669.

Toorani, M., Pan, L., Li, R., Idvorian, N. and Vincent, B. (2009). Advanced nonlinear flow-induced vibration and fretting-wear analysis capabilities. 6th CNS International Steam Generator Conference,. Toronto.

Wojewoda, J., Stefański, A., Wiercigroch, M. and Kapitaniak, T. (2008). Hysteretic effects of dry friction: modelling and experimental studies. Philosophical Transactions of the Royal Society A: Mathematical, Physical and Engineering Sciences 366(1866): 747-765.

CHAPTER 3
EXPERIMENTAL INVESTIGATION OF TUBE-SUPPORT NORMAL INTERACTION WITH A NONLINEAR IMPACT MODEL

This chapter is presented in the form of a paper submitted to *Journal of Pressure Vessel Technology* on 11 November 2012. Authors: Reza Azizian and Njuki Mureithi.

ABSTRACT

Flow-induced vibration in a steam generator may cause tube-support interaction. This long term interaction is a challenging problem as it may cause fretting-wear of the tube. An estimation of the normal impact force during tube-support interaction is important to precisely quantify material removal. Several authors have tried to model the normal interaction, using a linear spring-damper model. However, the inability of the model to correctly quantify fretting-wear raises interests to carefully investigate the force-displacement relation during tube-support interaction. A precise study of the interaction presents several challenges as a result of the many parameters involved during the interaction, including fluid forces, number and type of supports and geometry of contact.

This study investigates tube-support interaction using a simple experimental rig, consisting of a tube with a flat support which is positioned at the tube mid-span. This enables the investigation of normal impact forces in greater detail, using experimental tests and numerical simulation comparisons. The present work studies normal force-displacement relationship which leads to the estimation of an empirical parameter, associated with the nonlinearity in the relationship. In addition, the relationship is used to simulate tube-support interaction for various gap sizes and excitation forces. The comparisons indicate that using the nonlinear spring-damper model significantly reduces the predicted impact force error, to less than 20 percent, when compared to experimental tests. Additionally, this research investigates various energy dissipation mechanisms during tube-support interaction, including impact and structural damping. The effect of impact damping on the tube response is investigated, using the Hunt and Crossley model. The sensitivity of tube response to structural damping is also studied. The investigations suggest that using a higher structural damping during tube-support contact,

depending upon tube-support gap size, may improve the accuracy of the estimation of the tube response.

3.1 Introduction

In steam generator tube bundles, flow-induced vibration causes tube-support interaction. The long term interaction may lead to fretting-wear in the tube bundle which may consequently cause tube failure. Dynamic modeling of tube-support interaction is important due to a need to estimate the tube wear-rate at the support locations. Since the most important causes of wear are impact and friction between the tube and support, many authors have proposed models and developed numerical simulations for this interaction. Various developments have resulted from the continued works by, among others, Rogers and Pick (1977), Sauve and Teper (1987), Tan and Roger (1996), Hassan et al. (2000; 2002; 2003; 2005; 2008) and Tariku and Roger (2001). The model developers have mostly focused on developing proper models for friction force and computing tube-support interaction dynamics response. Several codes have been developed to provide a better estimation of the interaction response. These codes can be categorized into two main groups, based upon the approach used to solve the equation of motion. The first group was developed using the finite element method, including H3DMAP (Sauve and Teper, 1987), INDAP (Hassan, 2000; Hassan et al., 2002; Hassan et al., 2003) and FIVDYNA (Toorani et al., 2009). The most important challenge with the finite element codes is cost in terms of computation time. This is associated with the nonlinearity in the equation as a result of tube-support clearance. The second group was developed using the modal superposition method, including VIBIC (Rogers and Pick, 1977), GERBOISE (Axisa et al., 1986; Hassan et al., 2005) and VITRAN (Rubiolo, 2006). The modal superposition codes are competitive in terms of their computation time. However, the simplifications in the model, such as neglecting constrained modes, may reduce the modal precision compared to the FEM method.

Dynamic computation of tube-support interaction is a challenging task aimed at acquiring accurate results and optimum computation cost. Sauve and Teper (1987) developed a numerical integration code using the finite element method. The numerical integration was computed based upon the Newmark approach (Bathe, 1982). Furthermore, to form mass and damping matrices, the Lumped mass and Rayleigh approaches were adopted. However, it is vital to obtain an optimum time-step due to the cost of computation. This computation cost problem is associated

with the nonlinearity in the equations imposed by the tube-support clearance. Subbaraj and Dokainish (1989) adopted a pseudo force approach to model the tube-support gap using an external force in the equation of motion. This approach has been widely used to simulate the tube-support impact phenomenon (Hassan et al., 2002; Rubiolo, 2006).

As mentioned earlier, besides the finite element method for tube-support dynamic computation, another method is the modal superposition approach. Antunes et al. (1990) used the Euler-Bernoulli beam theory and the modal superposition technique for a nonlinear dynamic analysis of tube-support interaction. Later on, the modal superposition approach was adopted by Rubiolo (2006) in the VITRAN code to simulate the dynamic response of fuel rods. The modal superposition approach has some advantages to use due to its simplicity and lower computational cost. However, using the unconstrained mode shape may be problematic. Davies and Rogers (1979) investigated the effect of constrained versus unconstrained mode shape in the dynamic computations (Rubiolo, 2006). The study confirmed the feasibility of using unconstrained mode shapes for a tube with a very small structural damping coefficient.

Determining an accurate normal impact force is important due to its role when determining the friction force and wear work-rate. The normal impact model consists of two components (Goyal et al., 1994): the first component is the contact detection between two bodies and the second the relationship between impact force and normal displacement. This relationship is mainly dependent upon contact material and geometry. Accurately detecting the instance of contact and adopting a proper impact force function constitute a complete normal impact model (Goyal et al., 1994).

As described earlier, the nonlinearity of the force-displacement relationship during tube-support normal interaction grants an important role to the assumed form of the normal impact force. The form may be defined based upon contact conditions, geometry and level of accuracy needed for the analysis. The Hertz's contact theory is commonly used to estimate the normal impact force. However, there are some difficulties associated with the theory (Goldsmith, 1960; Johnson, 1985). In the Hertz theory, contact surfaces are assumed to be continuous and frictionless therefore the only force which can be transferred within the contact area is the normal force (Johnson, 1985). In most practical cases, however, the impact phenomenon includes energy dissipation while the Hertz's contact theory is formulated based upon an elastic impact process

(Goldsmith, 1960). In addition, the theory does not consider the boundary force originated as a result of impact deformation (Johnson, 1985). The geometry of contact may play an important role in an estimation of the normal impact force. In the present work, the two bodies under consideration are a thin-wall tube in contact with a flat support. The study conducted by Axisa et al. (1984) indicated that the ovalization stiffness may be the dominant stiffness during tube-support interaction as a result of the small thickness of tube.

The Hunt & Crossley (1975) damping model is commonly used to represent the energy dissipation as a result of impact. In this model, the coefficient of restitution is an important factor used to present the amount of dissipated energy. The coefficient generally depends on material, contact geometry and initial incident velocity (Werner and Robert, 2008). Based upon the nature of impact, different definitions for the coefficient of restitution may be used, including the Newtonian, Poisson and Stronge definitions (Stronge, 2000). Choosing a proper value for the coefficient of restitution is a challenging step as a result of the multi-modal behaviour of tube-support interaction. The experimental study by Thomson et al. (1994) suggested using a smaller coefficient of restitution for interaction involving a continuous system. This was attributed to the distribution of impact energy to the higher vibration modes. This transferred energy may then be easily dissipated in the form of sound, which may establish an inelastic impact process (de Weger et al., 1996; Wagg and Bishop, 2000). Another study by Werner and Robert (2008) also indicated that measuring the coefficient of restitution in a continuous system is problematic due to the multiple micro-impact behavior which may lead to a chaotic response. There have, however, been some attempts to measure the coefficient of restitution for continuous systems (Bao et al., 2004; Werner and Robert, 2008). The experimental study by Stoianovici and Hurmuzlu (1996) laid an emphasis on the sensitivity of the coefficient of restitution to internal elastic motion and micro-multiple impact phenomena.

In the development of numerical models, comprehensive efforts have been made to perform accurate experimental tests for model verifications. Weaver and Schneider (1983) performed experimental tests on U-bend tubes with flat supports; Chen et al. (1985) to understand support effectiveness; while Yetisir and Fisher’s (1997) aimed to estimate wear rates. These experimental tests were continued by Axisa et al. (1984), Haslinger and Steininger (1995), Pettigrew et al. (1998; 2003a; 2003b), Azizian et al. (2009) and Nowlan et al. (2009).

In the tube-support interaction dynamic computation codes, including VIBIC, H3DMAP, INDAP and VITRAN, the normal impact forces are modeled, with a similar method, using a parallel spring and damper. Fisher et al. (1989) compared tube-support impact forces in numerical simulations with experimental tests, using the VIBIC code. The results indicated the overestimation of impact forces by approximately a factor of 2 which indicated a significant difference. Hassan and Rogers (2005) predicted tube-support wear-rate, using the INDAP code. Their result comparisons with Yetisir and Fisher (1997) experimental tests indicated up to approximately 50% difference in work-rate estimation.

In the present study, the complicated behavior of the tube-support interaction in a steam generator is simplified to a two-span tube with a flat support positioned at the tube mid-span. This set-up is then used to measure impact forces and mid-span displacements for different combinations of gap sizes and excitation forces. The tests enable an accurate study of tube-support interaction dynamics. The results are also used as a reference database for the estimation of impact model parameters using comparisons with numerical simulations. In addition, a tube-support dynamics model is formulated using the Euler-Bernoulli beam theory. The equations are solved using the modal superposition method and Runge-Kutta numerical algorithm in Simulink.

Using an accurate impact model is a key factor to precisely simulate the interaction. The impact model is then divided into two parts including, elastic and inelastic impact. For elastic impact, three deflections during tube-support interaction including local deformation of tube, deflection of support and tube ovalization are studied. The impact model is then upgraded using an empirical parameter associated with nonlinearity in the force-displacement relationship. This nonlinearity is attributed to geometry of the contact interface and inability to precisely model the ovalization phenomenon. The model is then compared to experimental tests for different excitation forces and gap sizes. The source of energy dissipation in the tube-support interaction is mainly due to wave propagation, structural damping, friction and local impact damping. In this study, the effect of impact damping and the choice of nonlinear damping model parameters on tube response are investigated. Additionally, the effect of vibration amplitude on structural damping is studied. Furthermore, the mid-span displacement differences between the experimental tests and numerical simulation are investigated by upgrading the structural damping model. This is achieved using different damping magnitudes for contact and no-contact phases.

3.2 Experimental Rig and Measured Variables

As mentioned earlier, different authors have carried out experimental tests to construct a reliable reference to validate various tube-support interaction models. One of the most important components of the overall model is the impact model. The accuracy in the impact model is important due to its effect on the estimation of friction force and subsequently the tube-support dynamic response. In this section, the complicated structure of a tube bundle in a real heat exchanger is simplified to a simple experimental rig, including a two-span tube with a flat support in the middle. This makes it possible to precisely study the normal impact force. This section includes a description of the experimental rig, instrumentation, experimental procedure and the selection of measured variables.

3.2.1 Experimental test rig and instrumentation

To study the dynamics of tube-support interaction, an apparatus was designed which consists of a straight clamped-clamped tube, (with specifications presented in Table 3.1), interacting with a flat support. A schematic sketch of the experimental rig is shown in Figure 3-1.

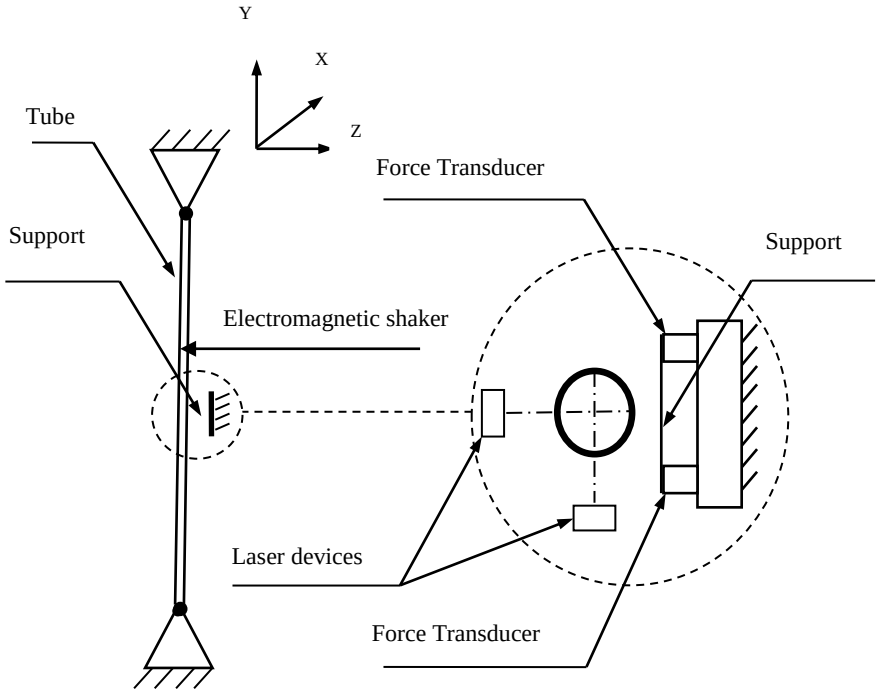

Figure 3-1 Tube-support experimental rig.

The tube is glued to two links at its lower and upper ends. The links are fastened to two steel blocks in the upper and lower parts of a large I-beam mounting post, as a support for the tube. The links have narrow neck regions to approximately produce pinned-pinned boundary conditions.

Table 3.1 Experimental test parameters.

Description	Variable	Unit	Value
Density	ρ	kg/m^3	8190
Inner diameter	D_i	m	0.0139
Outer diameter	D_o	m	0.0159
Tube length	L	m	2.5
Young's Modulus	E	GPa	200
Poisson ratio	ν	-	0.29
Damping ratio	ξ	%	0.12-0.2
Natural frequency	f	Hz	8.75

During the tube-support interaction, three external forces act on the tube: external excitation, impact and friction forces. Imparting an excitation force on the tube is a challenging process due to the need to avoid excessive vibration and noise resulting from the exciter contact with the tube. To achieve this, an electromagnetic shaker is used as an excitation source. As shown in Figure 3-2, the shaker is positioned at 1/8 of the tube length from the tube center in the direction normal to the support. The shaker is in turn installed on the I-beam mounting post using a rotating fixture. This fixture enables rotation of the shaker, along the tube longitude axis. The rotating mechanism is then used to adjust the tube-support inclination angle. In addition, the flat support is positioned at the tube mid-span while it is installed on a positioning system. This system can precisely produce various gap sizes between the tube and its flat support.

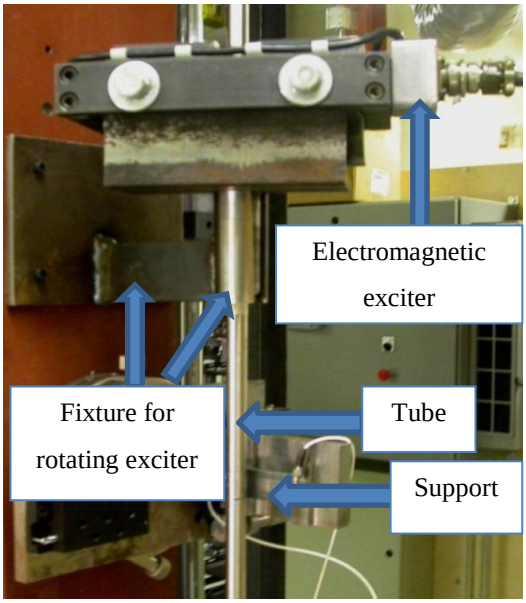

Figure 3-2 Experimental rig including tube, support, fixture and electromagnetic exciter.

To evaluate an incorporated impact model in a numerical simulation, it is important to measure the tube normal and tangential displacements as well as the tube-support impact force. To measure the tube mid-span displacements, two laser displacement sensors with 10 micron resolution are positioned in the horizontal plane, which is normal to the support.

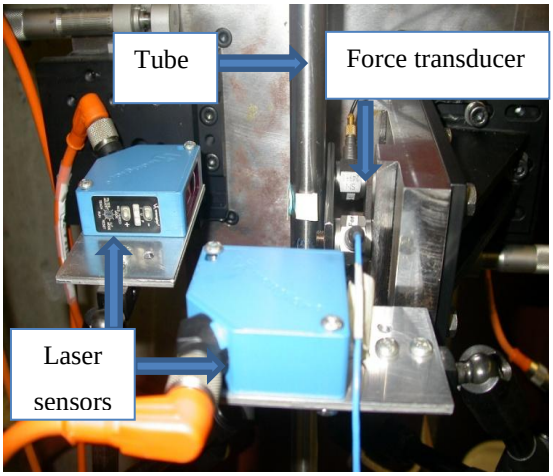

Figure 3-3 Experimental rig-measuring devices: force transducers and laser displacement sensors.

Using the laser sensors to measure the tube displacements with a circular cross-section is problematic as a result of the curvature of the cylindrical tube. Two flat bars are therefore positioned at the laser signs on the tube. In addition, two force transducers are installed under the

flat bar support to measure the impact forces. Figure 3-3 shows a close-up photo of the test region with the tube, support, force transducers and laser displacement sensors indicated.

3.2.2 Experimental procedure

The experimental test is conducted in four steps: the first is to accurately measure the tube structural damping coefficient and natural frequencies. To achieve this goal, an excitation force is employed on the tube using the electromagnetic shaker and then the shaker power is cut after a period of 30 seconds. The time domain response after the power-cut is used to measure the structural damping coefficient using the curve fitting method. In addition, the damping coefficient is measured for different mid-span displacements between 0.25 mm to 2.5 mm. This enables one to study the effect of tension in the tube structure and various nonlinearities, including the tube clamped-clamped condition and inhomogeneity in the tube material. The second step is to measure the tube mid-span displacements for different forcing amplitudes without interaction with the flat bar support. A sinusoidal excitation force is employed using a forcing frequency of 10.5Hz, which is approximately 10% higher than the tube first natural frequency and excitation force amplitude is chosen between 0.1 N-0.55 N. This step is valuable to validate a numerical code without considering the effect of interaction models. The third step is to excite the tube in the presence of the support to study its impact behaviour. To achieve this goal, a sinusoidal excitation force is imparted on the tube in the direction normal to the support using five different gap sizes of 0, 0.25, 0.5, 0.75 and 1 mm. The comparisons, for different gap sizes, make it possible to accurately examine the impact model parameters and damping coefficients. As shown in Table 3.2, four different excitation amplitudes, with the forcing frequency of 10.5 Hz, are employed for each gap size. The mid-span displacements and impact forces are then measured for each experimental test.

Table 3.2 Excitation force amplitude for each gap size.

Gap (mm)	Force Level-1 (N)	Force Level-2 (N)	Force Level-3 (N)	Force Level-4 (N)
0	0.0181	0.0410	0.1088	0.2617
0.25	0.1454	0.2616	0.3456	0.4510
0.5	0.2625	0.3462	0.4567	0.5747
0.75	0.3458	0.4559	0.5735	0.7062
1	0.3446	0.4541	0.5714	0.7060

The fourth step in the experimental test is to study energy dissipation during the tube-support interaction. The tube mid-span is therefore initially displaced to a fixed position and released resulting in imparting against the flat support, in the direction normal to the support. The different initial displacements for each gap size are listed in Table 3.3. The study of the tube mid-span displacement in a dissipative motion, without an instantaneous external excitation, is valuable to investigate the inelastic tube-support impact model.

Table 3.3 Initial displacements of the tube mid-span.

Gap(mm)	Disp-1 (mm)	Disp-2 (mm)	Disp-3 (mm)	Disp-4 (mm)
0	3.9	5.7	8.3	10.2
0.25	3.7	5.6	8.2	9.5
0.5	3.6	5.9	7.6	9.4
0.75	3.3	5.5	7.8	9.9
1	3.9	5.6	7.8	10.1

3.2.3 Measured variable

The tube-support interaction can be divided into elastic and inelastic interactions. In the elastic interaction, various elastic phenomena may be involved, including the tube local deformation, tube ovalization and support deflection. The most dominant impact force during the interaction is the elastic force. Therefore, the interaction force comparison between the experimental tests and numerical simulations is used to estimate the elastic impact model parameters. As mentioned in Section 3.2.2, the experimental results in the third step are used to make the comparisons. Using different combinations of gap sizes and forcing amplitudes enables one to examine a numerical model in greater detail. It is important to study the tube mid-span displacements and impact force differences between the experimental tests and numerical simulations. However, the study of the rate of change in the differences may also provide a number of insights into the investigation of elastic and inelastic impact dynamics.

On the other hand, tube-support inelastic interaction consists of different inelastic phenomena, including hysteretic energy dissipation, ovalization dissipation, wave propagation and higher modes structural dissipation. As mentioned in Section 3.2.2, the experimental tests, using tube initial displacement as an external excitation, are performed to study the dissipative

behaviour of the tube during the interaction. The mid-span displacements comparisons may therefore be valuable to study the inelastic dynamics.

3.3 Dynamic Computation of Tube-Support Interaction

In Section 3.2, the complicated structure of the tube-support interaction in a real heat-exchanger was simplified to a two-span tube. The simplification of the structure makes it possible to carefully study the impact dynamics. The first step of the study is to employ a proper dynamic computation method for tube-support modeling. In the present work, the Euler-Bernoulli beam equation and the modal superposition method are chosen to model the tube-support dynamics, as described by Antunes et al. (1990) and Rubiolo (2006).

3.3.1 Euler-Bernoulli beam modeling

For the nonlinear dynamic analysis of tube-support interaction, the modal superposition approach is used to solve the Euler-Bernoulli equation of motion. The tube partial differential equations of motion are formulated as,

$$\rho A\frac{\partial^2 z}{\partial t^2}+\eta\frac{\partial z}{\partial t}+EI\frac{\partial^4 z}{\partial y^4}=f_z(z,t)\ , \tag{3-1}$$

$$\rho A\frac{\partial^2 x}{\partial t^2}+\eta\frac{\partial x}{\partial t}+EI\frac{\partial^4 x}{\partial y^4}=f_x(x,t)\ , \tag{3-2}$$

where z and x are the normal and tangential directions to the support, respectively. ρ is the density of the tube material, A is the tube cross-sectional area, η is the structural damping coefficient and EI is the bending stiffness. In equations (3-1) and (3-2), the terms $f_z(z,t)$ and $f_x(x,t)$ are the total forces acting on the tube in the normal and tangential directions, respectively. The force terms may then be expressed as follows:

$$f_z(z,t)=F_{ez}(t)\delta(y-y_e)-F_i(z)\delta(y-y_i)\ , \tag{3-3}$$

$$f_x(x,t)=F_{ex}(t)\delta(y-y_e)-F_f(x,z)\delta(y-y_i)\ , \tag{3-4}$$

where F_{ez} and F_{ex} are the projection of the external excitation force in the z and x directions, respectively. F_i and F_f are the impact and friction forces, respectively. y_i and y_e are the axial positions of the external force and support along the tube span. The partial differential equations

of motion may then be simplified using the modal superposition approach. Thus, the displacements in the equations of motion may expressed as,

$$z = \sum_{n=1}^{N} \varphi_n(y) q_{nz}(t) \,, \tag{3-5}$$

$$x = \sum_{n=1}^{N} \varphi_n(y) q_{nx}(t) \,, \tag{3-6}$$

where q_{nz} and q_{nx} are the modal responses in the z and x directions, respectively, and $\varphi_n(y)$ is the n^{th} tube unconstrained mode of vibration.

The equations of motion are discretized using the normalized mode shapes and considering the orthogonality proprieties of the mode shapes. The discretized modal equations are obtained by substituting equations (3-5) and (3-6) into equations (3-1) and (3-2) and following a standard Galerkin procedure the following modal equations are obtained.

$$m_n \ddot{q}_{nz}(t) + 2m_n \xi \omega_n \dot{q}_{nz}(t) + m_n \omega_n^2 q_{nz}(t) = f_z^{\,p}(z,t), \tag{3-7}$$

$$m_n \ddot{q}_{nx}(t) + 2m_n \xi \omega_n \dot{q}_{nx}(t) + m_n \omega_n^2 q_{nx}(t) = f_x^{\,p}(x,t), \tag{3-8}$$

where the projected forces are given by

$$f_z^{\,p}(z,t) = \int_0^l \varphi_n(y) \left\{ F_{ez}(t)\delta(y - y_e) - F_i(z)\delta(y - y_i) \right\} dy, \tag{3-9}$$

$$f_x^{\,p}(x,t) = \int_0^l \varphi_n(y) \left\{ F_{ex}(t)\delta(y - y_e) - F_f(x,z)\delta(y - y_i) \right\} dy, \tag{3-10}$$

Equations (3-7)-(3-10) are numerically solved using the fourth-order Runge-Kutta algorithm in Simulink.

3.4 Tube-Support Impact Model

In the previous section, the basic dynamic model of the tube-support interaction was outlined. The model is based on Euler-Bernoulli beam theory and modal superposition technique. However, the incorporated interaction forces play an important role to determine a precise interaction response. The interaction forces are decomposed into impact and friction forces. As noted in Section 3.2.2, the effect of the friction force in the experimental tests was minimized by

considering the interaction in a normal direction to the support. The normal impact force can therefore be assumed as the effective interaction force, in the model. The normal impact force formulation consists of two models: elastic impact and inelastic impact models. In this section, these models are elaborated in greater detail.

3.4.1 Contact detection algorithm

The first step to estimate the interaction force is to define the condition of incipient contact between the tube and support. This can be achieved using a penalty function as formulated below (Delaune et al., 2010),

$$K = \begin{cases} K_{equ} \quad if \quad \sum_{n=1}^{N} \varphi_n(x) q_{nz}(t) - \Delta_1 \geq 0 \\ \\ 0 \quad if \quad \sum_{n=1}^{N} \varphi_n(x) q_{nz}(t) - \Delta_1 \leq 0 \end{cases}, \tag{3-11}$$

where Δ_1 is the tube-support clearance and K_{equ} is the equivalent normal contact stiffness. The above penalty equation may accurately define the contact moment, when a relatively small time-step is used.

3.4.2 Tube-support elastic interaction

Different phenomena may affect the elastic displacement during the tube-support interaction, including tube local deformation, ovalization and support deflection. Investigating such effects is important for a precise representation of the elastic impact force. The general normal elastic impact force, dependent upon the flatness of the contact interface, may be expressed as follows (Babistky, 1998):

$$F = c u_z^{\frac{2m+1}{2m}}, \tag{3-12}$$

where $1 \leq \frac{2m+1}{2m} \leq 3/2$ and u_z is the normal displacement. The flatter the contact surfaces the closer to linearity is the above equation. Using the parameter m in the tube-support contact force function allows one to consider the contact geometry effect during the tube-support interaction.

Choosing the factor *m* equal to 1 leads to an interaction force similar to the Hertz contact force. The interaction force then takes the following form (Johnson, 1985):

$$F = c_1 u_z^{3/2}, \tag{3-13}$$

The stiffness coefficient, c_1, may be determined based upon contact geometry and material proprieties. In the case of the tube-support local deformation, the geometry can be simplified by considering two cylinders in contact. The flat support is then modeled by choosing the radius of one of the cylinders equal to infinity. On the other hand, the axial curvature of the tube during interaction may vary as a result of the tube-support gap size. Thus, an elliptical contact region may be formed. Considering a point, line, circular or elliptical contact area, different values may be obtained for the Hertzian contact stiffness. However, in all cases, the value is relatively large compared to the tube ovalization stiffness.

The tube ovalization stiffness is the most effective stiffness compared to the tube local deformation and the support deflection stiffness during the tube-support interaction. The effect was proven by Axisa et al. (1988) work using the Morley's thin circular cylinder study (Morley, 1960). In the study, the shell equations were solved for a cylinder. The loading consisted of two equal point forces, acting at the cylinder mid-span and directed towards each other. The study introduced a dimensionless parameter ψ, which represents the ovalization force-displacement relationship. This parameter was formulated as (Morley, 1960),

$$\psi = w_z \sqrt{2} \left(\frac{Et^2}{FD} \right) \sqrt{\frac{t}{D}}, \tag{3-14}$$

where w_z is the ovalization displacement, F is the ovalization force, t is the tube thickness and D is the tube diameter.

The parameter ψ is mostly dependent upon the ratio of tube length to tube diameter. In this study, the ratio, $4L/D$, is greater than 40 which suggests a constant value of 0.737 for the parameter ψ, using the Flugge-Morley equation (Morley, 1960). Another deflection during tube-support interaction is attributed to the support deformation. The support used in this work is a fixed-fixed stainless steel flat bar. Assuming the occurrence of tube-support interaction in the middle of support, the support stiffness may then be formulated as,

$$k_s = \frac{192 E_s I_s}{L_s^{\,3}} \ , \tag{3-15}$$

where L_s is the support length and E_sI_s the support bending stiffness.

3.4.3 Tube-Support inelastic interaction

There are some limitations to using the Hertz and ovalization impact theories since these theories are developed for elastic bodies and frictionless contact interfaces. However, it is important to consider energy dissipation during impact. This can be achieved using the Hunt and Crossley model (Hunt and Crossley, 1975). This model is formulated as,

$$F_d = \frac{3}{2}\beta k z^p \dot{z}^q, \tag{3-16}$$

where F_d is the impact damping force, k is the contact stiffness and β is a ratio dependent upon energy dissipation during impact. p and q are empirical parameters depend upon the impact velocity, material and contact interfaces.

3.4.4 Tube-support spring-damper impact model

The mathematical tube-support impact model may be elaborated using a hybrid spring-damper system. As shown in Figure 3-4, the first part of the impact model consists of tube structural stiffness and damping. The second part consists of two parallel dampers and three springs in series. The dampers are associated with tube restitution and energy dissipation in the support while the springs are associated with tube local deformation, support deflection and tube ovalization.

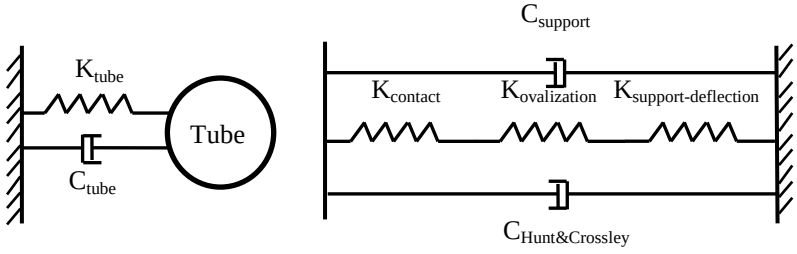

Figure 3-4 Tube-support impact model.

Tube structural stiffness is proportional to the tube elastic modulus and moment of inertia. However, the value may vary depending on the natural frequency of different modes of vibration.

3.5 Experimental Results and Numerical Simulation Comparisons

As noted in Section 3.2.2, the experimental tests were conducted in four steps to precisely evaluate the normal impact model used in tube-support numerical simulation. In this section, the experimental tests are compared to numerical simulations. In Section 3.5.1, the structural damping measurements are presented. Section 3.5.2 evaluates the elastic impact model by comparing the tube-support experimental tests with the related numerical simulations based on a nonlinear impact model. Section 3.5.3 investigates impact damping models by comparing the tube-support free vibration experimental tests with the corresponding numerical simulations.

3.5.1 Tube forced vibration comparison

As noted in Section 3.2.2, the first two steps of the experimental tests are designed to validate the numerical model and related code for the case of tube forced vibration, without support interaction. Accurate numerical simulation of tube-support interaction dynamics depends on correct modeling of the dependency of tube response on structural damping. Therefore, an accurate measurement of structural damping is important for a precise tube-support numerical simulation.

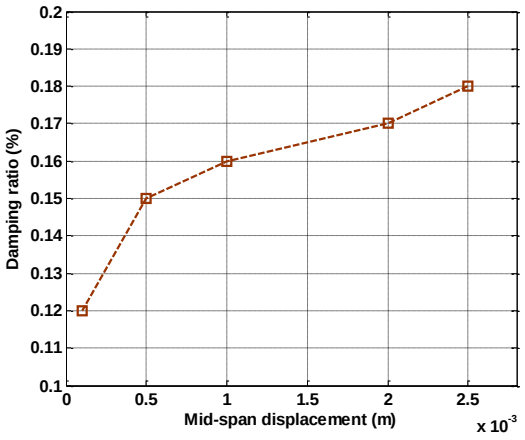

Figure 3-5 Experimental measurement of the tube structural damping.

As shown in Figure 3-5, the damping measurement is strongly dependent on the amplitude of the tube mid-span displacement. The damping magnitude increases from 0.12% to 0.18% as a result of an increase in the tube mid-span displacement from 0.2 mm to 2.5 mm.

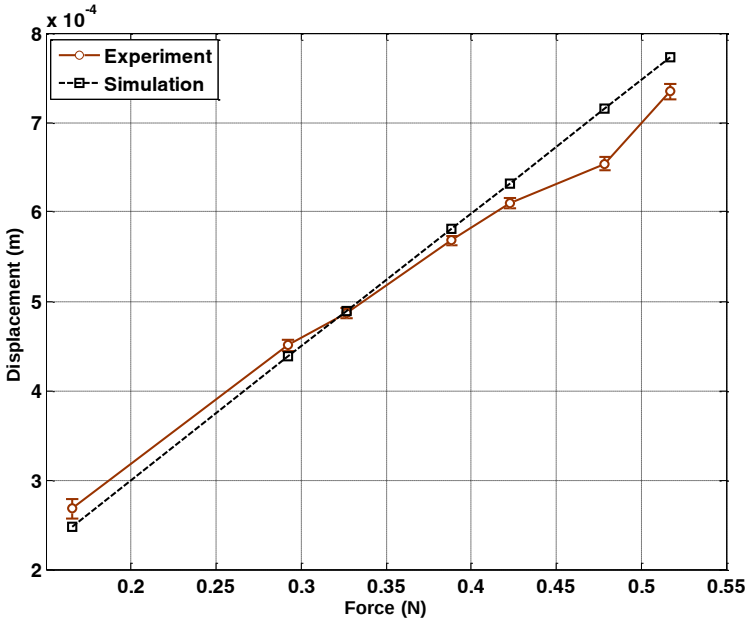

Figure 3-6 Tube mid-span displacement comparisons experiments and numerical simulations.

As noted in Section 3.2.2, the experimental tests are conducted using sinusoidal excitation forces. To examine the ability of the numerical model to reproduce the tube dynamic response, the steady-state normal mid-span displacements are compared to the related experimental tests for various forcing amplitudes in Figure 3-6. The results indicate reasonable agreements between the experiments and numerical simulations with a 2 % to 8 % difference. The small error may be associated with the experimental measurement error, nonlinearities in the supports and inhomogeneity in the tube material. However, the comparisons confirm the accuracy of the modal parameters, used in the numerical simulations.

3.5.2 Tube-support interaction with a sinusoidal excitation

The tube-support normal dynamic response is complex as a result of the nonlinearities involved in the impact process. As described in Section 3.4.2, the elastic impact force may be incorporated into the vibro-impact model using equation (3-12). In the equation, the empirical parameter *m* represents nonlinearities in tube-support force-displacement relationship. However,

assuming the contact interface as a perfectly flat surface may lead to the estimation of parameter *m* equal to infinity. This assumption will simplify the equation (3-12) to a linear form.

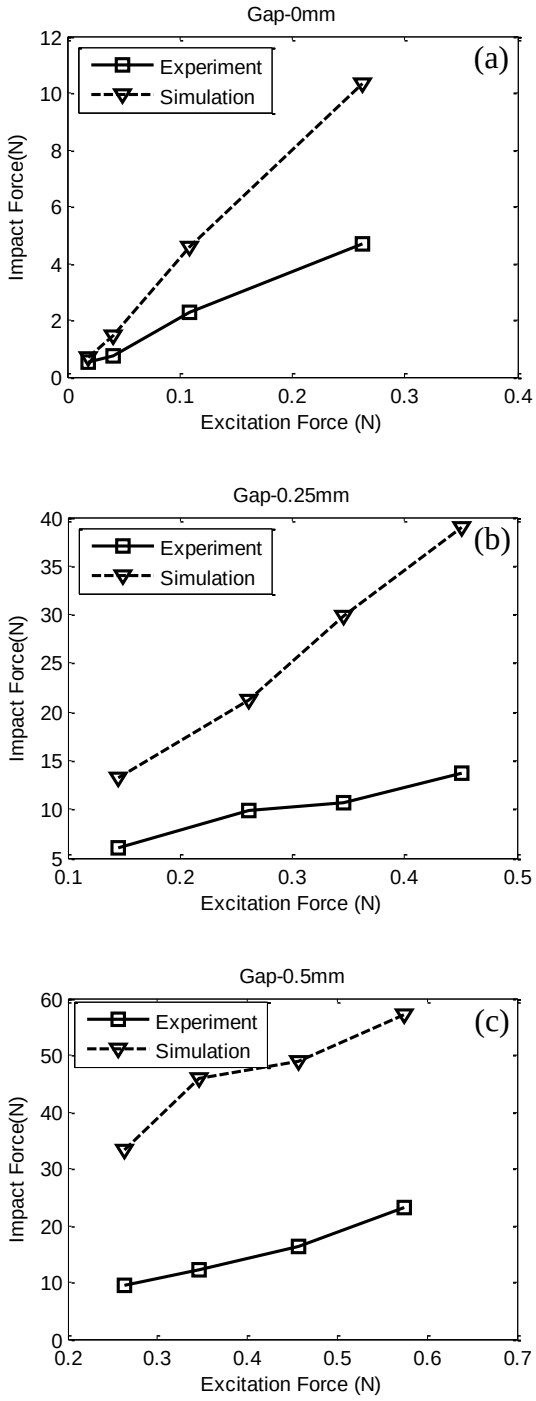

Figure 3-7 Impact forces comparison between simulations and experiments

(a) gap-0 mm (b) gap-0.25 mm (c) gap-0.5 mm.

Numerical simulations are conducted using the impact model parameters listed in Table 3-4. The simulation results indicated that choosing a number of modes higher than 20 leads to stable convergence of the numerical simulation. This is consistent with the sufficient number of modes suggested by Antunes et al. (1990) and Hassan et al. (2002). However, in this study the number of modes is chosen equal to 40 for higher accuracy.

Table 3.4 Simulation model parameters.

β	q	k	m	*N(modes)*
0.3	1	6.3e+6	infinity	40

As shown in Figure 3-7, the comparisons between the average peak impact forces in the experimental tests and numerical simulations show significant differences, when the parameter *m* is infinity. The error in the numerical simulations depends on gap size and excitation force. For 0 mm, 0.25 mm and 0.5 mm gap the simulations are off, compared to experiments, in the ranges of 0.5-2.5, 2.5-3.5 and 3.5-4, respectively.

The numerical simulation results indicate that the impact damping force obtained using the Hunt and Crossley model is associated with less than 5 percent of the total impact force. This indicates that the parameters β and q have a minor effect on the tube response. The effects of these two parameters on the tube response will be investigated in Section 3.5.3.1 in greater detail. In addition, a decrease in the contact stiffness by a factor of 0.1 leads to a 25% decrease in the average impact force. This may, however, not account for the significant differences between the experimental tests and numerical simulations.

The above differences may likely be attributed to nonlinearities in each contact stiffness coefficient. Since all the springs, in the current impact model, are assumed to be in a series, the smallest stiffness coefficient becomes the most effective one. This emphasizes the importance of the ovalization stiffness in the impact model. The ovalization stiffness, using the Morley's thin cylindrical shell (Morley, 1960), is derived based upon certain assumptions. The assumptions include a geometric limitation for the non-dimensional structural parameter χ. As this parameter is given by,

$$4\chi^4 = 12(1-\upsilon^2)\,R^2/t^2 \ , \tag{3-17}$$

where v is the Poisson ratio, R is the tube radius and t is the tube thickness. For valid of use Morley's shell equation, the dimensionless structural parameter χ must then satisfy the inequality as follows (Morley, 1960):

$$5 \leq \chi \leq 50 \,, \tag{3-18}$$

In this study, the parameter χ is estimated to be 3.69 which is out of range but not far below the lower limit of the validity range. Another assumption in Morley's model (Morley, 1960) is the type of loading which was considered as a point loading. However, in reality the loading area in the tube-support interaction is an elliptical region due to the tube diameter and longitudinal curvature during the interaction. Although the tube-support conditions may violate certain assumptions in Morley's model, the general phenomenon of ovalization during tube-support interaction is still admissible.

Therefore, to have a precise impact model, it is important to consider the nonlinearities in the force-displacement relationship by estimating a proper value for the empirical parameter m in equation (3-12). The optimal parameter is estimated by minimizing the impact force difference between the experimental tests and numerical simulations. The results indicate an optimal value of 1.67 for the parameter m. For comparison with the experimental tests, the tube-support model parameters are chosen according to Table 3.5, where analysis is done using m equal to infinity and 1.67.

Table 3.5 Tube-support simulation parameters

f_{exc}	F_{rms}	gap	m
10.5 *Hz*	0.4559 N	0.75 mm	Infinity-1.67

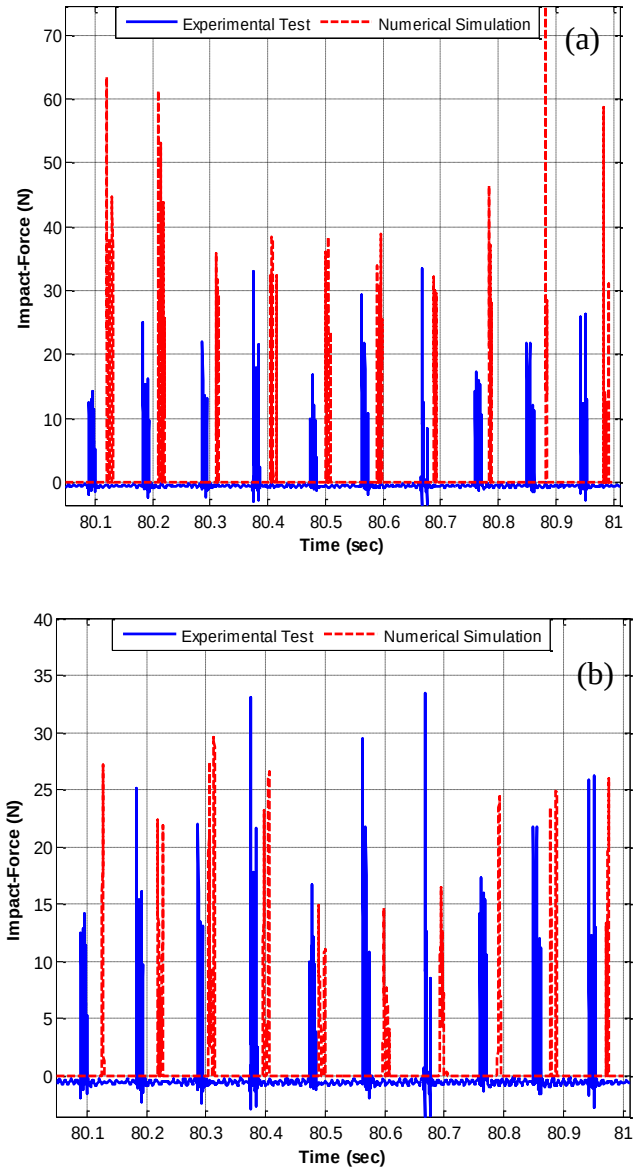

Figure 3-8 Impact force time history for the experimental test and numerical simulation using (a) *m*=infinity (b) *m*=1.67.

Seen in Figure 3-8(a), the numerical simulation, using *m* equal to infinity, overestimates the average peak impact force in the experimental test by a factor of 2.13 which indicates a significant difference. Equally or more importantly the maximum peak force is overestimated by approximately a factor of 2. A simulation conducted using the optimal parameter *m* equal to 1.67 is shown in Figure 3-8(b). The comparison shows a significant improvement in the impact force

difference which decreases to a 5% difference in the average peak impact force. The difference in maximum peak force also decreases to about 10%.

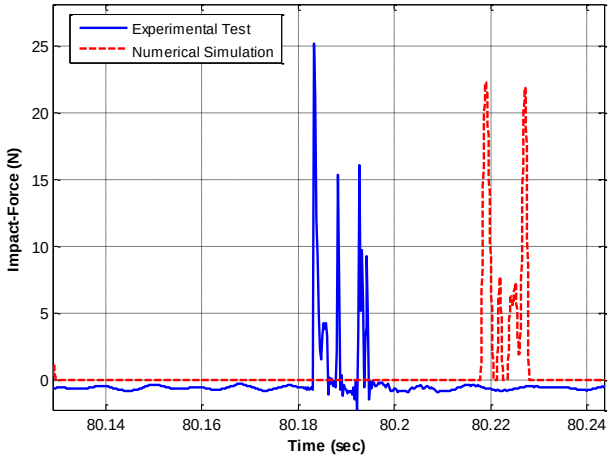

Figure 3-9 Close-up of a tube-support multiple impact during one interaction

Figure 3-9 shows a close up of the tube-support multiple impacts during an interaction using m=1.67. The result indicates a good agreement not only in the amplitude of the impact forces, but also in the number of multiple impacts and the overall interaction duration. Another comparison between the experimental tests and numerical simulations is made for the tube mid-span displacement, using the model parameters listed in Table 3.6.

Table 3.6 Tube-support experimental parameters.

f_{exc}	F_{rms}	gap	m
10.5 Hz	0.3456 N	0.25 mm	1.67

As shown in Figure 3-10, the mid-span peak to peak displacement in the numerical simulation using m=1.67, has a 20% difference with the experimental test. The difference may be explained by the different mechanisms of energy dissipation during the tube-support interaction. The elliptical motion of the tube contributes to the difference. Elliptical motion may cause energy dissipation due to friction by introducing a tangential velocity component. The elliptical motion can be explained by the non-homogeneity of the tube material, small misalignment of the forcing direction relative to the direction normal to the support and nonlinearities in the tube supports. In

spite of the existing errors in the experimental test, the difference between the numerical simulation and experimental test is still within a reasonable range.

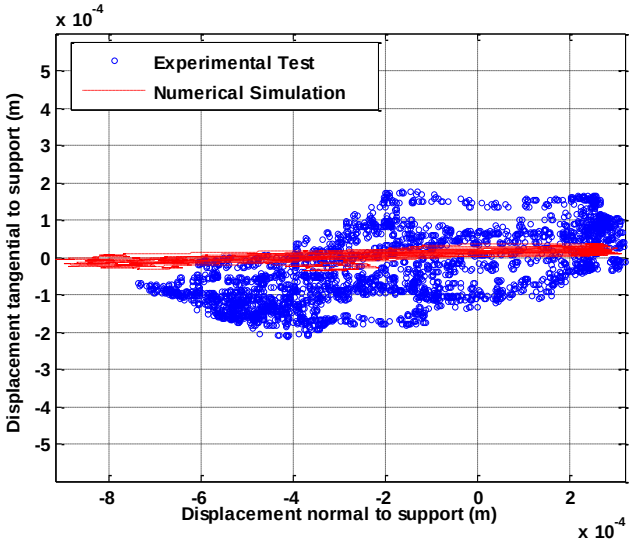

Figure 3-10 Experimental test and numerical simulation of the tube mid-span motion in the horizontal plane normal to the support.

As was shown in Figure 3-7(a), the comparisons indicate a significant difference between the experiments and simulations for $m \to \infty$. These results are reproduced in Figure 3-11 using m=1.67. The new comparisons clearly demonstrate the advantage of using the optimal parameter m.

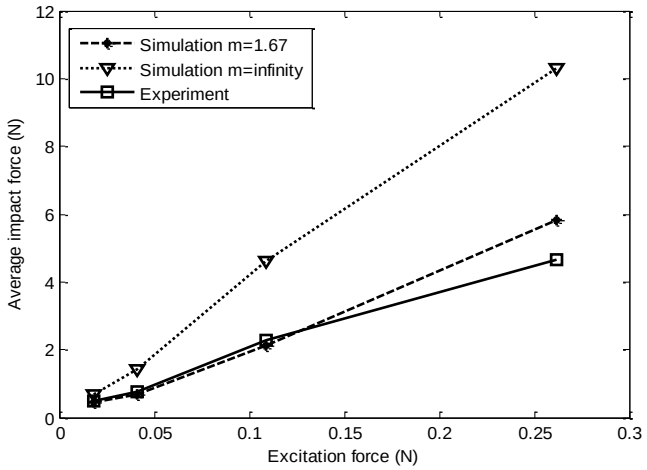

Figure 3-11 Impact force comparisons experiments and simulations for m=∞ and m=1.67.

To verify the precision of the impact model in detail, it is essential to compare the numerical simulations with the experimental tests for different boundary conditions and inputs. As shown in Figure 3-7, the comparisons between the experimental tests and numerical simulations, using the parameter *m* equal to infinity, showed significant differences. The trends indicated that nonlinearities underlay the differences. The numerical model errors can be expected to increase with an increase in gap size and excitation force magnitude. Therefore, the gap size and excitation force were chosen as variable parameters for more comparisons. As noted in Section 3.2.2, the experimental tests were done for five different gap sizes of 0, 0.25, 0.5, 0.75, 1.0 mm. For each gap size, the tube was subjected to four different excitation forces, as shown in Table 3.2.

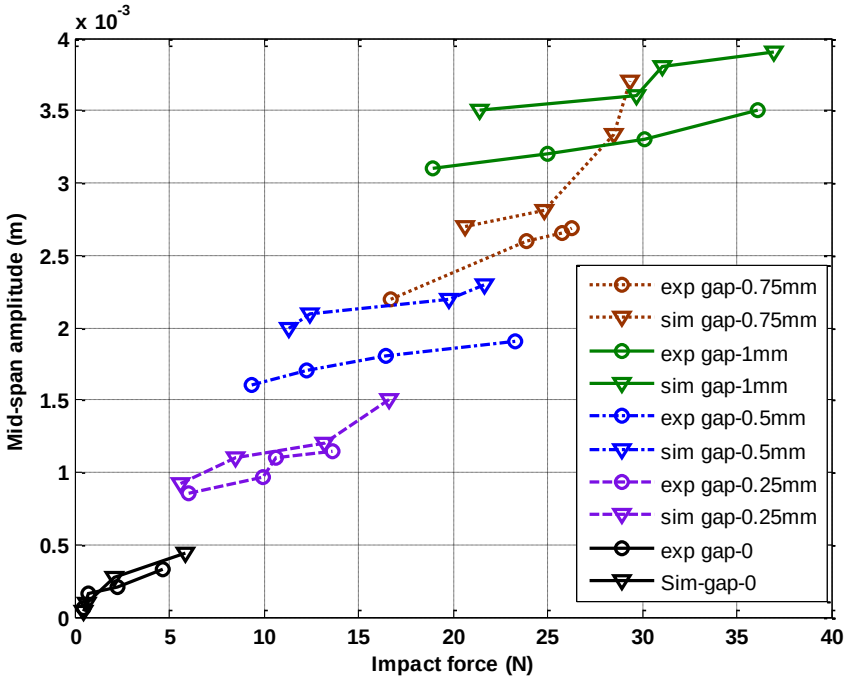

Figure 3-12 Mid-span displacements and impact forces for the experimental tests and numerical simulations.

Choosing *m* =1.67, the results of the tube mid-span displacements versus the tube-support impact forces are presented in Figure 3-12. The results indicate a good agreement between the experimental tests and numerical simulations. For each gap sizes, an increase in the excitation force may lead to a bigger difference for the impact forces and mid-span displacements.

However, the mid-span displacements have bigger percentage differences compared to the corresponding impact forces.

The differences in the impact forces and mid-span displacements are shown in Figure 3-13(a) and Figure 3-13(b), respectively. The force levels, which are presented in Figure 3-13, were obtained based on the parameters in Table 3.2.

As seen in Figure 3-13(a), the smallest difference in the impact forces is observed for the gap size of 0.5 mm and the second excitation force level. However, three zones of differences may be demarcated in Figure 3-13(a). The first zone is associated with the gap sizes bigger than 0.5 mm, the first and second levels of excitation forces. The zone corresponds to 15-20% difference in the average impact force. This difference may be explained by the tube elliptical path. The bigger gap size may cause a bigger elliptical motion for the tube in the experimental test. This motion may consequently cause more dissipation of energy. The second zone of the difference in Figure 3-13(a) is associated with gap sizes smaller than 0.5 mm, the third and fourth levels of the excitation forces. The zone corresponds to almost 20% difference in the average impact force. This difference is likely due to an underestimation of the impact energy dissipation in the numerical simulations. In addition, the experimental tests show that the tube forced vibration without support may also cause a narrow elliptical motion for the tube. This motion may be attributed to the nonlinearities associated with the tube supports. The experimental tests show that the elliptical motion of the tube may be narrowed with an increase in the excitation force magnitude. This may explain the third zone which corresponds to the smallest difference in the average impact force. This zone is found along the diagonal of Figure 3-13(a), within the region of increasing gap and increasing excitation force. The combined increases seem to decrease the offset elliptical motion of the tube and lead it to move in a narrower elliptical path which consequently improves the agreement with the numerical results.

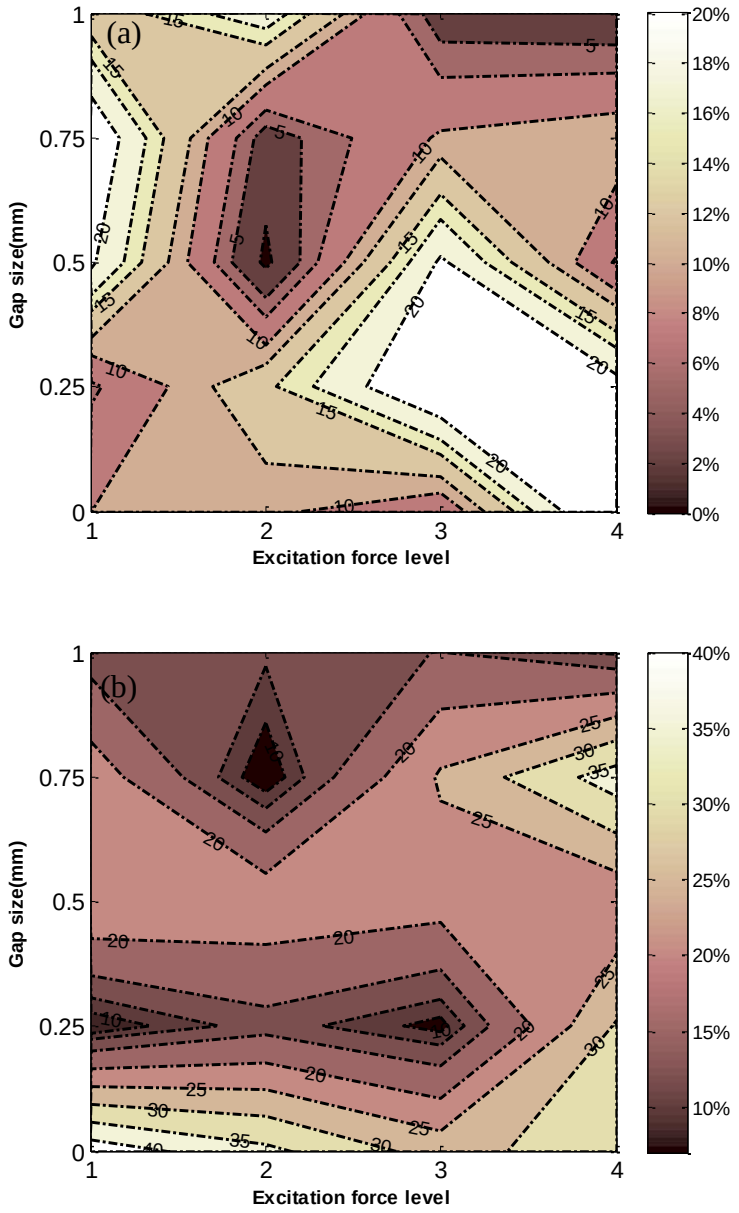

Figure 3-13 The differences between the experimental measurements and numerical simulations: (a) impact forces (b) mid-span displacements.

Figure 3-13(b) presents the mid-span displacement difference between the experimental measurements and numerical simulations as a function of excitation force level and gap size. The lowest difference is associated with two regions. The first region corresponds to 0.75 mm gap size and an excitation force of 0.4559 N. The second region corresponds to 0.25 mm gap size where the error is relatively low for the first three levels of excitation forces. As shown on the right side of Figure 3-13(b), the model error increases with increasing excitation force reaching

nearly 40 percent for the highest excitation force. This large error in the mid-span displacement cannot be explained only by the elliptical motion of the tube and dissipation of energy due to friction. The difference may also be attributed to the type of damping model incorporated in the numerical simulation. Figure 3-14 compares the change in the impact force and mid-span displacement errors with excitation force level. This may provide insight into the weaknesses of the impact damping model.

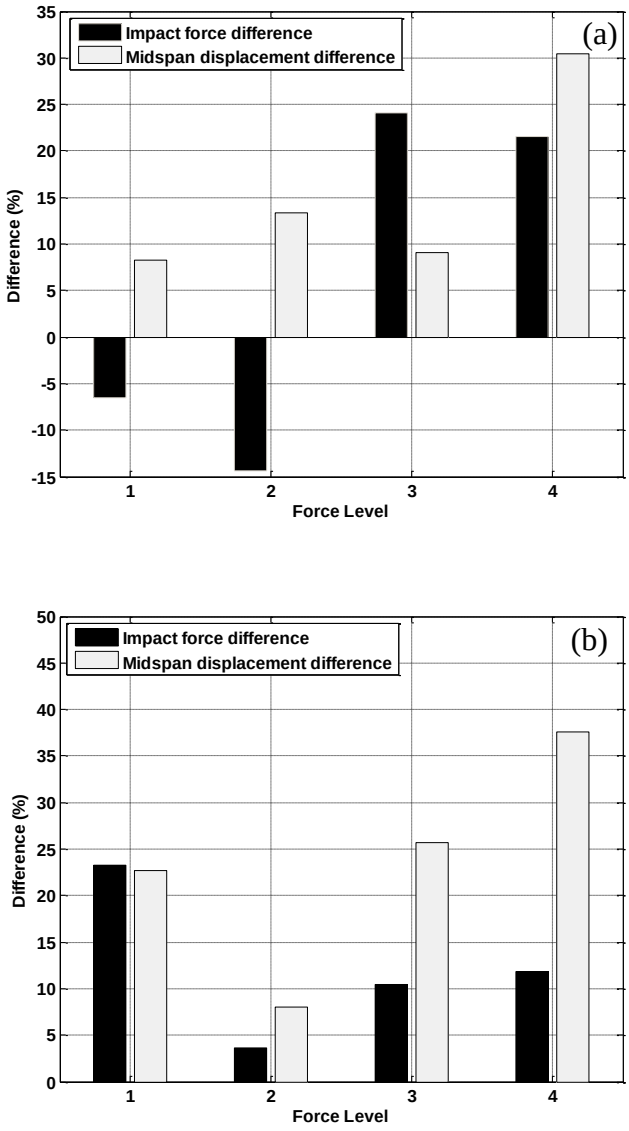

Figure 3-14 Impact force and mid-span displacement between the experimental measurements and numerical simulations (a) 0.25 mm gap size (b) 0.75 mm gap size.

Figure 3-14(a) and Figure 3-14(b) compare the differences in the impact force and mid-span displacement for 0.25 mm and 0.75 mm gap sizes, respectively. The two gap sizes are associated with the minimum difference for the mid-span displacement as shown in Figure 3-13(b).

As shown in Figure 3-14(a), the simulations underestimate the impact forces and overestimate the mid-span displacement for the low excitation forces. However, the impact force difference trend reverses by overestimating the impact force for the force levels 3 and 4. On the other hand, the mid-span displacement error gradually increases with increasing excitation force. The trends may be explained by the weak impact damping, incorporated in the numerical simulation.

For the 0.75 mm gap, Figure 3-14(b), the differences in the impact force and mid-span displacement decrease and subsequently increase with the same trend. This indicates the propagation of the impact force difference in the mid-span displacement difference. However, the change in the impact force difference, with the excitation force level, is smaller than that in the mid-span displacement, particularly after the second level of excitation force. This may also be explained by the weaknesses of the damping models, including the nonlinearities in the Hunt and Crossley model and the structural damping. In addition, the damping dissipation associated with the mounted force transducer behind the support may partially affect the differences. This may be evaluated by an increase in the gap size resulting in a smaller impact velocity. The decrease in impact velocity may lead to a lower energy dissipation associated with the Hunt and Crossley model and the force transducers, as discussed in the next section.

3.5.3 Tube-support interaction with initial displacements

As noted in Section 3.5.2, the tube mid-span displacement difference between the experimental tests and numerical simulations may be attributed to underestimation of the damping coefficients in the model. Impact damping, structural damping and friction damping dissipations are three energy dissipation mechanisms involved during the tube-support interaction. To minimize the dissipation as a result of friction, the experimental rig is designed to maintain interactions in the normal direction to the support. In this section, the effect of impact damping by the Hunt and Crossley model (Hunt and Crossley, 1975) and the structural damping

on the tube response are investigated. As noted in Section 3.2.2, to precisely study the damping effect a series of experimental tests are conducted. The experimental tests consist of exciting the tube with initial displacements in the presence of the support. Gap sizes of 0 mm, 0.25 mm, 0.5 mm, 0.75 mm and 1.0 mm are used to investigate the dynamics of interactions. The tube is subjected to four initial displacements for each gap sizes, as listed in Table 3.3. The advantage of the free vibration experimental test is it simplifies the problem by not subjecting the tube to a persistent excitation force. The damping effects may therefore be studied in greater detail.

3.5.3.1 Impact damping

As discussed in Section 3.4.2, the impact damping force is incorporated in the numerical simulation, using equation (3-16). The two parameters β and q determine the impact damping coefficients in the equation. It is important to study the effect of the coefficients on the tube-support response. Therefore, the tube mid-span displacements between the experimental test and numerical simulation are compared, using the simulation parameters listed in Table 3.7.

Table 3.7 Simulation parameters.

d_{exc}	*gap*	β	q	*N (modes)*
8.2 mm	0.25 mm	0.3	1	40

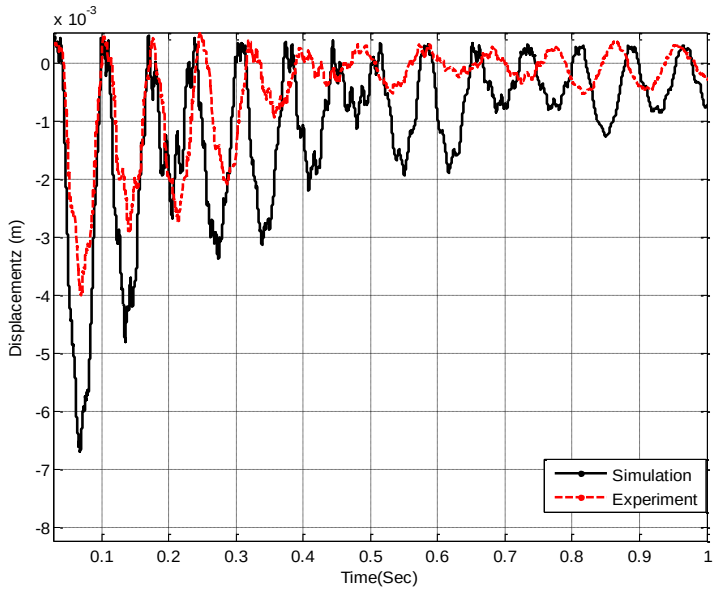

Figure 3-15 Tube-support response comparison between simulation and experiment, beginning with the first tube-support interaction.

As shown in Figure 3-15, the result indicates a significant difference of up to 55 percent in the average mid-span displacement between the experimental test and numerical simulation. The overestimation of the vibration amplitude by the numerical simulation suggests possible weaknesses in the incorporated damping models.

According to equation (3-16), β is an empirical coefficient associated with energy dissipation during impact. This coefficient is chosen in a physical range of 0.08-0.32 sec/m, to study the effect of the parameter β on the mid-span amplitude. As shown in Figure 3-16, the result indicates less than 5% difference in the tube mid-span amplitude, when β is decreased to 0.08.

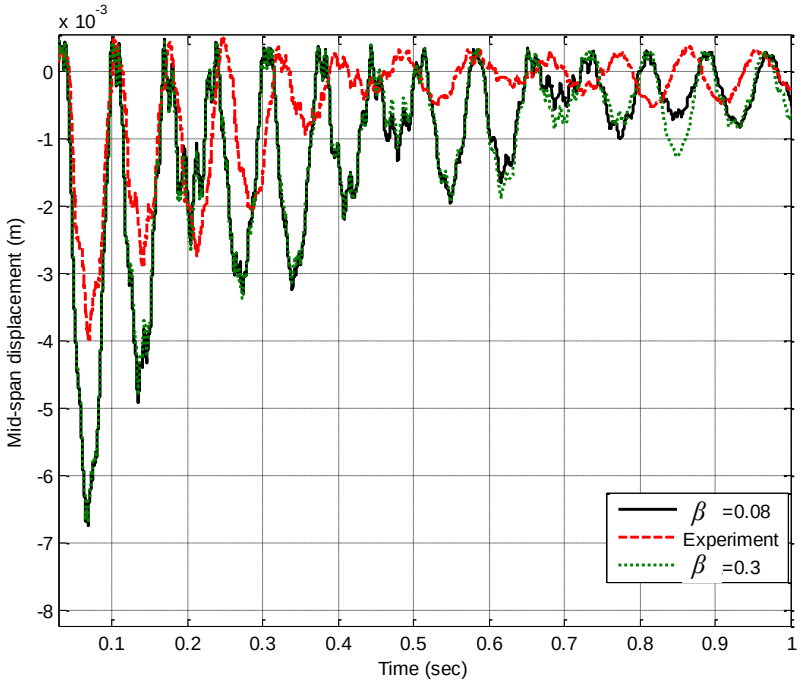

Figure 3-16 Tube-support response comparison between simulation and experiment with β=0.3 and β=0.08.

Computations were also done to investigate the effect of the parameter q on tube amplitude. As shown in Figure 3-17, the result indicates little change in the amplitude when the value of q varied between 0.5 and 1.5. In conclusion, the simulation results confirm the minimal effect of the impact damping, using the Hunt and Crossley model, on the tube response.

However, the difference in the tube amplitude between the simulation and experiment suggests the importance of other mechanisms of energy dissipation rather than impact damping.

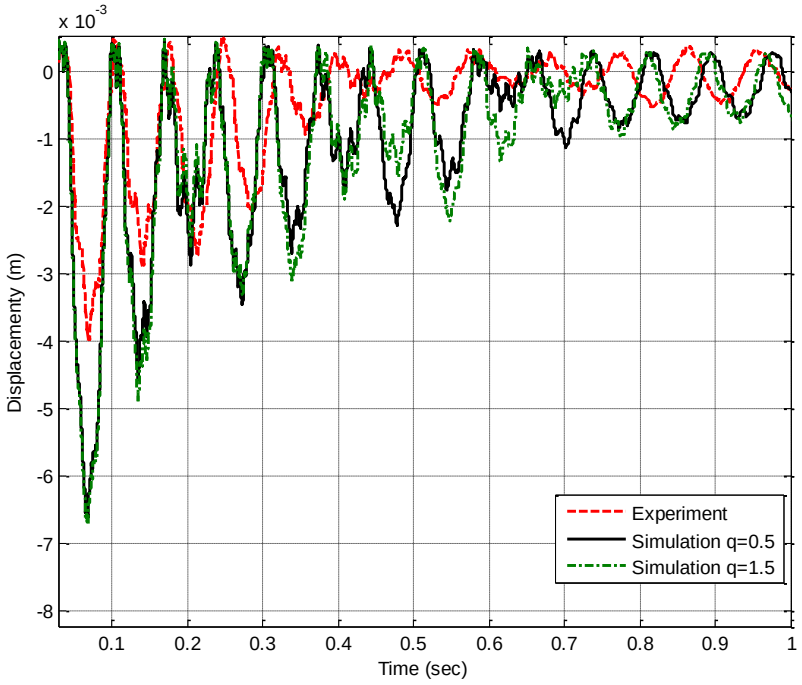

Figure 3-17 Tube-support response comparison between simulation and experiment with parameter q=0.5 and 1.5.

3.5.3.2 Structural damping

As noted in Section 3.2.2, the experimental test was designed to maintain the interaction in the normal direction to the support. Therefore, the friction energy dissipation may be a negligible source. On the other hand, the Hunt and Crossley impact damping does not have a significant effect on the tube response. One of the methods to characterize the energy dissipation is to measure the coefficient of restitution as the ratio of the velocity after and before impact. However, in a continuous system such as tube-support, the coefficient of restitution is not strictly meaningful due to chaotic multiple impact behaviour of the interaction in the short contact time (Werner and Robert, 2008). In addition, the coefficient of restitution does not represent the real phenomenon of the energy dissipation. The energy may be 'hidden' as internal elastic motions, transferred and dissipated to higher modes and propagated in the form of waves (de Weger et al., 1996).

The tube-support interaction occurs in a situation where the tube bending may impose both tensile and compressive stresses along the tube material depending on the tube-support gap. These pre-stress conditions may accompany with other stresses, associated with the impact, including ovalization, wave propagation and higher modes excitation. The mentioned pre-stress conditions may change the tube structural damping. Lesieutre (2009) studied the effect of axial loading on structural damping. The study indicated that the structural damping increases as a result of an axial compressive load and decreases as a result of axial tensile load. However, the effects of the above mentioned pre-stress conditions on the tube structural damping have not so far been studied. On the other hand, different mechanisms during the tube-support interaction, including ovalization, wave propagation and higher modes excitation may also directly affect the tube structural damping. To account for the effects of these mechanisms and the above mentioned pre-stress conditions on the tube structural damping, the structural damping model is modified by employing the parameter ε as follows:

$$\begin{cases} \sum_{n=1}^{N} \varphi_n(x) q_{nz}(t) - \Delta_1 \geq 0 \rightarrow \xi = \varepsilon \xi_s & contact \\ \sum_{n=1}^{N} \varphi_n(x) q_{nz}(t) - \Delta_1 \leq 0 \rightarrow \xi = \xi_s & no-contact \end{cases}, \tag{3-20}$$

ξ_s is the measured structural damping as shown in Figure 3-5 and ε is a coefficient representing an increase in structural damping during tube-support contact phase.

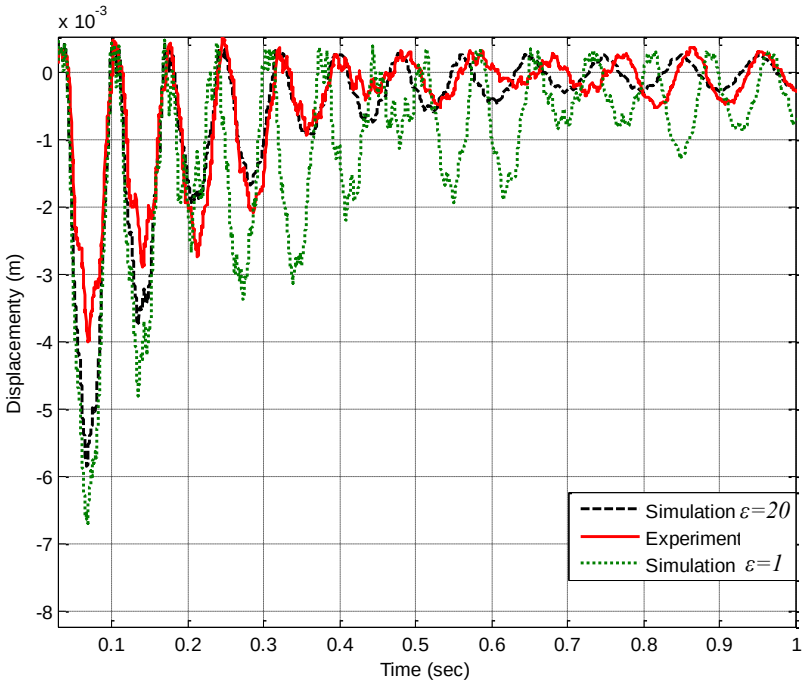

Figure 3-18 Experimental and numerical simulation of tube-support interaction for ε=1 and ε=20.

The parameter ε is adjusted to reproduce the experimental result with minimum difference possible, as shown in Figure 3-18. The simulation result indicates better agreement with the experimental result choosing the parameter ε equal to 20.

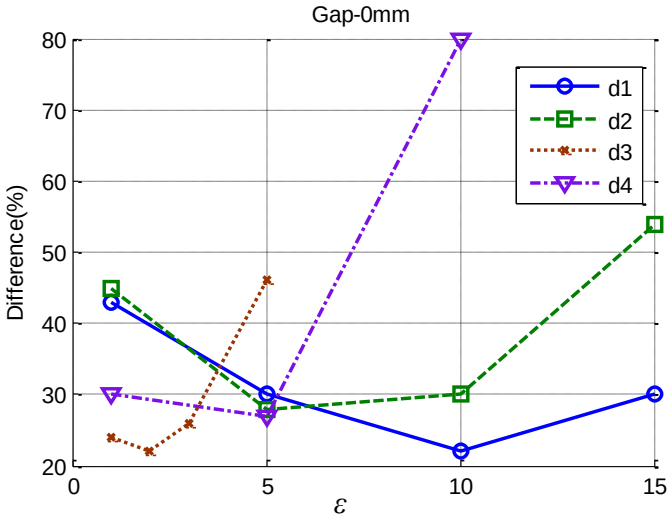

Figure 3-19 Experiment and simulation differences versus parameter ε for the initial displacements d1-d4 and gap size 0 mm.

As mentioned Section 3.2.2, the tube is subjected to four different initial displacements for each gap size, as defined in Table 3.3. Figure 3-19 shows the differences in the average peak amplitudes between the experimental tests and numerical simulations for the gap size of 0 mm. The general trends of the differences, for the four initial displacements, decrease with increasing ε until they reach optimal values. For 0 mm gap size, the range of optimal parameter ε is between 2 and 10. Having bigger magnitudes for the parameter ε, associated with the displacements d1 and d2, compared to the magnitudes, associated with the displacements d3 and d4, can be explained by nonlinearities which may cause a bigger tube-support impact inclination angle. This may then cause more energy dissipation as a result of friction hence the need for a larger value of ε to account for the higher dissipation.

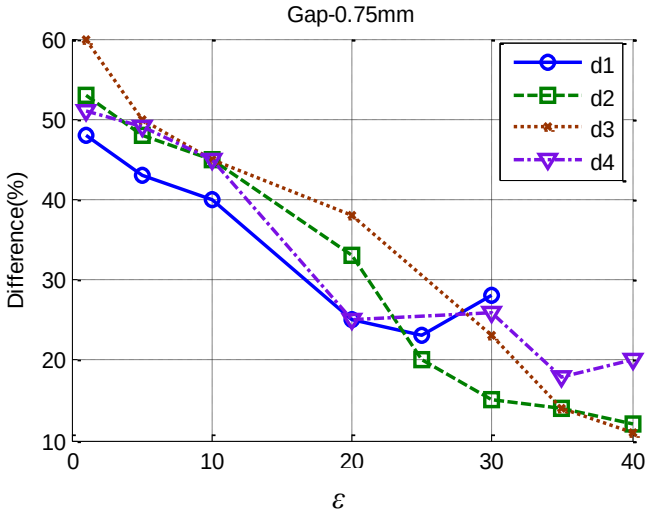

Figure 3-20 Experiment and simulation differences versus parameter ε for initial displacements d1-d4 and gap size 0.75 mm.

Figure 3-20 shows that the optimal parameter ε is in the range 25-40, for a gap size of 0.75 mm. This indicates a higher value of the parameter ε for 0.75 mm gap size compared 0 mm. The incident impact velocity of tube mid-span in the case of 0.75 mm gap size is smaller than the case of 0 mm gap size. However, the estimated parameter ε increases with decreasing incident velocity. This can be explained by higher structural energy dissipation. As noted earlier, the higher structural damping may be associated with various phenomena related to pre-stress conditions including ovalization effect, tube displacement, wave propagation and a successive multiple excitation of higher modes.

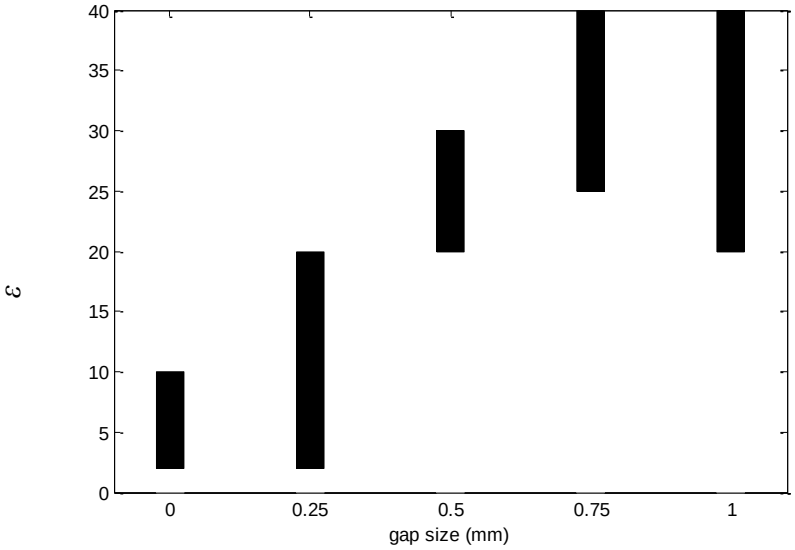

Figure 3-21 Ranges of the optimum parameter ε for different gap sizes.

Figure 3-21 shows the ranges of the optimal parameter ε for different gap sizes. The range of the parameter for each gap size is associated with four initial displacements, as noted in Section 3.2.2. The results indicate an increase in the parameter ε value as the tube-support gap size increases.

3.6 Conclusions

Impact modeling of tube-support interaction is an important step due to its role in quantifying tube fretting-wear. This study was aimed at carefully investigating the tube-support impact models, identifying the sources of differences with experimental tests and upgrading the models to better represent the dynamics of tube-support interaction. These goals were achieved by conducting a series of experimental tests and evaluating elastic and inelastic impact models for tube-support interaction.

In this work, the complicated structure of tube-support interaction in a heat exchanger was simplified to a two-span tube with a flat bar supported in the middle of the tube. The experimental rig allows one to carefully evaluate the normal impact model in a numerical simulation. The tube structural damping measurements indicated a nonlinear behaviour depending on tube displacement. The damping increased from 0.12% to 0.2% for a mid-span displacement in the range of 0.2-2.5 mm. In addition, the effects of elastic and inelastic impact

forces on the tube response were investigated, using tube-support interaction experimental data with sinusoidal excitation forces. The results confirm the minor effect of impact damping, using the Hunt and Crossley model, on total impact force. On the other hand, two elastic impact force parameters m and k were also investigated. The parameter k was estimated, using ovalization stiffness based on the Morley shell equation. The results indicated that a decrease in the parameter k by a factor of 0.1 leads to a decrease of less than 25 percent in the average impact force. In an extension of the above investigations, this study provided a unique insight into the nonlinear elastic force-displacement relation, associated with the parameter m. The results indicated that using the optimal value of 1.67 for the parameter m, significantly reduced the impact force differences between the experimental tests and numerical simulations. The comparisons for different gap sizes and excitation amplitudes indicated up to 20% difference in the impact forces and 40% difference in the mid-span displacements, using the nonlinear force-displacement relationship.

A series of experimental tests were conducted considering the tube-support interaction with a tube initial displacement as an external excitation. This enabled a detailed investigation of the tube response in a dissipative motion without continuous external excitation. The results confirmed the small effect of the Hunt and Crossley impact damping force on the tube displacement. For improved accuracy, the tube-support structural damping model was modified by introducing the coefficient ε, to increase the structural damping in the tube-support contact duration. This was explained by a variation in structural damping due to an increase in the tube stress condition. The result indicated a significant improvement in compatibility of the numerical simulations with the experimental tests using the optimal coefficient ε. Additionally, the optimal value of the coefficient was also estimated for different gap sizes and tube initial displacements. The results indicated an increasing trend for the coefficient ε, with increasing gap size.

3.7 References

Antunes, J., Axisa, F., Beaufils, B. and Guilbaud, D. (1990). Coulomb friction modelling in numerical simulations of vibration and wear work rate of multispan tube bundles. Journal of Fluids and Structures 4(3): 287-304.

Axisa, F., Antunes, J. and Villard, B. (1988). Overview of Numerical Methods for Predicting Flow-Induced Vibration. ASME Journal of Pressure Vessel Technology 110(1): 6-14.

Axisa, F., Anunes, J. and Villard, B. (1986). Overview of numerical methods for predicting flow-induced vibration and wear of heat-exchanger tubes. ASME Flow-Induced Vibration 104: 147-159.

Axisa, F., Desseaux, A. and Gibert, R. J. (1984). Experimental study of tube/support impact forces in multi-span PWR steam generator tubes. Symposium on Flow-Induced Vibrations. New Orleans, LA, USA. 6**:** 139 -148

Azizian, R., Mureithi, N. W. and Sawadogo, T. P. (2009). Dynamic modeling of heat exchanger tube-to-support Interaction. 6th CNS International Steam Generator Conference. Toronto.

Babistky, V. I. (1998). Theory of Vibro-Impact Systems and Applications. Berlin, Springer.

Bao, Z., Goyal, S., Leu, L.-J. and Mukherjee, S. (2004). The role of beam flexibility and ground contact model in the clattering of deformable beams. Journal of Dynamic Systems, Measurement, and Control 126(2): 421-425.

Bathe, K. J. (1982). Finite Element Procedures in Engineering Analysis. New Jersey, Prentice-Hall.

Chen, S., Jendrzjczyk, J. and Wambsganss, M. (1985). Dynamics of tubes in fluid with tube-baffle interaction. . ASME Journal of Pressure Vessel Technology 107: 7–17.

Davies, H. G. and Rogers, R. J. (1979). The vibration of structures elastically constrained at discrete points. Journal of Sound and Vibration 63(3): 437-447.

de Weger, J., Binks, D., Molenaar, J. and van de Water, W. (1996). Generic behavior of grazing impact oscillators. Physical Review Letters 76(21): 3951-3954.

Delaune, X., Antunes, J., Debut, V., Piteau, P. and Borsoi, L. (2010). Modal techniques for remote identification of nonlinear reactions at gap-supported tubes under turbulent excitation. ASME Journal of Pressure Vessel Technology 132(3): 031801.

Fisher, N. J. O., M. J.; Rogers, R.J.; Ko, P. L. (1989). Simulation of tube-to-support dynamic interaction in heat exchange equipment. Transactions of the ASME 111(4): 378 - 384.

Goldsmith, W. (1960). The Theory and Physical Behaviour of Colliding Solids. Bungay Suffolk, Edward Arnold LTD.

Goyal, S., Pinson, E. N. and Sinden, F. W. (1994). Simulation of dynamics of interacting rigid bodies including friction I: General problem and contact model. Engineering with Computers 10(3): 162-174.

Haslinger, K. H. and Steininger, D. A. (1995). Experimental characterization of sliding and impact friction coefficients between steam generator tubes and avb supports. Journal of Sound and Vibration 181(5): 851-871.

Hassan, M. (2000). Dynamics of loosely supported heat exchanger tubes. PhD, McMaster University.

Hassan, M. and Hayder, M. (2008). Modelling of fluidelastic vibrations of heat exchanger tubes with loose supports. Nuclear Engineering and Design 238(10): 2507-2520.

Hassan, M. A. and Rogers, R. J. (2005). Friction modelling of preloaded tube contact dynamics. Nuclear Engineering and Design 235(22): 2349-2357.

Hassan, M. A., Weaver, D. S. and Dokainish, M. A. (2002). A simulation of the turbulence response of heat exchanger tubes in lattice-bar supports. Journal of Fluids and Structures 16(8): 1145-1176.

Hassan, M. A., Weaver, D. S. and Dokainish, M. A. (2003). The effects of support geometry on the turbulence response of loosely supported heat exchanger tubes. Journal of Fluids and Structures 18(5): 529-554.

Hassan, M. A., Weaver, D. S. and Dokainish, M. A. (2005). A new tube/support impact model for heat exchanger tubes. Journal of Fluids and Structures 21(5-7): 561-577.

Hunt, K. H. and Crossley, F. R. E. (1975). Coefficient of restitution interpreted as damping in vibroimpact. ASME Journal of applied mechanics 42(2): 440-445.

Johnson, K. L. (1985). Contact Mechanics. Cambridge, Cambridge University Press.

Lesieutre, G. A. (2009). How membrane loads influence the modal damping of flexural structures. AIAA Journal 47(7): 1642-1646.

Morley, L. S. D. (1960). The thin-walled circular cylinder subjected to concentrated radial loads. The Quarterly Journal of Mechanics and Applied Mathematics 13(1): 24-37.

Nowlan, I., Ross, A. and Pettigrew, M. J. (2009). Dynamic interaction between a straight tube and an anti-vibration bar. ASME Conference Proceedings 2009(43673): 437-445.

Pettigrew, M. J. and Taylor, C. E. (2003a). Vibration analysis of shell-and-tube heat exchangers: an overview--Part 1: flow, damping, fluidelastic instability. Journal of Fluids and Structures 18(5): 469-483.

Pettigrew, M. J. and Taylor, C. E. (2003b). Vibration analysis of shell-and-tube heat exchangers: an overview--Part 2: vibration response, fretting-wear, guidelines. Journal of Fluids and Structures 18(5): 485-500.

Pettigrew, M. J., Taylor, C. E., Fisher, N. J., Yetisir, M. and Smith, B. A. W. (1998). Flow-induced vibration: recent findings and open questions. Nuclear Engineering and Design 185(2-3): 249-276.

Rogers, R. J. and Pick, R. J. (1977). Factors associated with support plate forces due to heat-exchanger tube vibratory contact. Nuclear Engineering and Design 44(2): 247-253.

Rubiolo, P. R. (2006). Probabilistic prediction of fretting-wear damage of nuclear fuel rods. Nuclear Engineering and Design 236(14–16): 1628-1640.

Sauve, R. G. and Teper, W. W. (1987). Impact simulation of process equipment tubes and support plates: a numerical algorithm. ASME Journal of Pressure Vessel Technology 109(1): 70-79.

Stoianovici, D. and Hurmuzlu, Y. (1996). A critical study of the applicability of rigid-body collision theory ASME Journal of Applied Mechanics 63(2): 307-316.

Stronge, W. J. (2000). Impact Mechanics. Cambridge, Cambridge Unviversity Press.

Subbaraj, K. and Dokainish, M. A. (1989). A survey of direct time-integration methods in computational structural dynamics II. Implicit methods. Computers and Structures 32(6): 1387-1401.

Tan, X. and Rogers, R. (1996). Dynamic friction modelling in heat exchanger tube simulations. Flow-Induced Vibrations. Montreal, ASME. 328**:** 347–358.

Tariku, F. A. and Rogers, R. J. (2001). Improved Dynamic Friction Models for Simulation of One-Dimensional and Two-Dimensional Stick-Slip Motion. Journal of Tribology 123(4): 661-669.

Thomson, M. G., Bishop, S. R. and Foale, S. (1994). An experimental study of low velocity impact. Machine Vibration 3: 10-17.

Toorani, M., Pan, L., Li, R., Idvorian, N. and Vincent, B. (2009). Advanced nonlinear flow-induced vibration and fretting-wear analysis capabilities. 6th CNS International Steam Generator Conference,. Toronto.

Wagg, D. J. and Bishop, S. R. (2000). A note on modeling multi-degree-of-freedom vibro-impact systems using coefficient of restitution models. Journal of Sound and Vibration 236(1): 176-184.

Weaver, D. S. and Schneider, W. (1983). The effect of flat bar supports on the crossflow induced response of heat exchanger U-tubes. ASME Journal of Engineering for Power 105(4): 775-781.

Werner, S. and Robert, S. (2008). Impacts on beams. Computational Structural Dynamics and Earthquake Engineering, Taylor & Francis**:** 137-148.

Yetisir, M. and Fisher , N. J. (1997). Prediction of pressure tube fretting-wear damage due to fuel vibration. Nuclear Engineering and Design 176: 261-271.

CHAPTER 4
GENERAL DISCUSSION

This chapter will summarize the main objectives of the thesis and evaluate them with brief discussions. The chapter is divided into four sections. The first Section 4.1 briefly outlines and reviews the objectives. Section 4.2 lists the main conclusions with further discussions. In Section 4.3 the main contributions made in this study are presented, and finally Section 4.4 contains recommendations for future research in the area.

4.1 Review of Objectives

The objectives of this Thesis were listed in Section 1.3, so in conclusion it may be beneficial to evaluate the progress made through this research and highlight its achievements. As noted in this thesis introduction, this research was directed towards developing and evaluating friction and impact models to improve the estimation of tube-support fretting-wear.

The first objective was to design and develop a friction model to represent the real bristle behavior from zero velocity to the gross-slip state. To achieve this goal, the tangential stress distribution within the contact region was studied. Based upon this distribution, a hybrid spring-damper friction model was designed to demarcate the elastic, plastic and partial-slipping regions during the friction process.

The second objective of the research was to study the effect of the break-away force and Stribeck phenomenon on the stick-slip regime. The study emphasized the importance of considering the above effects in a friction model. This objective was materialized by comparing the stick-slip regimes in the velocity-limited and LuGre friction models.

The third objective was to conduct a series of experiments designed to measure the impact forces and mid-span displacements. Therefore, the complicated structure of the tube-support interaction in a heat exchanger was simplified to a two-span tube with a flat support at mid-span. Tests were conducted for different gap sizes and excitation amplitudes. The results were then used to validate the tube-support interaction dynamics model.

The fourth objective was to develop a numerical code to simulate the tube-support dynamic interaction. This code was developed using the Euler-Bernoulli beam theory and the modal superposition technique. The numerical computations were performed based upon the forth-order Runge-Kutta algorithm in Simulink.

The fifth objective was directed towards the analysis of the nonlinearity in the force-displacement relation, during tube-support interaction. An investigation was conducted comparing impact forces in experimental tests to numerical simulations. To carefully study the dynamics of this interaction, different gap sizes and excitation amplitudes were considered.

The sixth objective was to study the source of energy dissipation during the tube-support interaction. To achieve this goal, a series of the tube-support experiments were conducted, where the tube initial displacement was adopted as the excitation force. Finally, the effects of the Hunt and Crossley damping and the structural damping on the mid-span displacement were also investigated.

4.2 Further Discussion

Detailed discussions on the friction and impact models were presented in Chapters 2 and 3. In this Section, overall discussions and main conclusions of the research are presented.

4.2.1 Friction model discussion

The friction model discussion is geared to look at the hybrid spring-damper friction model, which was developed to accurately estimate the slipping distance. To analyze the various developments, the stick-slip regime of a simple mass-spring system was investigated by implementing different forcing functions. Two different friction models including the velocity limited-friction model and LuGre friction model were incorporated into the system. Applying a constant pulling velocity as the external excitation, a slipping time difference of up to 5 percent was reported between the two friction models. The difference was mainly attributed to the conceptual design of the friction models. In the LuGre model, the varying break-away force and the Stribeck effect played an important role to define the stick-slip regime. This was demonstrated by an increase in the magnitude of the constant pulling velocity in the range of 0.1-

0.3 m/s, which led to a decrease in the break-away force in the range of 1.26-1.39N. Additionally, the ability of the velocity-limited and LuGre friction models to accurately detect the stick-slip region was examined by implementing a chirp function, which is a frequency varying function. For the chirp excitation force with the frequency range of 1-5 Hz, the slipping time difference of 1-2 percent was found. However, an increase in the target frequency to 1-10 Hz led to a difference of 10 percent. This increase in the difference was then explained based upon the inability of the velocity-limited friction model to adjust the magnitude of the limiting velocity based upon the change in the break-away force.

Further detailed analysis of the LuGre friction equations inspired the idea to develop an equivalent spring-damper model. The equivalent model attributed physical meaning to the mathematical functions. This is valuable because it associates the physical parameters such as the Stribeck damping, bristle stiffness and bristle damping to the friction model parameters. However, the reorganization of the mathematical equation to a spring-damper model leads to a 5-10 percent difference in the slipping-time between the two models. Despite this difference developing a physical hybrid model, which may represent the real behavior of the bristle in the contact region, is clearly beneficial. In the development, the comprehensive study of the tangential stress distribution within the contact region was essential. As mentioned in the state of the art review, Cattaneo (1938) and Mindlin (1949) associated a tangential stress distribution to the real bristle behavior within the contact region. The stress distribution was established based upon the different regions of elastic and partial slipping. As an extension, Mindlin and Deresiewicz (1953) determined the energy dissipation associated to the partial-slipping region. Furthermore, Odfalk and Vingsbo (1992) upgraded the tangential stress distribution by considering the plastic deformation and yielding effect within the contact region. As shown in Figure 4-1, the contact region was demarcated into the three main regions of elastic, plastic and partial-slipping based upon the above tangential stress distributions. This led to associating a spring or damper to each region based upon the elastic or inelastic behaviors.

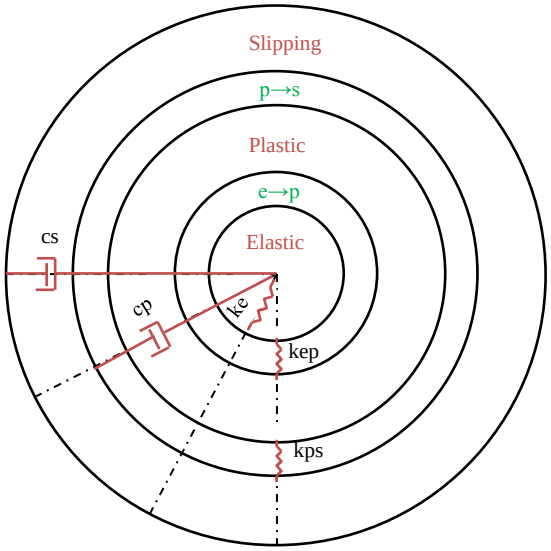

Figure 4-1 Displacement field in the contact area and hybrid spring-damper model.

As a result, the conceptual design of the phenomena led to the development of the hybrid spring-damper friction model shown in Figure 4-2.

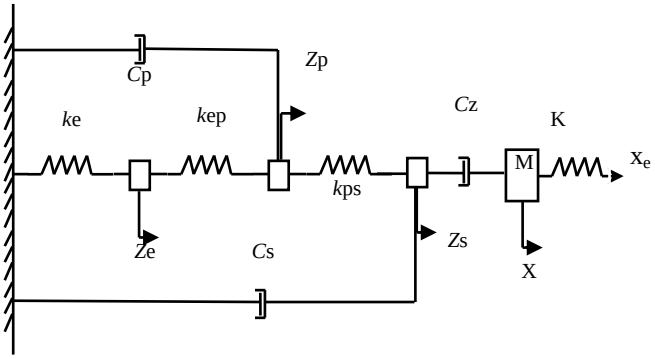

Figure 4-2 New hybrid spring-damper friction model.

The research also examined the ability of the hybrid model to reproduce experimental tests. The examination presented several challenges due to the estimation of the model parameters. The parameters were therefore divided into two main groups, the first group including the parameters associated with the pre-sliding displacement and the second the general gross-slip phase parameters. An inverse numerical method was then adopted to estimate the model parameters. The displacement-time history was compared among the Ozaki and Hashiguchi model (Ozaki and Hashiguchi, 2010), the experimental tests conducted by Baumberger et al. (Baumberger et al., 1994) and the hybrid spring-damper model. The

comparisons confirmed a better reproduction of the experimental tests, both qualitatively and quantitatively, by using the hybrid spring-damper model rather than the Ozaki and Hashiguchi model.

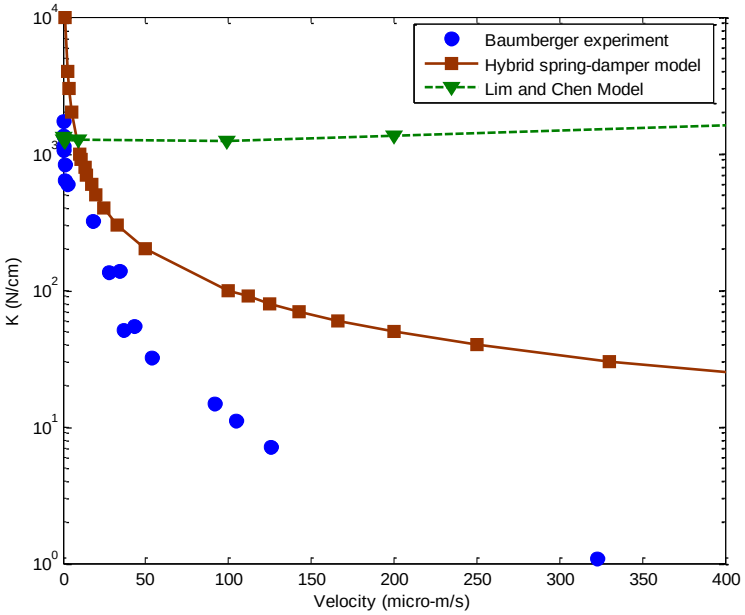

Figure 4-3 K-V dynamic phase diagram for the stick-slip stability for the Baumberger experimental test (Baumberger et al., 1994) , Lim and Chen model (Lim and Chen, 1998) and Hybrid spring-damper model.

Furthermore, the stability dynamic phase diagram was considered for detailed comparisons between the models. As shown in Figure 4-3, the Baumberger experimental test (Baumberger et al., 1994) was compared with the Lim and Chen theoretical model (Lim and Chen, 1998) and the hybrid spring-damper friction model. As reported in the Lim and Chen study, their model has a weakness when reproducing the correct slope of the stability diagram. The results indicated that the model mostly approximates the stability diagram with a constant line which does not represent the system behavior particularly for the creep dominated regions. On the other hand, the hybrid spring-damper friction model reproduced the experimental stability diagram with a qualitatively good agreement. However, the magnitude of the stability velocity has some differences with the experimental test. The differences may have different interpretations in the different regions of the stability diagram: in the region with the high spring stiffness, the difference may be mostly associated with the underestimation of the Stribeck velocity. A higher Stribeck velocity leads to a lower stability velocity. On the other hand, in the

region with the lower spring stiffness, the differences may be mostly associated with the underestimation of the damping coefficients in the hybrid friction model.

4.2.2 Impact model discussion

The impact model in the tube-support dynamic interaction was also studied. The first step in the research was to conduct a series of experiments to create a reference database for the numerical code validation. The structural damping measurements of the tube indicated nonlinearity in the damping magnitude which was dependent on the tube mid-span amplitude. For instance, structural damping coefficients of 0.12-0.18 were obtained for the mid-span displacements of 0.2-2.5 mm. The comparisons of the tube mid-span displacement without the supports present indicated 2 to 8 percent differences between the experimental tests and numerical simulations. The results provided credence to the accuracy of the magnitude of the modal parameters incorporated in the numerical simulation. To study the force-displacement relation during the tube-support interaction, experimental tests were conducted with different gap sizes and excitation amplitudes. As discussed in Section 3.5.2, a linear force-displacement assumption led to a significant difference between the impact force in the experimental tests and numerical simulations. The difference became larger with increasing gap size and excitation force. In addition, the study of the empirical parameter, *m*, in Equation 3-13, indicated the sensitivity of the response to the parameter magnitude. As a result, the optimal parameter, *m*, equal to 1.67 was deduced to minimize difference between the experimental measurements and numerical simulations.

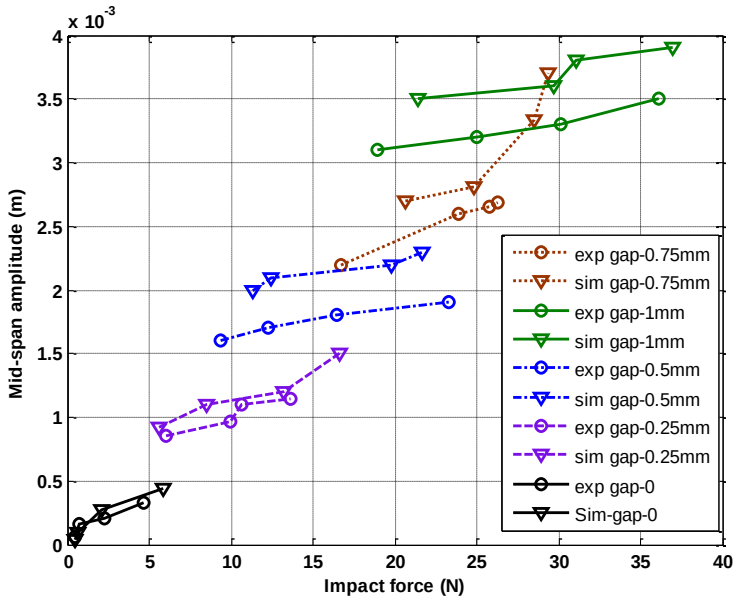

Figure 4-4 Mid-span displacements and impact forces for the experimental tests and numerical simulations.

As shown in Figure 4-4, the diagram of the mid-span displacement versus the impact force shows a reasonable agreement between the experimental tests and numerical simulations using the optimal parameter. The results indicated up to 20 percent difference for the impact forces and 40 percent difference for the mid-span displacements. As noted in Section 3.5.2, the differences originated mainly from the error associated with the tube elliptical motion and weaknesses of the incorporated damping model. This led us to study the energy dissipation during the tube-support interaction in great detail. The study consisted of a series of experimental tests for the tube-support interaction adopting the tube initial displacements as the origin of the excitation force. The experimental tests allowed careful examination of the damping model. The experimental tests and numerical simulation comparisons indicated a significant difference in the mid-span displacements, which was mainly attributed to the damping model. This necessitated the investigation of the Hunt and Crossley damping model based upon equation (3-16). In the damping model, the two parameters, β and q, were varied in the physical range of 0.08-0.32 sec/m and 0.5-1.5, respectively. The results indicated less than 5 percent difference in the tube mid-span displacement for these parameter variations. The energy dissipation was then interpreted based upon a higher structural damping coefficient during the interaction. Thus, the structural damping was modified by introducing the parameter, ε, according to Equation 3-20. To

have reasonable agreements between the experimental tests and numerical simulations, the magnitude of the parameter, ε, was then estimated as shown in Figure 4-5.

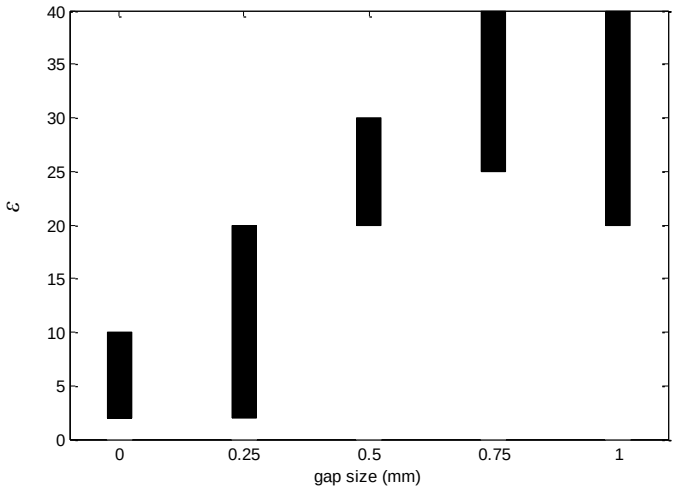

Figure 4-5 Range of the optimum parameter ε for different gap sizes.

4.3 Main Contributions

This study was conceptualized to better estimate fretting-wear during the tube-support interaction. The two quantities on which the work-rate is mainly dependent are the normal force and sliding distance. The study therefore focused mainly on the improvement and upgrade of the related friction and impact models.

In evaluating the relevance of this study, the primary contribution was the development of a new hybrid spring-damper friction model. The model was developed based upon the tangential stress distribution within the contact region. The model is able to demarcate the different regions of elastic, plastic and partial-slipping during the friction process. The Stribeck stick-slip transition effect was also incorporated in the model in the form of a nonlinear damper. The model makes it possible for the work-rate calculation to associate different wear coefficients to different regions in the friction process. The friction model was then compared against the Baumberger et al. experimental test (Baumberger et al., 1994). The comparison indicated a reasonable compatibility with the dynamic phase diagram of the stick-slip stability. Furthermore, the weakness that exists in the Lim and Chen friction model (Lim and Chen, 1998) to reproduce the slope of the dynamic phase diagram was significantly overcome by the new hybrid elasto-plastic friction model.

Secondly this research also contributes to improve and upgrade the impact model for tube-support interaction. The improvement was achieved by studying the tube-support elastic and inelastic impact models. The first stage of the study was to conduct experimental tests for the tube-support interaction as a reference to carefully evaluate the impact model. The experimental tests were subsequently advanced to different gap sizes and excitation amplitudes to study the dynamics of the interaction. The second stage was to study the elastic impact model and the nonlinearity involved in the force-displacement relation. These analyses were able to estimate an empirical parameter associated with the nonlinearity, which significantly reduces the difference between impact forces in the numerical simulations and experimental tests. The third stage was to analyze the inelastic impact model. This objective was accomplished by conducting a series of tube-support experimental tests using a tube initial displacement as an external excitation. The study demonstrated the minor effect of the Hunt and Crossley inelastic impact model on the tube response. Therefore, the difference in the mid-span displacement was interpreted as resulting from the energy "dissipation" in the forms of the higher mode excitation, wave propagation and ovalization.

4.4 Recommendations for Future Work

In pursuance of this or similar research in the future, the following recommendations are put forward:

1) Performance of experimental tests to produce the stability phase diagram for the case of the tube and support. This will require an accurate measuring instrument to precisely measure the pre-sliding displacement. The results may be used to estimate the parameters of the new hybrid spring-damper friction model for the case of the tube-support interaction;
2) A study of the effect of the variation of the normal force on the pre-sliding displacement;
3) Experimental investigation of the tube-support oblique interaction may also be beneficial to precisely evaluate the energy dissipation due to friction force;
4) Performance of tube-support experimental test in the presence of fluids would be useful for the evaluation of squeeze-film effects and viscous friction.

CONCLUSIONS

This thesis mainly focused on accurate estimation of work-rate which is an important parameter to quantify fretting-wear during tube-support interaction. The work-rate is mostly dependent upon two factors, sliding distance and normal force. Therefore, this study consisted of two main parts including the development of a new hybrid spring-damper friction model and upgrading tube-support impact model.

In the first part of this study, the weaknesses and advantages of the velocity-limited and the LuGre friction models, to detect stick-slip regions, were investigated. This achieved by examining the ability of these friction models to demarcate the stick-slip motion of a simple mass-spring system subjected to different types of pulling velocity. The results underlined the importance of the varying break-away force and the Stribeck effects on the estimation of the sliding distance. In addition, the incorporations of the Stribeck effect and the presliding damping in the LuGre mathematical formulations were studied. This led to the development of an extended LuGre model using an equivalent spring-damper system which attributes physical meanings to the mathematical functions. Additionally, a new hybrid elasto-plastic friction model was developed by considering different regions during the friction process from zero velocity to the gross-slip state. This was achieved by demarcating elastic, plastic and partial slipping displacements using the tangential stress distribution within the contact area. Finally, the new hybrid spring-damper friction model was examined using the Baumberger et al. experimental tests and the Lim and Chen friction model. The stability velocity phase diagram was chosen to make the comparisons between the experimental tests and numerical simulations. The results indicated better agreement between the experimental tests and numerical simulations using the new hybrid friction model compared to the Lim and Chen friction model.

The second part of this study investigated the normal impact model during the tube-support interaction. This was achieved by undertaking an experimental program for the tube-support interaction as a reference database. The experimental tests were conducted for different combinations of the tube-support gap size and excitation force to carefully investigate the dynamics of the interaction. This interaction was then simulated using the Euler-Bernoulli beam

theory and the modal superposition technique. The elastic and inelastic normal impact models were also investigated. The impact force comparisons between the experimental tests and numerical simulations underlined a nonlinear force-displacement relationship. This relationship was defined by the estimation of the empirical parameter m equal to 1.67. The numerical simulations and experimental test comparisons indicated a significant reduction, up to 20 percent, in the differences by adopting the nonlinear force-displacement relationship. In addition, the inelastic impact force was investigated. The results indicated the minor effect of the Hunt and Crossley impact model on the tube response. For improved accuracy, the structural impact model was modified by adopting the empirical parameter ε. The optimal value for the parameter ε was estimated for different gap sizes and excitations. The result indicated a good agreement between experimental results and numerical simulation using the optimal parameter ε.

REFERENCES

Antunes, J., Axisa, F., Beaufils, B. and Guilbaud, D. (1990). Coulomb friction modelling in numerical simulations of vibration and wear work rate of multispan tube bundles. Journal of Fluids and Structures 4(3): 287-304.

Argon, A. S. and Im, J. (1975). Cavity formationfrom inclusion in ductile fracture. Metallurgical and Materials Transactions 6(4): 825-837.

Armstrong-Helouvry, B. (1991). Control of machines with friction. Boston, Kluwer.

Armstrong, B. (1990). Control of machines with non-linear, low-velocity friction: A dimensional analysis. Experimental Robotics I. Heidelberg, Springer 139**:** 180-195.

Armstrong, B. and Qunyi, C. (2008). The Z-properties chart. IEEE Control Systems 28(5): 79-89.

Armstrong, D. and Canudas, C. (1994). A survey of models, analysis tools and compensation methods for the control of machines with friction. Automatica 30(7): 1083-1138.

Astrom, K. J. and Canudas de Wit, C. (2008). Revisiting the LuGre friction model. Control Systems, IEEE 28(6): 101-114.

Attia, H., Gessesse, Y. B. and Osman, M. O. M. (2007). New parameter for characterizing and correlating impact-sliding fretting wear to energy dissipation--experimental investigation. Wear 263(1-6): 419-429.

Attia, M. H. and Magel, E. (1999). Experimental investigation of long-term fretting wear of multi-span steam generator tubes with U-bend sections. Wear 225-229(1): 563-574.

Axisa, F., Antunes, J. and Villard, B. (1988). Overview of Numerical Methods for Predicting Flow-Induced Vibration. ASME Journal of Pressure Vessel Technology 110(1): 6-14.

Axisa, F., Anunes, J. and Villard, B. (1986). Overview of numerical methods for predicting flow-induced vibration and wear of heat-exchanger tubes. ASME Flow-Induced Vibration 104: 147-159.

Axisa, F., Desseaux, A. and Gibert, R. J. (1984). Experimental study of tube/support impact forces in multi-span PWR steam generator tubes. Symposium on Flow-Induced Vibrations. New Orleans, LA, USA. 6**:** 139 -148

Azizian, R., Mureithi, N. W. and Sawadogo, T. P. (2009). Dynamic modeling of heat exchanger tube-to-support Interaction. 6th CNS International Steam Generator Conference. Toronto.

Babistky, V. I. (1998). Theory of Vibro-Impact Systems and Applications. Berlin, Springer.

Bao, Z., Goyal, S., Leu, L.-J. and Mukherjee, S. (2004). The role of beam flexibility and ground contact model in the clattering of deformable beams. Journal of Dynamic Systems, Measurement, and Control 126(2): 421-425.

Bathe, K. J. (1982). Finite Element Procedures in Engineering Analysis. New Jersey, Prentice-Hall.

Baumberger, T., Heslot, F. and Perrin, B. (1994). Crossover from creep to inertial motion in friction dynamics. Nature 367(6463): 544-546.

Canudas de Wit, C., Olsson, H., Astrom, K. J. and Lischinsky, P. (1995). A new model for control of systems with friction. IEEE Transactions on Automatic Control 40(3): 419-425.

Cattaneo, C. (1938). Sul contato di due corpo elastici. Accademia dei Lincei, Rendiconti, 27: pp342-348, 434-436, and 474-478.

Chen, S., Jendrzjczyk, J. and Wambsganss, M. (1985). Dynamics of tubes in fluid with tube-baffle interaction. . ASME Journal of Pressure Vessel Technology 107: 7–17.

Chen, S. S. (1991). Dynamic tube/support interaction in heat exchanger tubes. Washington, DC Argonne National Lab**:** 1-28.

Dahl, P. R. (1968). A solid friction model, Technical report, Space and Missile Systems Organization Air Force Systems Command.

Davies, H. G. and Rogers, R. J. (1979). The vibration of structures elastically constrained at discrete points. Journal of Sound and Vibration 63(3): 437-447.

de Weger, J., Binks, D., Molenaar, J. and van de Water, W. (1996). Generic behavior of grazing impact oscillators. Physical Review Letters 76(21): 3951-3954.

Delaune, X., Antunes, J., Debut, V., Piteau, P. and Borsoi, L. (2010). Modal techniques for remote identification of nonlinear reactions at gap-supported tubes under turbulent excitation. ASME Journal of Pressure Vessel Technology 132(3): 031801.

Dierecks, D. R., Shak, W. J. and Muscara, J. (1996). Overview of steam generator tube degredation and integrity. Argonne,Illinois, Argonne National Laboratory.

Dieterich, J. H. (1978). Time-dependent friction and the mechanics of stick-slip. Pure and Applied Geophysics 116(4): 790-806.

Dupont, P., Hayward, V., Armstrong, B. and Altpeter, F. (2002). Single state elastoplastic friction models. IEEE Transactions on Automatic Control 47(5): 787-792.

Fisher, N. J., Han, Y. and Taylor, C. E. (2001). Threory manual VIBIC code. Chalk River.

Fisher, N. J., Ing, J. G., Pettigrew, M. J. and Rogers, R. J. (1992). "Tube-to-support dynamic interaction for a multispan steam generator tube." Proceedings ASME Congress on Pressure Vessels and Piping 242: 301-316.

Fisher, N. J. O., M. J.; Rogers, R.J.; Ko, P. L. (1989). Simulation of tube-to-support dynamic interaction in heat exchange equipment. Transactions of the ASME 111(4): 378 - 384.

Fleming, J. R. and Suh, N. P. (1977). Mechanics of crack propagation in delamination wear. Wear 44: 39-56.

Fouvry, S., Kapsa, P., Zahouani, H. and Vincent, L. (1997). Wear analysis in fretting of hard coatings through a dissipated energy concept. Wear 203-204: 393-403.

Gauland, D. J. and Duquette, D. J. (1980). Cyclic wear behavior (Fretting) of a tempered martensite steel. Metallurgical Transactions 11(9): 1581-1588.

Gessesse, Y. B. (2000). On the fretting wear of nuclear power plant heat exchanger tubes using a fracture mechanics approach: Theory and verification. Ph.D, Concordia University

Gessesse, Y. B. and Attia, M. H. (2004). On the mechanics of crack Initiation and propagation in elasto-plastic materials in impact fretting wear. Journal of Tribology 126(2): 395-403.

Goldsmith, W. (1960). The Theory and Physical Behaviour of Colliding Solids. Bungay Suffolk, Edward Arnold LTD.

Goyal, S., Pinson, E. N. and Sinden, F. W. (1994). Simulation of dynamics of interacting rigid bodies including friction I: General problem and contact model. Engineering with Computers 10(3): 162-174.

Haslinger, K. H., Martin, M. L. and Steininger, D. A. (1990). Experimental characterization of fluid and squeeze film effects in heat exchanger tube supports. Journal of Fluids and Structures 4(6): 605-629.

Haslinger, K. H. and Steininger, D. A. (1995). Experimental characterization of sliding and impact friction coefficients between steam generator tubes and avb supports. Journal of Sound and Vibration 181(5): 851-871.

Hassan, M. (2000). Dynamics of loosely supported heat exchanger tubes. PhD, McMaster University.

Hassan, M. and Hayder, M. (2008). Modelling of fluidelastic vibrations of heat exchanger tubes with loose supports. Nuclear Engineering and Design 238(10): 2507-2520.

Hassan, M. A. and Rogers, R. J. (2005). Friction modelling of preloaded tube contact dynamics. Nuclear Engineering and Design 235(22): 2349-2357.

Hassan, M. A., Weaver, D. S. and Dokainish, M. A. (2002). A simulation of the turbulence response of heat exchanger tubes in lattice-bar supports. Journal of Fluids and Structures 16(8): 1145-1176.

Hassan, M. A., Weaver, D. S. and Dokainish, M. A. (2003). The effects of support geometry on the turbulence response of loosely supported heat exchanger tubes. Journal of Fluids and Structures 18(5): 529-554.

Hassan, M. A., Weaver, D. S. and Dokainish, M. A. (2005). A new tube/support impact model for heat exchanger tubes. Journal of Fluids and Structures 21(5-7): 561-577.

Heslot, F., Baumberger, T., Perrin, B., Caroli, B. and Caroli, C. (1994). Creep, stick-slip, and dry-friction dynamics: Experiments and a heuristic model. Physical Review E 49(6): 4973.

Hess, D. P. and Soom, A. (1990). Friction at a Lubricated Line Contact Operating at Oscillating Sliding Velocities. Journal of Tribology 112(1): 147-152.

Hofmann, P. J., Schettler, T. and Steininger, D. A. (1992). PWR steam generator tube fretting and fatigue wear phenomena and correlations. Symposium on flow-induced vibration and noise.

Hunt, K. H. and Crossley, F. R. E. (1975). Coefficient of restitution interpreted as damping in vibroimpact. ASME Journal of applied mechanics 42(2): 440-445.

Jahanmir, S. and Suh, N. P. (1977). Mechanics of subsurface void nucleation in delamination wear. Wear 44(1): 17–38.

Johannes, V. I., Green, M. A. and Brockley, C. A. (1973). The role of the rate of application of the tangential force in determining the static friction coefficient. Wear 24(3): 381-385.

Johnson, K. L. (1955). Surface Interaction between Elastically Loaded Bodies under Tangential Forces. Proceedings of the Royal Society of London. Series A. Mathematical and Physical Sciences 230(1183): 531-548.

Johnson, K. L. (1961). Energy Dissipation at Spherical Surfaces in Contact Transmitting Oscillating Forces. Journal of Mechanical Engineering Science 3 (4): 362-368

Johnson, K. L. (1985). Contact Mechanics. Cambridge, Cambridge University Press.

Johnson, K. L., Kendall, K. and Roberts, A. D. (1971). Surface energy and the contact of elastic Solids. Proceedings of the Royal Society of London, Mathematical and Physical Sciences 324(1558): 301-313.

Karnopp, D. (1985). Computer simulation of stick-slip friction in mechanical dynamic systems. Journal of Dynamic Systems, Measurement, and Control 107(1): 100-103.

Ko, P. L. (1986). Metallic wear-a review, with special references to vibration-induced wear in power plant components. Proceedings ASME Pressure Vessels and Piping Conference. Chicago, Illinois. 20**:** 66-78.

Lee, Y.-H., Kim, I.-S., Kang, S.-S. and Chung, H.-D. (2001). A study on wear coefficients and mechanisms of steam generator tube materials. Wear 250(1-12): 718-725.

Lesieutre, G. A. (2009). How membrane loads influence the modal damping of flexural structures. AIAA Journal 47(7): 1642-1646.

Lever, J. H. and Weaver, D. S. (1982). A Theoretical model for fluid-elastic instability in heat exchanger tube bundles. ASME Journal of Pressure Vessel Technology 104(3): 147-158.

Lim, Y. F. and Chen, K. (1998). Dynamics of dry friction: A numerical investigation. Physical Review E 58(5): 5637–5642.

Magaziner, R., Jin, O. and Mall, S. (2004). Slip regime explanation of observed size effects in fretting. Wear 257(1-2): 190-197.

Mindlin, R. D. (1949). Compliance of elastic bodies in contact. ASME Journal of Applied Mechanics 16(3): 259-268.

Mindlin, R. D. and Deresiewicz, H. (1953). Elastic Spheres in Contact under Varying Oblique Forces. ASME Journal of applied mechanics 20: 327-344.

Moretti, P. M. and Lowery, R. L. (1973). Heat exchanger tube vibration characteristics in a "no flow" condition , School of Mechanical and Aerospace Engineering, Oklahoma State University, TEMA experimental program**:** Technical Report.

Morley, L. S. D. (1960). The thin-walled circular cylinder subjected to concentrated radial loads. The Quarterly Journal of Mechanics and Applied Mathematics 13(1): 24-37.

Nowlan, I., Ross, A. and Pettigrew, M. J. (2009). Dynamic interaction between a straight tube and an anti-vibration bar. ASME Conference Proceedings 2009(43673): 437-445.

Ödfalk, M. and Vingsbo, O. (1990). Influence of normal force and frequency in fretting. Tribology Transactions 33(4): 604-610.

Ödfalk, M. and Vingsbo, O. (1992). An elastic-plastic model for fretting contact. Wear 157(2): 435-444.

Oengoren, A. and Ziada, S. (1995). Vortex shedding, acoustic resonance and turbulent buffeting in normal triangle tube arrays. Flow-Induced Vibrations. Balkema, Rotterdam. 6**:** 295–313.

Ozaki, S. and Hashiguchi, K. (2010). Numerical analysis of stick-slip instability by a rate-dependent elastoplastic formulation for friction. Tribology International 43(11): 2120-2133.

Païdoussis, M. P., Price, S. and de Langre, E. (2010). Fluid-Structure Interactions, Cambridge University Press.

Pettigrew, M. J., Sylvestre, Y. and Campagna, A. O. (1978). Vibration analysis of heat exchanger and steam generator designs. Nuclear Engineering and Design 48(1): 97-115.

Pettigrew, M. J. and Taylor, C. E. (1994). Two-phase flow-induced vibration: An overview. ASME Journal of Pressure Vessel Technology 116(3): 233-253.

Pettigrew, M. J. and Taylor, C. E. (2003a). Vibration analysis of shell-and-tube heat exchangers: an overview--Part 1: flow, damping, fluidelastic instability. Journal of Fluids and Structures 18(5): 469-483.

Pettigrew, M. J. and Taylor, C. E. (2003b). Vibration analysis of shell-and-tube heat exchangers: an overview--Part 2: vibration response, fretting-wear, guidelines. Journal of Fluids and Structures 18(5): 485-500.

Pettigrew, M. J., Taylor, C. E., Fisher, N. J., Yetisir, M. and Smith, B. A. W. (1998). Flow-induced vibration: recent findings and open questions. Nuclear Engineering and Design 185(2-3): 249-276.

Popp, K. (2005). Modelling and control of friction-induced vibrations. Mathematical and Computer Modelling of Dynamical Systems 11(3): 345 - 369.

Rabinowicz, E. (1951). The nature of the static and kinetic coefficients of friction. Journal of Applied Physics 22(11): 1373-1379.

Rice, J. R. and Ruina, A. L. (1983). Stability of steady frictional slipping. Journal of applied mechanics 50(2): 343-349.

Rogers, R. J. and Pick, R. J. (1977). Factors associated with support plate forces due to heat-exchanger tube vibratory contact. Nuclear Engineering and Design 44(2): 247-253.

Rubiolo, P. R. (2006). Probabilistic prediction of fretting-wear damage of nuclear fuel rods. Nuclear Engineering and Design 236(14–16): 1628-1640.

Ruina, A. (1983). Slip instability and state variable friction laws. Journal of Geophysical Research 88(B12): 10359-10370.

Sauve, R. G. and Teper, W. W. (1987). Impact simulation of process equipment tubes and support plates: a numerical algorithm. ASME Journal of Pressure Vessel Technology 109(1): 70-79.

Shaw, S. W. (1985). Forced vibrations of a beam with one-sided amplitude constraint: Theory and experiment. Journal of Sound and Vibration 99(2): 199-212.

Stevens, A. B. and Hrenya, C. M. (2005). Comparison of soft-sphere models to measurements of collision properties during normal impacts. Powder Technology 154(2-3): 99-109.

Stoianovici, D. and Hurmuzlu, Y. (1996). A critical study of the applicability of rigid-body collision theory ASME Journal of Applied Mechanics 63(2): 307-316.

Stribeck, R. (1902). Die wesentlichen Eigenschaften der Gleit- und Rollenlager. VDI-Zeitschrift 46: 1341-1348.

Stronge, W. J. (2000). Impact Mechanics. Cambridge, Cambridge Unviversity Press.

Subbaraj, K. and Dokainish, M. A. (1989). A survey of direct time-integration methods in computational structural dynamics II. Implicit methods. Computers and Structures 32(6): 1387-1401.

Suh, N. P. (1973). The delamination theory of wear. Wear 25(1): 111–124.

Tan, X. and Rogers, R. (1996). Dynamic friction modelling in heat exchanger tube simulations. Flow-Induced Vibrations. Montreal, ASME. 328**:** 347–358.

Tariku, F. A. and Rogers, R. J. (2001). Improved Dynamic Friction Models for Simulation of One-Dimensional and Two-Dimensional Stick-Slip Motion. Journal of Tribology 123(4): 661-669.

Thomson, M. G., Bishop, S. R. and Foale, S. (1994). An experimental study of low velocity impact. Machine Vibration 3: 10-17.

Thornton, C. and Randall, C. W., Eds. (1988). Micromechanics of granular materials. Amsterdam, Elsevier.

Toorani, M., Pan, L., Li, R., Idvorian, N. and Vincent, B. (2009). Advanced nonlinear flow-induced vibration and fretting-wear analysis capabilities. 6th CNS International Steam Generator Conference,. Toronto.

Tustin, A. (1947). The effects of backlash and of speed-dependent friction on the stability of closed-cycle control systems. Journal of the Institution of Electrical Engineers 94(1): 143-151.

Vingsbo, O. and Schön, J. (1993). Gross slip criteria in fretting. Wear 162-164(1): 347-356.

Wagg, D. J. (2005). Periodic sticking motion in a two-degree-of-freedom impact oscillator. International Journal of Non-Linear Mechanics 40(8): 1076-1087.

Wagg, D. J. (2007). A note on coefficient of restitution models including the effects of impact induced vibration. Journal of Sound and Vibration 300(3–5): 1071-1078.

Wagg, D. J. and Bishop, S. R. (2000). A note on modeling multi-degree-of-freedom vibro-impact systems using coefficient of restitution models. Journal of Sound and Vibration 236(1): 176-184.

Waterhouse, R. B. (1981). Fretting Fatigue. London, Applied Science.

Weaver, D. S. and Schneider, W. (1983). The effect of flat bar supports on the crossflow induced response of heat exchanger U-tubes. ASME Journal of Engineering for Power 105(4): 775-781.

Weaver, D. S., Ziada, S., Au-Yang, M. K., Chen, S. S., Paidoussis, M. P. and Pettigrew, M. J. (2000). Flow-induced vibrations in power and process plant components---progress and prospects. ASME Journal of Pressure Vessel Technology 122(3): 339-348.

Werner, S. and Robert, S. (2008). Impacts on beams. Computational Structural Dynamics and Earthquake Engineering, Taylor & Francis**:** 137-148.

Wojewoda, J., Stefański, A., Wiercigroch, M. and Kapitaniak, T. (2008). Hysteretic effects of dry friction: modelling and experimental studies. Philosophical Transactions of the Royal Society A: Mathematical, Physical and Engineering Sciences 366(1866): 747-765.

Yetisir, M. and Fisher , N. J. (1997). Prediction of pressure tube fretting-wear damage due to fuel vibration. Nuclear Engineering and Design 176: 261-271.

APPENDIX 1

Proceedings of the Pressure Vessels & Piping Conference
ASME2012
July 15-19, 2012, Toronto, Ontario, CA

PVP2012-78699

NUMERICAL ANALYSIS OF INTERMITTENT STICK-SLIP BEHAVIOUR OF TUBE-SUPPORT INTERACTION IN HEAT-EXCHANGERS

Reza Azizian
BWC/AECL/NSERC Chair of Fluid-Structure Interaction, Department of Mechanical Engineering, École Polytechnique de Montréal
Montreal, Canada
Email:reza.azizian@polymtl.ca

Njuki Mureithi
BWC/AECL/NSERC Chair of Fluid-Structure Interaction, Department of Mechanical Engineering, École Polytechnique de Montréal
Montreal, Canada
Email:njuki.mureithi@polymtl.ca

ABSTRACT

Flow induced excitation forces in heat exchangers cause tube-support interactions. The long-term interaction is an important phenomenon which may cause fretting-wear of the tubes. Experimental tests of the interaction show the occurrence of stick-slip intermittent behavior in the tube response. Many factors are involved to precisely predict the interaction behavior including flow excitation forces, impact and friction forces. One of the explanations behind the intermittent stick-slip behavior may be interpreted by refinements in the conceptual choice of friction model and coefficient of friction. Therefore, among the factors above, the incorporated friction model plays an important role in the determination of the level of fretting-wear in the system. The friction model should satisfy two important criteria: the first important aspect is the strategy of the friction model to detect the cessation of sticking, the beginning of partial slipping and establishment of the sliding region. The second important aspect is defining a friction coefficient function for the entire system response to precisely represent the transient stick-slip regions. In the present work, the velocity limited friction model was compared with the LuGre model which is a rate dependent friction model. The effect of varying the break-away force and Stribeck effect on the stick-slip region was also investigated. Furthermore, the criteria to demarcate the stick-slip region in the LuGre model are discussed and a different method to incorporate the Stribeck effect and presliding damping in the Dahl friction model are proposed. Finally, a new hybrid spring-damper friction model inspired by the Cattaneo-Mindlin stress distribution in the contact region is proposed.

INTRODUCTION

During interaction between metallic components, friction and wear play important roles. These phenomena cause material to be removed at the points of interaction which may lead to component failure. Different wear processes may be involved during the interaction such as abrasion, delamination, fatigue, corrosion and fretting wear [1, 2]. Tube-support interaction in heat exchanger tube bundles may cause the same problem. Different experimental tests have been carried out to determine the exact mechanism of the wear process and material removal [3, 4]. The results indicate that cracks propagate in the sub-layer parallel to the contact surface and gradually turn toward the contact surface due to stress concentration [3, 5]. The process may cause wear debris which explains the main mechanism of material removal during the wear process [3, 6].

For tube-support interaction simulation, especially in the presence of wear, it is vital to incorporate a proper friction model. The friction model should have certain capabilities to

precisely reproduce the interaction behavior. During interaction, three phases of relative motion may be considered: sticking, partial-slip and gross-slip. Thus, it is important for the friction model to be able to demarcate the boundaries between the different phases of the relative motion and measure the length of the relative motion in each phase. Switching among different phases of the relative motion has been observed in the different experimental test [7, 8]. Moreover, different mathematical functions were incorporated in the friction models to reproduce the intermittent stick-slip behavior especially in the vicinity of zero velocity where there is a nonlinear transient behavior from the stick to slip phase [7, 9-11].

For numerical simulation of the tube-support interaction, different numerical codes have been developed to reproduce the interaction behavior. These include VIBIC [12], H3DMAP [13] and FIVDYNA [14]. As mentioned earlier, a proper friction model is vital to determine the amount of wear in the simulations. The Velocity Limited Friction Model (VLFM), Force-Balanced Friction Model (FBFM) and Spring-Damper Friction Model (SDFM) are three friction models which have been used in the simulations.

In the present work, the advantages and weaknesses of different friction models were investigated for a simple mass-spring system. Furthermore, a hybrid friction model is proposed which is capable of estimate of the length of sticking, partial-slip and gross-slip during movement. Physical parameters were introduced into the friction model based on the stress-distribution in the contact area considering bristle elastic displacement, bristle yielding and the relative tangential displacement of bristles [15-17].

FRICTION MODELS

The main purpose of developing different friction models is to have capabilities to reproduce the exact behavior of the movement before the cession of sticking. Moreover, due to nonlinear friction behavior in the vicinity of zero velocity, it is important for the friction model to have a more realistic transient function for this period in contrast with the simple Coulomb friction model.

The basic friction model is the Coulomb friction model. All the different types of friction models use the Coulomb friction model to determine the friction forces during sliding. However, different methods are used for demarcating between the stick - slip regions, which plays an important role in our research since more slipping regions may increase the work-rate and consequently increase estimated fretting during tube-support interaction.

Different friction models were developed to evaluate the stick-slip regions and estimate the sticking friction forces as follows [18]:

1- Velocity-limited friction models (VLFM) [19]
2- Force balance friction models (FBFM) [20]
3- Spring damper friction models (SDFM) [18]

Each type of friction model has limitations and advantages. Researchers have tried to combine the friction models to compensate for the weaknesses of each individual model to be able to precisely determine the slipping distance [21].

RATE DEPENDENT FRICTION MODELS

To have a more precise friction model, the model should be able to reproduce the process from an absolute zero velocity to the condition of incipient gross slip. The contact interaction process contains different regions of elastic, plastic and partial slipping before the complete cession of sticking [15, 17, 22]. Much effort has been dedicated to precisely simulating the different parts of the process. Ozaki and Hashiguchi [10] have simulated the non-linear intermittent stick-slip behavior by introducing a mathematical function for the friction coefficient. The function not only depends on the rate of change of the friction coefficient but also the plastic sliding velocity and the friction coefficient itself [10]. With the help of the transient function the pre-sliding displacement and the stick-slip switching may be reproduced based on an equation as follows [10]:

$$\dot{\mu} = -k(\frac{\mu}{\mu_k} - 1)v_p + \xi(1 - \frac{\mu}{\mu_s}). \qquad (1)$$

Lim and Chen [9] developed a model considering a conceptual choice of the friction coefficient by taking into account velocity weakening and creep before the cession of sticking as follows [9, 23]:

$$\mu(\phi, \dot{x}) = A\,\mathrm{sgn}(\dot{x}) \sinh^{-1}\left\{\frac{1}{2}\exp\left[\frac{\bar{\mu}}{A}\right]\right\} + \eta\dot{x}, \qquad (2)$$

$$\bar{\mu} = a_v + b_v \ln\frac{\phi V_0}{D_0} + A\ln\frac{\phi|\dot{x}|}{D_0}, \qquad (3)$$

$$\dot{\phi}(t) = 1 - \frac{|\dot{x}|\phi}{D_0}. \qquad (4)$$

Another effort has been made to consider the Stribeck effect in a state variable model for switching from the sticking state to the slip state [11, 24]. The LuGre model was developed based on the elastic displacement of a conceptual bristle and considering a rate-dependent break-away force, presliding displacement and hysteretic behavior and has the following form [11, 24, 25] :

$$F_f = \sigma_0 z + \sigma_1 \frac{dz}{dt} + \sigma_2 \dot{x}, \qquad (5)$$

$$\frac{dz}{dt} = \dot{x} - \frac{|\dot{x}|}{g(\dot{x})} z, \qquad (6)$$

$$g(\dot{x}) = \frac{1}{\sigma_0}\{F_c + (F_s - F_c)\exp(-(\dot{x}/v_s))\}, \qquad (7)$$

where F_s, F_c, v_s and z are the static friction force, coulomb friction force, Stribeck velocity and average bristle deflection, respectively. σ_0, σ_1 and σ_2 are the stiffness coefficient and damping coefficients, respectively.

Figure 1. shows the transient function modeling the switching between the stick state and slip state in the LuGre model. The effect of varying the Stribeck velocity, v_s, is shown. The Stribeck velocity is the parameter which defines how fast switching takes place in the friction model.

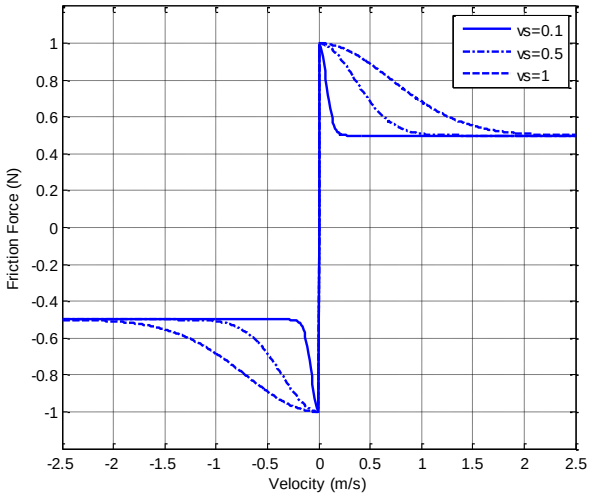

FIG. 1 STRIBECK VELOCITY EFFECT ON SWITCHING FROM STICK STATE TO SLIP STATE

MASS-SPRING MODEL

As shown in Fig. 2, a mass attached to a spring was chosen to perform the simulations. The system allows us to precisely study the effect of the friction model parameters on the predicted friction force and slick-slip regions.

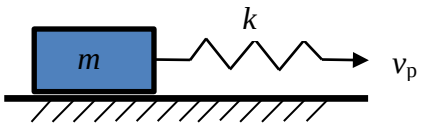

FIG. 2 MASS-SPRING SYSTEM

The equation of the motion of the system may is,

$$m\ddot{x} + kx = kv_p t - F_f. \qquad (8)$$

In Eq. (8), the mass, m, and stiffness, k, are chosen respectively equal to 1 kg and 20 N/m^2. v_p and F_f are the pulling velocity and friction force, respectively. In this study, different types of pulling velocities are chosen to examine friction model behavior under various conditions.

The first applied excitation consisted of a constant pulling velocity to the mass-spring model. In Fig.3, the friction force histories obtained using the velocity-limited friction model and the LuGre model are shown. For pulling velocities of 0.1, 0.2 and 0.3 m/s, break-away forces of 1.39, 1.34 and 1.26 N were respectively obtained for the LuGre model.

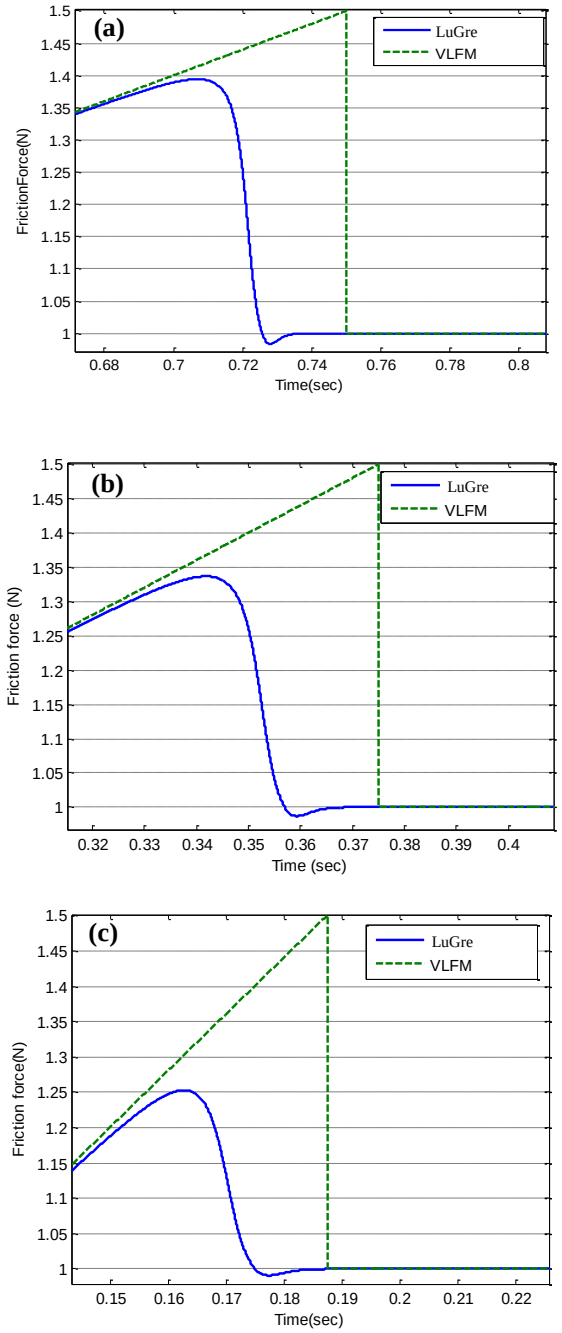

FIG.3 BREAK-AWAY FORCES COMPARISON FOR THE VELOCITY LIMITED FRICTION MODEL AND THE LUGRE MODEL WITH DIFFERENT PULLING VELOCITY (a) vp = 0.1 (m/s^2), (b) vp = 0.2(m/s^2), (c) vp = 0.4 (m/s^2)

The results show that the break-away force in the LuGre model decreases with increasing the excitation force in contrast with the velocity-limited friction model which gives a constant break-away force. The comparison shows not only the importance of the varying break-away force but also the change in the stick-slip regions due to the difference. In other words, the LuGre model switches to the gross-slip regime sooner than the velocity-limited friction model in the study.

In Fig. 4, the differences between the slipping times for different simulation times for both models are presented. The results show an increase in the slipping time percentage with increasing in simulation time for both models which eventually attains a steady state after passing a certain time. The results indicate approximately a 4% difference in slipping duration between the LuGre and VLFM models.

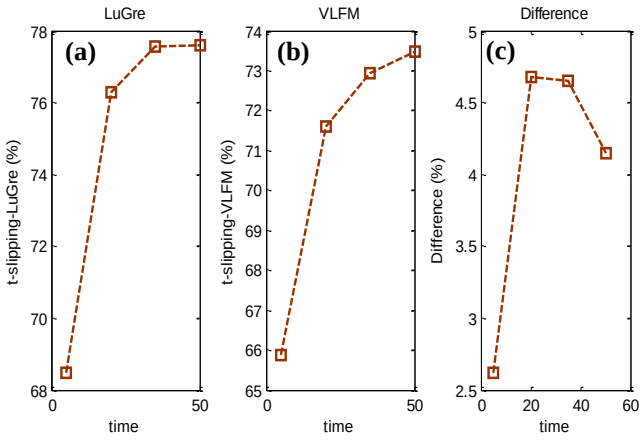

FIG. 4 SLIPPING TIME FOR LUGRE MODEL AND VELOCITY-LIMITED FRICTION MODEL (a) THE LUGRE SLIPPING TIME (b) THE VLFM SLIPPING TIME (c) DIFFERENENCE BETWEENTHE LUGRE AND VLFM

To more carefully investigate the ability of the friction models to capture the stick-slip regions, the chirp excitation function was chosen. The chirp is a cosine function with a linearly increasing instantaneous frequency with time. As shown in Fig. 5, four different chirp excitation functions are applied to the pulling velocity. The chirp functions with 0.2 m amplitude have target frequencies increase from 5 Hz to 30 Hz for cases 1 to 4, respectively, in 10 second simulation time. The results indicate decreasing in the slipping time with the LuGre model in contrast with the VLFM.

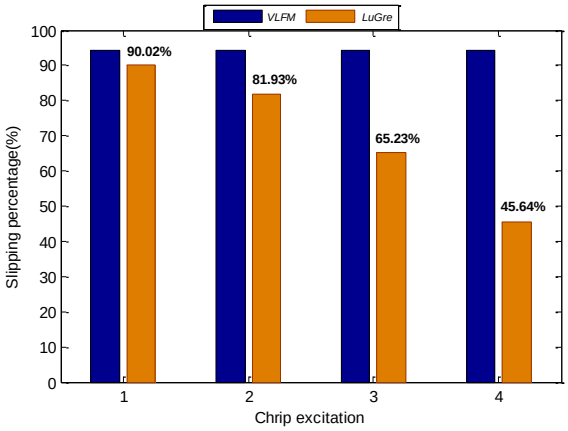

FIG. 5 SLIPPING TIME COMPARISON VLFM AND LUGRE (1) CHIRP [1,5] (2) CHIRP [1,10] (3) CHIRP [1,20] (4) CHIRP [1,30]

Based on the slipping time duration for the LuGre and the VLFM models, it is vital to choose a proper criterion to demarcate the stick-slip regions. In the LuGre model, the rate of average bristle deflection is chosen as the criterion for detection of incipient gross-slip displacement. Based on the mathematical formulation of the LuGre model, the parameter, *dz/dt*, needs to be chosen small enough to capture all sticking regions. In Fig.6, the effect of decreasing the rate of the average bristle deflection is investigated. Decreasing the parameter from 1e-9 (m/s^2) to 1e-12 (m/s^2) shows only a slight difference in the slipping time until the critical point of 1e-12 (m/s^2). The results indicate that by choosing an average bristle deflection smaller than 1e-11 (m/s^2), the LuGre model assumes a big portion of the movement to fall in the sticking region. Therefore, a steep decrease from 62.37% to 3% of the slipping time is observed.

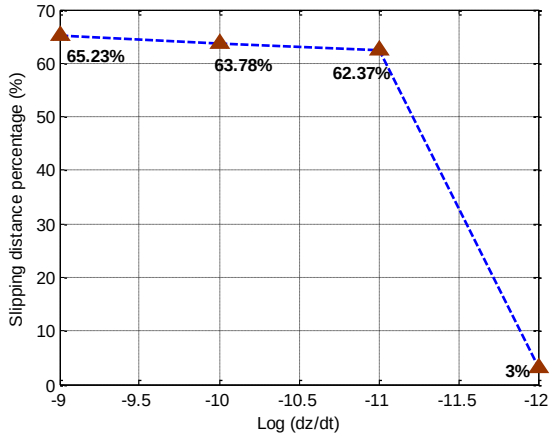

FIG.6 SLIPPING TIME PERCENTAGE VERSUS LOGARITHMIC AVERAGE BRISTLE DEFLECTION

EQUIVALENT SPRING-DAMPER FRICTION MODEL

In this section the LuGre model is expressed in the form of an equivalent physical nonlinear spring-damper model .The LuGre model is a friction model which was developed based on the Dahl friction model by considering hysteretic behavior and

presliding displacement [11, 26]. To achieve these goals, the Stribeck function, Eq. (6), is incorporated into Eq. (5). Moreover, two additional damping terms are introduced in Eq. (5) which represent the damping associated with the rate of the average bristle deflection and viscous damping.

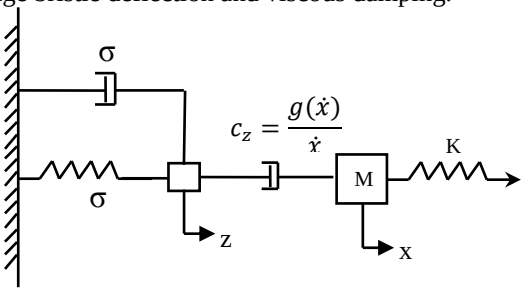

FIG. 7 SPRING-DAMPER MODEL EQUIVQLENT TO THE LUGRE MODEL

As shown in Fig. 7, it is proposed to represent the Stribeck function and damping term by a physical hybrid spring-damper model.

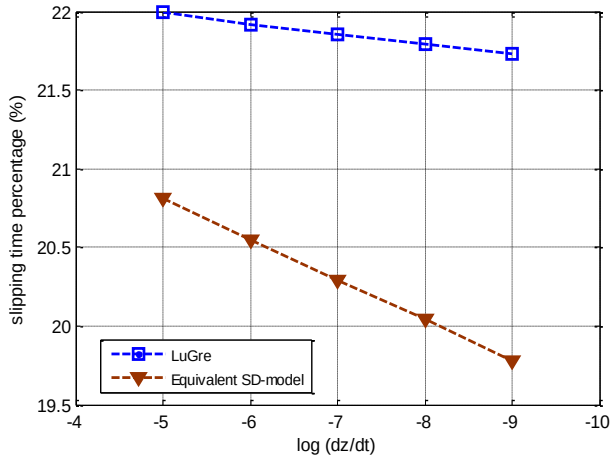

FIG. 8 SLIPPING TIME COMPARISON BETWEEN LUGRE AND REVISED SDFM FOR DIFFERENT LOGARITHMIC RATE OF AVERAGE BRISTLE DEFLECTION

As shown in Fig. 8, the simulation results show 5-9% difference for the slipping time between the LuGre model and the physical equivalent spring-damper friction model. The advantage of the latter model is that gives an intuitive physical meaning to the mathematical functions in the LuGre model.

NEW HYBRID SPRING-DAMPER FRICTION MODEL

In this study, different weaknesses and advantages of the LuGre model were investigated. Two important aspects of the friction model are considered. The first aspect is the criterion to demarcate the stick-slip regions. The second aspect is incorporation of different friction phenomena such as the Stribeck effect and presliding displacement based on a physical hybrid spring-damper model. The issues are vital due to sensitivity of fretting-wear to slipping distance. The demarcating parameter was chosen as the rate of the average bristle deflection. However, as shown in Fig.6, the slipping time may strongly depend on the magnitude of the limiting parameter.

Researchers have investigated the micro-behaviour in the contact area during the stick-slip states. Mindlin [27] developed a model for the tangential stress distribution in the contact area. The model suggests two regions within the contact area. A sticking region inside of the contact area and a partial slipping region in a peripheral region outside of the contact area which progressively develops towards the contact center with increase in the friction force [17]. Johnson [28] experimentally proved the theory. Moreover the Cattaneo-Mindlin [27] theory was further developed to consider the effect of plastic deformation and yielding in the border between the sticking and slip regions [15].

To develop a new friction model, three regions of sticking, yielding and partial slipping are considered before incipient gross-slip based on relations as follows:

$$F_f = k_e z_e + c_p \dot{z}_p + c_s \dot{z}_s, \quad (9)$$

$$\delta = \delta_e + \delta_p + \delta_s, \quad (10)$$

where k_e , c_s , c_p are the stiffness, plastic-damping and slip-damping coefficients. z_e, z_p and z_s are the elastic, plastic and partial slipping displacements.

Based on the Eq. (9) and (10), a new hybrid spring-damper friction model is proposed as shown in Fig. 9.

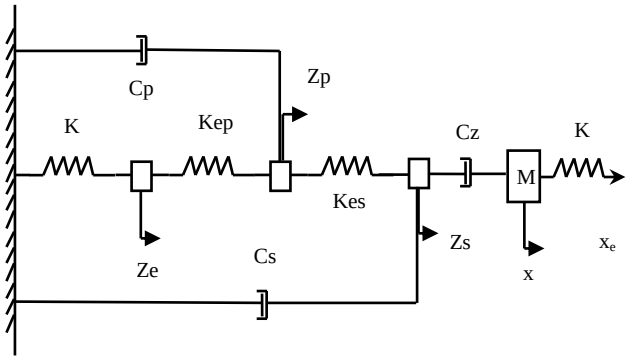

FIG. 9 HYBRID SPRING-DAMPER FRICTION MODEL

The new model consists of two damping coefficients for the plastic and partial slipping. Moreover, three stiffness coefficients for the elastic, elasto-plastic and elasto-slipping displacements are incorporated in the model. One of the important properties of the new hybrid friction model is the capability to explicitly determine the elastic displacement, plastic displacement and partial slipping displacement. To demonstrate this, the system is excited below the break-away force with a function as follows:

(11)

$$x_e = 0.1\cos(10t) + 0.1.$$

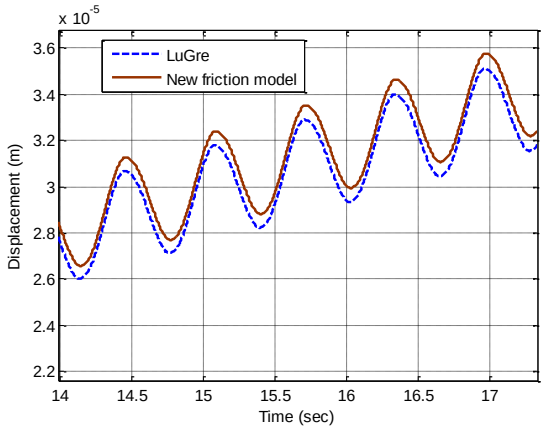

FIG. 10 DISPLACEMENT COMPARISON BETWEEN THE LUGRE AND THE NEW FRICTION MODELS

In Fig. 10, the displacements of the mass-spring system obtained using the LuGre and the new friction model are presented. Both models behave similarly with slight differences in the displacements. However, as shown in Fig. 11. the new friction model has the capability to demarcate elastic, plastic and partial slipping displacements during the motion.

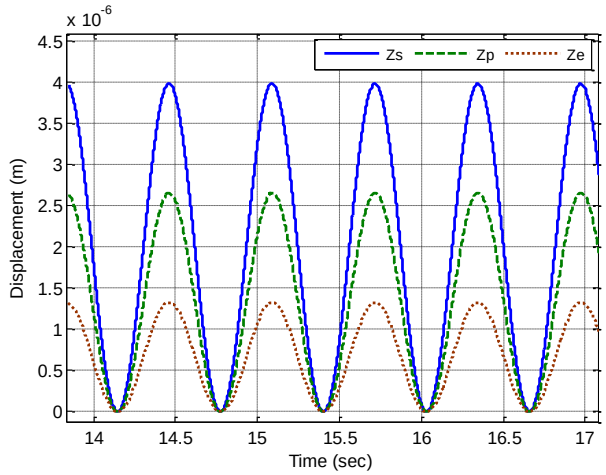

FIG. 11 ELASTIC, PLASTIC, PARTIAL SLIPPING DISPLACEMENT

In the numerical simulation of stick-slip motions, it is important to precisely estimate the pre-sliding displacement. The LuGre model is an elastic model with the weakness of inability to demarcate between the elastic, plastic and partial slipping regions within the presliding displacement. As shown in Fig. 11, the new hybrid model overcomes this difficulty. Furthermore, the demarcating capability makes the new hybrid friction model more flexible in terms of reproducing the pre-sliding displacement. To examine the flexibility, another comparison between the LuGre model and the new friction model is made by implementing an excitation displacement as follows:

$$x_e = \left\{0.05 + e^{-0.05t}\right\}\cos 2t. \qquad (12)$$

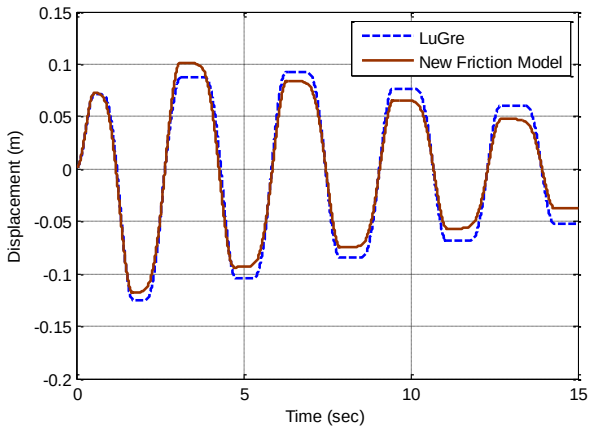

FIG. 12 DISPLACEMENT COMPARISON THE LUGRE AND NEW FRICTION MODELS

The displacements of the mass-spring system are compared in Fig. 12 for the two friction models. The results show the capability of the hybrid friction model to reproduce a bigger presliding displacement while at same time reproducing the correct general motion. In contrast with the LuGre model, the new friction model is an elasto-plastic model. The elasto-plasticity property enables the new friction model not only reproduce a more precise presliding displacement but also the capability to reproduce the nonlinear behaviour in the vicinity of zero velocity.

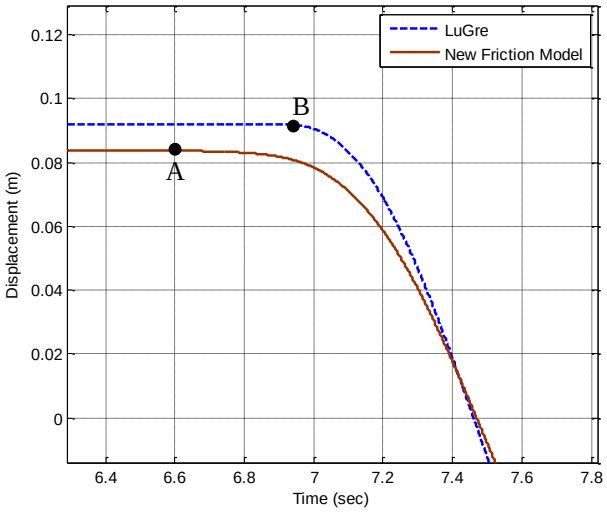

FIG. 13 PRESLIDING DISPLACEMENT IN THE LUGRE MODEL AND NEW HYBRID FRICTION MODEL

In Fig.13, the presliding displacement in the LuGre model and new hybrid friction model are presented in greater detail. The points 'A' and 'B' represent the beginning of the presliding displacement in the new hybrid friction model and LuGre model, respectively. The results emphasize the flexibility of the

new hybrid friction model to reproduce a bigger presliding displacement while maintaining the general trend of the motion.

CONCLUSION

In this study, commonly used friction models for tube-support interaction simulation were discussed. The weaknesses and advantages of the models are compared with a rate dependent friction model. For comparison a simple mass-spring system was used. The Stribeck effect and effect of changing the break-away force on the stick-slip regions were investigated. To have better comparison between the models, different excitation forces were applied on the mass-spring system and the capabilities of the models to capture all the sticking regions were examined.

Furthermore, two aspects in the LuGre model were investigated. The first aspect is the criterion for demarcating the stick-slip regions and the second aspect is incorporation of the Stribeck effect and presliding damping in the Dahl [11] friction model. A modified and extended LuGre model based on an equivalent spring-damper was then proposed. The slipping time comparison was made for the two models which indicated 5-9% difference.

To have a precise estimation of the slipping distance, it is important for the friction model to be able to detect different regions during the motion especially before incipient gross slip. To achieve this, a new elasto-plastic model was proposed to determine the elastic, plastic and partial slipping regions within the contact area. The model was developed based on a hybrid spring-damper model. Simulation results confirm the capability of the new friction model to accurately demarcate the different regions of elastic, plastic and partial-slipping within the presliding displacement. Consequently, the capability makes the new friction model more precise not only in reproducing the presliding displacement but also reproducing the nonlinear trend of the displacement in the vicinity of zero velocity.

REFERENCES

1. Ko, P.L., *Metallic wear-a review, with special references to vibration-induced wear in power plant components*, in *Proceedings ASME Pressure Vessels and Piping Conference*1986: Chicago, Illinois. p. 66-78.
2. Gessesse, Y.B., *On the fretting wear of nuclear power plant heat exchanger tubes using a fracture mechanics approach: Theory and verification*, 2000, Concordia University
3. Suh, N.P., *The delamination theory of wear.* Wear, 1973. **25**(1): p. 111–124.
4. Gauland, D.J. and D.J. Duquette, *Cyclic wear behavior (Fretting) of a tempered martensite steel.* Metallurgical Transactions, 1980. **11**(9): p. 1581-1588.
5. Fouvry, S., P. Kapsa, H. Zahouani, and L. Vincent, *Wear analysis in fretting of hard coatings through a dissipated energy concept.* Wear, 1997. **203-204**: p. 393-403.
6. Fleming, J.R. and N.P. Suh, *Mechanics of crack propagation in delamination wear.* Wear, 1977. **44**: p. 39-56.
7. Baumberger, T., F. Heslot, and B. Perrin, *Crossover from creep to inertial motion in friction dynamics.* Nature, 1994. **367**(6463): p. 544-546.
8. Heslot, F., T. Baumberger, B. Perrin, B. Caroli, and C. Caroli, *Creep, stick-slip, and dry-friction dynamics: Experiments and a heuristic model.* Physical Review E, 1994. **49**(6): p. 4973.
9. Lim, Y.F. and K. Chen, *Dynamics of dry friction: A numerical investigation.* Physical Review E, 1998. **58**(5): p. 5637–5642.
10. Ozaki, S. and K. Hashiguchi, *Numerical analysis of stick-slip instability by a rate-dependent elastoplastic formulation for friction.* Tribology International, 2010. **43**(11): p. 2120-2133.
11. Canudas de Wit, C., H. Olsson, K.J. Astrom, and P. Lischinsky, *A new model for control of systems with friction.* IEEE Transactions on Automatic Control, 1995. **40**(3): p. 419-425.
12. Rogers, R.J. and R.J. Pick, *Factors associated with support plate forces due to heat-exchanger tube vibratory contact.* Nuclear Engineering and Design, 1977. **44**(2): p. 247-253.
13. Sauve, R.G. and W.W. Teper, *Impact Simulation of Process Equipment Tubes and Support Plates---A Numerical Algorithm.* Journal of Pressure Vessel Technology, 1987. **109**(1): p. 70-79.
14. Toorani, M., L. Pan, R. Li, N. Idvorian, and B. Vincent, *Advanced nonlinear flow-induced vibration and fretting-wear analysis capabilities*, in *6th CNS International Steam Generator Conference,*2009: Toronto.
15. Ödfalk, M. and O. Vingsbo, *An elastic-plastic model for fretting contact.* Wear, 1992. **157**(2): p. 435-444.
16. Mindlin, R.D. and H. Deresiewicz, *Elastic Spheres in Contact under Varying Oblique Forces.* ASME Journal of applied mechanics, 1953. **20**: p. 327-344.
17. Johnson, K.L., *Contact Mechanics*1985, Cambridge: Cambridge University Press.
18. Hassan, M.A. and R.J. Rogers, *Friction modelling of preloaded tube contact dynamics.* Nuclear Engineering and Design, 2005. **235**(22): p. 2349-2357.
19. Tan, X. and R. Rogers, *Dynamic friction modelling in heat exchanger tube simulations*, in *Flow-Induced Vibrations,*1996, ASME: Montreal. p. 347–358.
20. Karnopp, D., *Computer Simulation of Stick-Slip Friction in Mechanical Dynamic Systems.* Journal of Dynamic Systems, Measurement, and Control, 1985. **107**(1): p. 100-103.

21. Tariku, F.A. and R.J. Rogers, *Improved Dynamic Friction Models for Simulation of One-Dimensional and Two-Dimensional Stick-Slip Motion.* Journal of Tribology, 2001. **123**(4): p. 661-669.
22. Johnson, K.L., K. Kendall, and A.D. Roberts, *Surface energy and the contact of elastic Solids.* Proceedings of the Royal Society of London, Mathematical and Physical Sciences 1971. **324**(1558): p. 301-313.
23. Ruina, A.L., *Unsteady motions between sliding surfaces.* Wear, 1986. **113**(1): p. 83-86.
24. Armstrong, B. and C. Qunyi, *The Z-properties chart.* IEEE Control Systems 2008. **28**(5): p. 79-89.
25. Astrom, K.J. and C. Canudas de Wit, *Revisiting the LuGre friction model.* Control Systems, IEEE, 2008. **28**(6): p. 101-114.
26. Armstrong, B., *Control of machines with non-linear, low-velocity friction: A dimensional analysis*, in *Experimental Robotics I*1990, Springer Heidelberg. p. 180-195.
27. Mindlin, R.D., *Compliance of elastic bodies in contact.* ASME Journal of Applied Mechanics 1949. **16**(3): p. 259-268.
28. Johnson, K.L., *Energy Dissipation at Spherical Surfaces in Contact Transmitting Oscillating Forces.* Journal of Mechanical Engineering Science, 1961. **3** (4): p. 362-368

APPENDIX 2

Proceedings of the ASME 2012 International Design Engineering Technical Conferences & Computers and Information in Engineering Conference
IDETC/CIE 2012
August 12-15, 2012, Illinois, Chicago, USA
ACCPTED BUT NOT PUBLISHED IN PROCEEDING

DETC2012-70168

A HYBRID FRICTION MODEL FOR DYNAMIC MODELING OF STICK-SLIP BEHAVIOUR

Reza Azizian
BWC/AECL/NSERC Chair of Fluid-Structure Interaction, Department of Mechanical Engineering, École Polytechnique de Montréal
Montreal, Canada

Njuki Mureithi
BWC/AECL/NSERC Chair of Fluid-Structure Interaction, Department of Mechanical Engineering, École Polytechnique de Montréal
Montreal, Canada

ABSTRACT

Fretting wear is a common problem in different industries especially when it comes to interactions between metallic components. In heat exchangers, the problem plays a destructive role due to long term interaction between tubes and supports which may consequently lead to tube failure. In the present work, the tube-support fretting wear problem was investigated by refining models for friction effects in the stick-slip regions. The Slip distance is the most important parameter for wear estimation. Using the tangential stress distribution in the contact area, a new hybrid spring-damper friction model was developed. The model is able to estimate elastic, plastic and partial slipping distances during relative motion. The ability of the model to reproduce experimental tests is investigated in the present work.

INTRODUCTION

The long term tube-support interaction in heat exchangers may cause tube-support fretting-wear [1]. In numerical simulations of the phenomenon the type of incorporated friction model plays an important role. Nonlinearities of the friction models in the vicinity of zero velocity pose serious difficulties when developing and incorporating these models in numerical simulations. Experimental studies of tube-support interaction show significant chattering between stick-slip regions during the tube-support interaction [1, 2]. The friction model should therefore be designed to give details and boundaries of three different modes of relative movement: slip, stick and stick-slip. The velocity limited friction model (VLFM) [3], force balanced friction model (FBFM) [4] and spring-damper friction model (SDFM) [5, 6] are the three major friction models which are commonly used in tube-support numerical simulations.

Azizian and Mureithi [7] compared the LuGre [8] friction model which is a rate-dependent friction model with the velocity-limited friction model. The results indicated the importance of considering the presliding displacement and the Stribeck effect in the stick-slip regions. In the present work, the process of transition from absolute zero velocity to entirely gross slipping was refined by considering the tangential stress distribution over the contact region. The results indicate three main regions of elastic, yielding (plastic) and partial slipping before incipient gross-slip. Each region of the motion is represented by a theoretical model. The elastic displacement is represented by Cattaneo-Mindlin theory [9]. The plastic displacement and yielding are characterized with the Odfalk and Vingsbo method [10]. The partial-slipping displacement is

associated with a damping coefficient based on the Cattaneo and Deresiewicz method [9]. Moreover, the Stribeck effect is modeled with a transient function based on the LuGre model [8, 11] .

Finally, to consider the different effects, a hybrid spring damper friction model was designed. A simple mass-spring system was chosen according to experimental tests by Baumberger et al. [12] to test the new friction model.

FRICTION MODELS

A friction model is a key element in wear-rate estimation. The importance of choosing a proper friction model can be recognized in establishing accurate stick-slip regions. A larger slipping distance may lead to more material removal due to fretting-wear. The Coulomb friction model is the fundamental basis of all friction models. The model gives the friction force in the gross slip state. The model, however, cannot predict incipient gross slip or estimate the friction force in the sticking region.

Different friction models have been proposed to overcome these short comings as follows [5, 13, 14]:

1-Velocity-Limited Friction Model (VLFM) [14]

In the velocity-limited friction model, a limiting velocity is defined to demarcate stick-slip regions.

$$|F_f| = \mu F_n \qquad if \quad |V_t| > V_0 \quad , \tag{1}$$

$$|F_f| = \frac{|V_t|}{V_0}\mu F_n \qquad if \quad |V_t| \le V_0 \ , \tag{2}$$

where V_0 , μ and F_n are the limiting velocity, friction coefficient and normal force, respectively.

2-Force Balanced Friction Model (FBFM) [4]

In the force-balanced friction model, the slipping friction force is determined similarly to the Coulomb's friction model but the sticking friction force is determined as follows:

$$F_f = Ku - F_e \ , \tag{3}$$

where Ku and F_e are internal and external forces, respectively.

3-Spring Damper Friction Model (SDFM) [5]

In the spring-damper friction model, the friction force during sticking is composed of two terms: damping force and spring force. The model is formulated as,

$$F_f = \mu F_n \qquad \text{sliding} \ , \tag{4}$$

(5)

$$F_f = K_a(u_c - u_0) + C_a V_t \qquad \text{sticking} \ ,$$

where the parameters u_c and u_0 are, respectively, the current and the zero velocity tangential displacement. K_a and C_a are stiffness and damping coefficients.

RATE DEPENDENT FRICTION MODELS

To have a precise estimation of the slipping distance, it is vital for the friction model to be able to recognize different regions where sticking, presliding and sliding occurs. Moreover, incorporating a proper mathematical function in the friction model to represent the transient process of switching between the sticking phase and slip phase is important. The function can affect the stick-slip regime.

Different studies have been conducted to examine the weaknesses and advantages of the traditional friction models. Azizian and Mureithi [7] made a comparison between the velocity-limited friction model and LuGre model. The study indicated the weaknesses of the traditional friction models compared to a rate dependent friction specially in terms of estimating the precise slipping distance.

LuGre Friction Model [8]

The LuGre friction model is an elastic rate-dependent friction model. In the model, phenomena such as varying break-away force, friction hysteretic behavior and presliding displacement are considered [11]. The model is expressed mathematically as follows:

$$F_f = \sigma_0 z + \sigma_1 \frac{dz}{dt} + \sigma_2 \dot{x} \ , \tag{6}$$

$$\frac{dz}{dt} = \dot{x} - \frac{|\dot{x}|}{g(\dot{x})} z \ , \tag{7}$$

$$g(\dot{x}) = \frac{1}{\sigma_0}\left\{F_c + (F_s - F_c)\exp(-(\dot{x}/v_s))\right\} \ , \tag{8}$$

where σ_0, σ_1 and σ_2 are the stiffness, presliding damping and viscous damping coefficient, respectively. F_s , F_c and v_s are the static friction force, coulomb friction force and Stribeck velocity, respectively.

In the LuGre model, the Stribeck effect was considered by introducing an exponential function according to equation (8). The Stribeck velocity, v_s, determines the rate of changing from the sticking phase to gross slipping phase. Moreover, the presliding displacement is taken into account by introducing a damping term, σ_1, as shown in equation (6).

Ozaki and Hashiguchi Friction Model [15]

Ozaki and Hashiguchi [15] developed a rate-dependent friction model based on a conceptual definition of a friction coefficient for the entire motion. The model may describe as follows:

$$\dot{\mu} = -k(\frac{\mu}{\mu_k} - 1)v_p + \xi(1 - \frac{\mu}{\mu_s}) \,, \qquad (9)$$

where k and ξ are the rate of decrease and recovery of the friction coefficient, respectively. v_p , μ_s , μ_k are the plastic sliding velocity, static coefficient of friction and kinetic coefficient of friction, respectively.

In the model, the instantaneous friction coefficient depends not only on the plastic velocity, static and dynamic friction coefficient but also depends on the coefficient friction's rate of changing.

STRESS DISTRIBUTION IN THE CONTACT AREA

To come up with a physical model capable of demarcating different regions in the contact area, it is vital to study the tangential stress distribution in the contact surface between two objects. Cattaeno-Mindlin [16] developed a mathematical formula to describe the tangential stress distribution over the contact area as follows:

$$q(r) = \begin{cases} \mu p_0 \left\{ \left(1 - \dfrac{r^2}{a^2}\right)^{1/2} - \left(1 - \dfrac{r^2}{c^2}\right)^{1/2} \right\} & 0 \le r < c \\ \mu p_0 \left(1 - \dfrac{r^2}{a^2}\right)^{1/2} & c \le r \le a \end{cases} \,, \qquad (10)$$

where μ is the coefficient of friction and P_0 the normal stress.

Based on equation (10), the contact area is divided into two regions: a sticking region with elastic displacement and a partial slip region. Fig.1 shows the differences in the stress distribution in the two regions which are demarcated by the parameter 'c'.

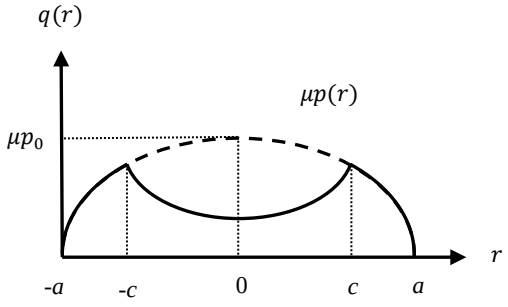

Figure 1 Cattaneo-Mindlin tangential stress distribution [17]

In the region $0 \le r \le c$, the coincident contact points on the contact interface move together which represents the sticking region as shown in Fig.2 by the point 'A' [16, 17]. However, for the region $c \le r \le a$, the contact points on the two bodies have a relative tangential movement which represents the slipping region as shown in Fig.2 by the points 'B' and 'C' [16, 17].

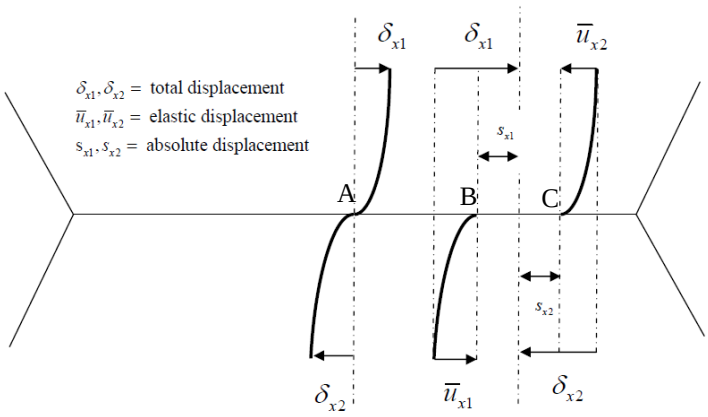

Figure 2 Stick and slip point in contact region [18]

In later development of the Cattaneo-Mindlin theory [16], Cattaneo and Deresiewicz [19] studied the effect of varying tangential force on the stress distribution in the contact area. Consequently, the study determined the energy dissipation during oscillatory tangential displacement. Moreover, Odfalk and Vignsbo [20] measured the presliding displacement dependence on the excitation frequency. The results indicated underestimation of presliding displacement by the Cattaneo-Mindlin elastic theory. To correct for this, Odfalk and Vignsbo [10] developed a plastic model to consider yielding effect in the contact region.

Using Cattaneo-Mindlin theory for flat surfaces without losing its cogency needs to be explained and justified. Considering two flat surfaces in contact, with condition of neither gross-slip nor partial-slip, the system is similar to a flat punch with the same displacement in the loading direction all over the contact region. The tangential stress distribution is [18],

$$Q(x) = \frac{Q_x}{\pi(w^2 - x^2)^{1/2}} \,, \qquad (11)$$

where x is the position of the coincident points within the contact width and w is the contact width.

The tangential stress distribution shows the amount of infinity on the border line of $x=w$ which brings into question the condition of no-slip. In other words, the coefficient of friction needs to infinite to sustain the condition of no-slip on the border of the contact area. This leads us to infer the presence of the partial-slipping region for the two-flat surfaces similarly to the spherical contact [18].

Since the Cattaneo-Mindlin theory is valid for a spherical contact, certain assumptions needed to be considered to be able to use the theory for flat surfaces including: (1) two smooth flat surfaces in contact with each other and one of them includes certain waviness [20]. (2) the surfaces are in contact at least in three contact points [20]. (3) considering a spherical shape for the contact tip between flat surfaces [20]. The experimental test conducted by Odfalek & Vingsbo [20] confirmed that the presliding displacement is proportional to the *2/3* power of the normal force which emphasizes the validity of the Cattaneo-Mindlin theory for flat surfaces. Based upon the assumptions, conceptual incorporation the Cattaneo-Mindlin theory in a friction model for flat surfaces is admissible.

NEW HYBRID SPRING-DAMPER FRICTION MODEL

Based upon the stress distribution in the contact region, different phases of displacement may be identified in the contact area [10, 18]. Three main regions of elastic displacement, plastic displacement and slipping are shown in Fig.3. Moreover, to have a precise friction model, two transient regions of elastic to plastic and plastic to slipping transition are considered.

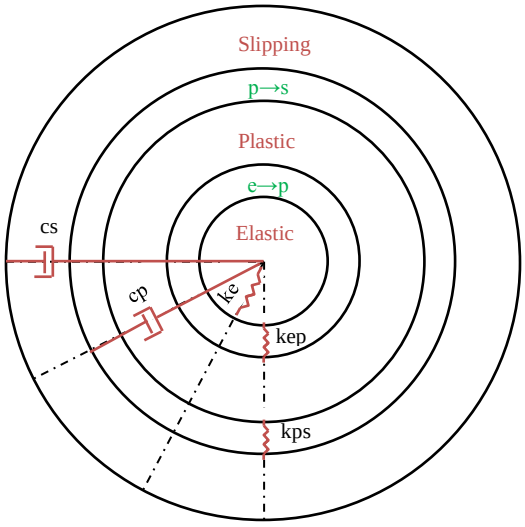

Figure 3 Displacement field in the contact area and equivalent spring-damper model

The hybrid spring-damper friction model was developed based on different regions in the contact area which satisfy following conditions:

$$F_f = k_e z_e + c_p \dot{z}_p + c_s \dot{z}_s \ , \tag{12}$$

$$z = z_e + z_p + z_s \ , \tag{13}$$

where z_e , z_p and z_s are the elastic, plastic and partial slipping displacements, respectively. k_e , c_s , c_p are the stiffness, plastic-damping and slip-damping coefficients, respectively.

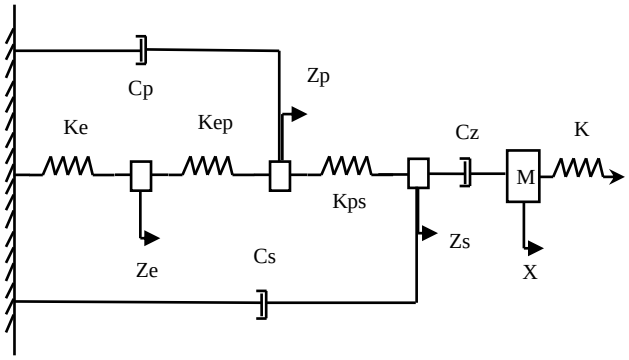

Figure 4 New hybrid spring-damper friction model

As shown in Fig.4 , the hybrid friction model consists of four important effects: The average elastic bristle displacement inspired by the Cattaneo-Mindlin theory [9], plastic displacement inspired by the Odfalk-Vignsbo method [10] , partial-slipping displacement inspired by the Cattaneo-deresiewicz method [9] and finally the Stribeck phenomenon based on the LuGre model [8].

$$\underbrace{k_e z_e}_{\text{bristle elastic}} + \underbrace{k_{ep}(z_e - z_p)}_{\text{transient } e\to p} = 0, \tag{14}$$

$$\underbrace{k_{ep}(z_p - z_e)}_{\text{transient p}\to e} + \underbrace{k_{ps}(z_p - z_s)}_{\text{transient p}\to s} + \underbrace{c_p \dot{z}_p}_{\substack{\text{plastic}\\ \text{dissipation}}} = 0, \tag{15}$$

$$\underbrace{k_{ps}(z_p - z_s)}_{\text{transient s}\to p} + \underbrace{c_z(\dot{z}_s - \dot{x})}_{\substack{\text{transient}\\ \text{partial-slipp}\to\text{slip}}} + \underbrace{c_s \dot{z}_s}_{\substack{\text{slipping}\\ \text{dissipation}}} = 0. \tag{16}$$

The Friction model can be expressed based on equations (14)-(16) which include the four different effects. C_z in equation (16) is the Stribeck damping [7] which may be determine based on equation (8). Considering these effects, the pre-sliding displacement may be more accurately modeled. C_z in equation (16) is the Stribeck damping [7].

MASS-SPRING SYSTEM

A simple mass-spring model is considered for numerical simulation as shown in Fig.5.

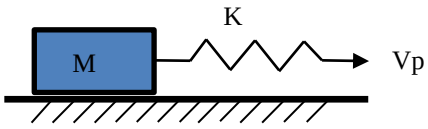

Figure 5 Mass-Spring system

Table.1 shows constants for the mass-spring system. The parameters were chosen to be consistent with the experimental test conducted by Baumberger et al. [12] for model verification.

Table 1 mass-spring model parameters

M (kg)	K (Ncm^{-1})	Vp (μms^{-1})
0.8	580	1

RESULTS AND DISCUSSION

To evaluate the new hybrid spring-damper friction model, the Baumberger [12] experimental test was chosen. That was the only fully documented test program the authors have found in the open literature. The experimental test consists of a mass attached to a spring with a constant pulling velocity. The set-up makes it possible to produce periodic stick-slip motion due to the spring force and friction resistance to the motion. To reproduce the experimental test's displacement, choosing proper model parameters is a challenging step. Four parameters k_e , F_s , F_c ,v_s affect the general stick-slip behavior. On the other hand, four other parameters k_{ep} , k_{ps} , c_s , c_p mostly affect the presliding distance.

To estimate the parameters, the nonlinear least-squares method was used. The optimization was conducted in two steps. The first step involved defining the general motion behavior by optimizing the first set of parameters. In this step the objective function is the quadratic difference between the displacement time-history in the experiment and numerical simulation for the entire stick-slip motion. In Table 2, the first set of the optimized parameters is presented.

Table 2 New friction model parameters

k_e	F_s	F_c	v_s
5.2e+7	1.07	0.707	1e-6

The second optimization step contains the estimation of the second set of parameters which is more sensitive in terms of defining the presliding displacement. In this step the objective function is the quadratic difference for the time-history of the presliding displacement. In Table 3, the second set of the optimized parameters is presented.

Table 3 New friction model parameters

k_{ep}	k_{ps}	c_s	c_p
1.9e+7	8.5e+7	2.3e+3	6.3e+2

The first-step of the optimization is more costly since the objective function is highly sensitive to these parameters. On the other hand, the second set of the optimization captured the presliding displacement which required a more refined time step to more accurately run the simulation and capture the entire process. The time step is chosen equal to 1e-6 sec.

Fig.6 shows a comparison of the Baumberger et al. [12] experimental test data with the new friction model as well as the Ozaki and Hashiguchi [15] model. The new friction model can reproduce the same number of the stick regions as reported in the experiment contrary to the Ozaki and Hashiguchi [15] model which detects five out of eight sticking phases. Furthermore, the duration of the sticking region in the new friction model has reasonable agreement with the experimental test.

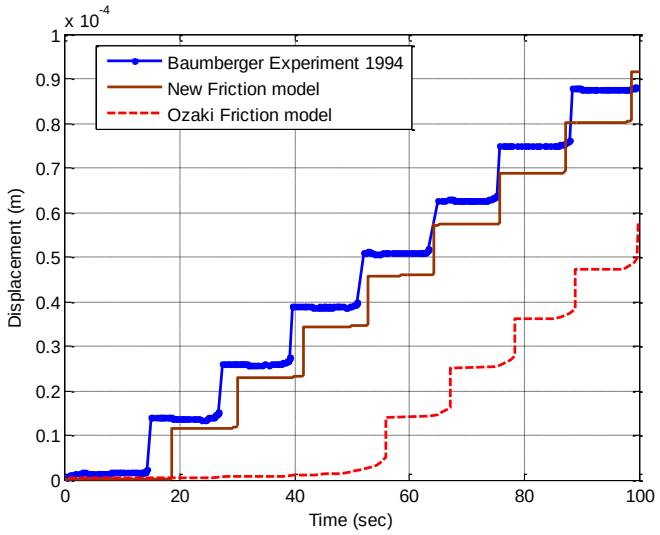

Figure 6 New hybrid friction model, Ozaki and Hashiguchi friction model [15] and Baumberger et al. [12] experimental test comparison

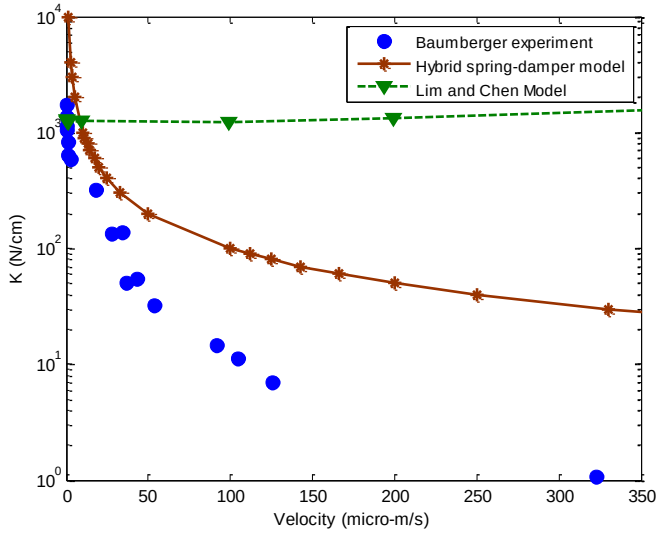

Figure 7 K-V dynamic phase diagram for the stick-slip stability for the Baumberger experimental test [12] , Lim and Chen model [21] and Hybrid spring-damper model

After identifying the system parameters with the optimization method, the friction model is evaluated with different inputs for the spring stiffness and pulling velocity. The K-V stability diagram based upon Baumberger et.al. [12] experimental test data is used to compare the stability velocities. The velocity may be determined for each spring stiffness coefficient by subjecting the mass-spring model to a linearly increasing velocity. For low velocity the motion begins with the stick-slip behavior until it reaches the stability velocity which transfers the motion to a more stable mode of gross-slip.

As shown in Fig.7, the stability velocity for different spring stiffnesses is compared against the hybrid spring damper and Lim-Chen friction model [21]. For each set of data, the transient stick-slip may occur below the curve whereas the more stable motion is located for velocities above the curve.

As reported by Lim and Chen [21], their friction model has a good agreement with the theoretical friction model developed by Rice and Ruina [22]. However, the models have limitation to reproduce the slope of dynamic stability diagram. As shown in Fig.7, the Lim and Chen model produced approximately a constant line for the stability curve with highly sensitive stability velocity to the stiffness in contrast to experimental results. The new hybrid spring damper friction model with the optimized parameters may be able to reproduce the experimental result with a qualitatively good agreement. Quantitatively, the dynamic stability diagram is divided into three regions based on the agreement between the experimental test and hybrid friction model. The first region of the stability velocity of $0 \leq v_c \leq 10(\mu ms^{-1})$ shows magnitude differences between the model and experimental test. The differences may be explained based upon the nature of the creep dominated region which may need a higher Stribeck velocity as the motion changes slowly from the static to the dynamic. However, the trends of the experimental test and numerical simulation have a good agreement showing v_c tends to zero for high spring stiffness. The second region of $10 \leq v_c \leq 50$ (μms^{-1}) has a fairly good agreement with experimental test. Furthermore, in the third stability region of $50 \leq v_c \leq 350$ (μms^{-1}) the numerical simulation is able to reproduce the general experimental trends. However, the simulations overestimate the stability velocity. This is likely due to overestimation of the damping coefficients in the friction model.

CONCLUSION

A new hybrid spring-damper friction model was conceptually designed incorporating different phenomena which have a role in establishing stick-slip regions. Based on the stress distribution in a contact area, different regions of elastic, yielding (plastic) and partial slipping are considered. Moreover, the Stribeck phenomenon was also considered which plays an important role in transition stick-slip regions. The hybrid spring-damper friction model was compared to experimental tests and shown to correctly predict not only the number of the stick-slip events but also the correct duration of the sticking phase. The model is therefore a significant improvement over the Ozaki and Hashiguchi model. Other comparisons were made against a series of experimental tests conducted by Baumberger et al. The numerical simulation results indicated a qualitatively good agreement with the measured stability velocity. However, the differences in the stability velocity magnitude were reported. The differences were interpreted based upon underestimation of the Stribeck velocity and overestimation of the damping coefficients in the hybrid friction model parameters.

REFERENCES

1. Pettigrew, M.J. and C.E. Taylor, *Vibration analysis of shell-and-tube heat exchangers: an overview--Part 2: vibration response, fretting-wear, guidelines.* Journal of Fluids and Structures, 2003. **18**(5): p. 485-500.
2. Haslinger, K.H. and D.A. Steininger, *Experimental characterization of sliding and impact friction coefficients between steam generator tubes and avb supports.* Journal of Sound and Vibration, 1995. **181**(5): p. 851-871.
3. Rogers, R.J. and R.J. Pick, *Factors associated with support plate forces due to heat-exchanger tube vibratory contact.* Nuclear Engineering and Design, 1977. **44**(2): p. 247-253.
4. Karnopp, D., *Computer Simulation of Stick-Slip Friction in Mechanical Dynamic Systems.* Journal of Dynamic Systems, Measurement, and Control, 1985. **107**(1): p. 100-103.
5. Hassan, M.A. and R.J. Rogers, *Friction modelling of preloaded tube contact dynamics.* Nuclear Engineering and Design, 2005. **235**(22): p. 2349-2357.
6. Tan, X. and R. Rogers, *Dynamic friction modelling in heat exchanger tube simulations*, in *Flow-Induced Vibrations*,1996, ASME: Montreal. p. 347–358.
7. Azizian, R. and N. Mureithi. *A Numerical Analysis of Intermittent Stick-slip Behavior of Tube-support Interaction in Heat Exchangers*. in *Proceedings of the Pressure Vessels & Piping Conference* 2012. Toronto, Ontario, CA.
8. Johanastrom, K. and C. Canudas-de-Wit, *Revisiting the LuGre friction model.* Control Systems, IEEE, 2008. **28**(6): p. 101-114.
9. Johnson, *Contact Mechanics*1985, Cambridge: Cambridge University Press.
10. Ödfalk, M. and O. Vingsbo, *An elastic-plastic model for fretting contact.* Wear, 1992. **157**(2): p. 435-444.
11. Canudas de Wit, C., H. Olsson, K.J. Astrom, and P. Lischinsky, *A new model for control of systems with friction.* Automatic Control, IEEE Transactions on, 1995. **40**(3): p. 419-425.

12. Baumberger, T., F. Heslot, and B. Perrin, *Crossover from Creep to Inertial Motion in Friction Dynamics.* Nature, 1994. **367**(6463): p. 544-546.
13. Tariku, F.A. and R.J. Rogers, *Improved Dynamic Friction Models for Simulation of One-Dimensional and Two-Dimensional Stick-Slip Motion.* Journal of Tribology, 2001. **123**(4): p. 661-669.
14. Tan, X. and R. Rogers, *Dynamic friction modelling in heat exchanger tube simulations*, in *Flow-Induced Vibrations,*1996, ASME: Montreal. p. 347–358.
15. Ozaki, S. and K. Hashiguchi, *Numerical analysis of stick-slip instability by a rate-dependent elastoplastic formulation for friction.* Tribology International, 2010. **43**(11): p. 2120-2133.
16. Mindlin, R.D., *Compliance of elastic bodies in contact.* Journal of Applied Mechanics ,1949. **16**(3): p. 259-268.
17. Johnson, K.L., *Surface Interaction between Elastically Loaded Bodies under Tangential Forces.* Proceedings of the Royal Society of London. Series A. Mathematical and Physical Sciences, 1955. **230**(1183): p. 531-548.
18. Johnson, *Contact Mechanics,*1985, Cambridge: Cambridge University Press.
19. Mindlin, R.D. and H. Deresiewicz, *Elastic Spheres in Contact under Varying Oblique Forces.* Journal of applied mechanics, 1953. **20**: p. 327-344.
20. Odfalk, M. and O. Vingsbo, *Influence of Normal Force and Frequency in Fretting.* Tribology Transactions, 1990. **33**(4): p. 604-610.
21. Lim, Y.F. and K. Chen, *Dynamics of dry friction: A numerical investigation.* Physical Review E, 1998. **58**(5): p. 5637–5642.
22. Rice, J.R. and A.L. Ruina, *Stability of Steady Frictional Slipping.* Journal of applied mechanics, 1983. **50**(2): p. 343-349.